MSc thesis Biosystems Engineering

Dynamic simulation and control of potato bulk storage

J.C. Mol

March, 2015
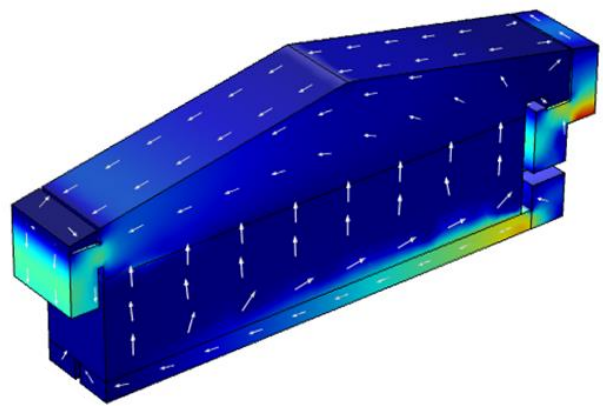
CONFIDENTIAL

Dynamic simulation and control of potato bulk storage

Course title   : MSc thesis Biosystems Engineering
Course code   : BCT-80436
Study load   : 36 credits
Report number   : BCT-001
Date   : March 26th , 2015

Student   : Jordi Mol
Registration number   : 920405-576-090
Study programme   : Biosystems Engineering (MAB)

Supervisors   : dr. ir. K.J. Keesman
                             : MSc N.L.M. Grubben
Examiner   : dr. ir. L.G. van Willigenburg
Chair group   : Biobased Chemistry and Technology (BCT)
                            Gerda Bos
                            Bornse Weilanden 9
                            6708 WG Wageningen
                            Tel.:   +31 (317) 48 06 94
                            Mail: office.bct@wur.nl

Abstract

Agricultural products play an important role in the continuous demand for feed and food. Additional to that, an increasing amount of agricultural products is used as raw material for biobased industrial processes. Since the production of agricultural products is season dependent, storage of these products is necessary in order to guarantee a continuous supply towards the customers. To maintain the product climate at least at a certain level, modern storage facilities are controlled by advanced controllers.

In this research, a fully spatially distributed model of an advanced potato bulk storage is developed, including air conditioning equipment, as a mechanical cooling unit and a humidifier. In addition, a controller based on the potato temperature is designed and evaluated by simulations. The control input variables are the pressure drop over the system fans and the difference between the ventilated air temperature and potato temperature. For different settings of the control input variables, the system behaviour is evaluated with respect to necessary ventilation time and dehydration of the product. Furthermore, the effect of the air conditioning equipment on the system behaviour is evaluated.

Finally, cost functions are derived for energy consumption by the system fans and the air condition equipment and for weight losses of the product caused by dehydration. Using these cost functions, optimal control settings, which minimize the total costs for a specific storage period, were found.

Table of Contents

Acknowledgements

I would like to thank my supervisors, dr.ir. K.J. (Karel) Keesman and N.L.M. (Nik) Grubben for the assistance during this thesis project. I would also like to thank ir. L. (Luuk) Salamons, director of Omnivent, for his support and interest to cooperate in this study.

Wageningen University
March 26, 2015

1   Introduction

1.1 Background

From the beginning of mankind, agricultural products play an important role in live, since agricultural products were used for food and feed. Last decades, agricultural products are also used for another purpose, namely as raw material for bio based industrial processes (Yokoyama, 2008). Due to this new purpose and the growing world population, the worldwide demand for agricultural products is increasing every year. Since most agricultural products are season dependent, storage of the products is necessary in order to deliver a continuous, seasonable independent stream of agricultural products to the costumer and industry.

According to van't Ooster (1996), two basic storage methods for agricultural products can be distinguished, namely indoor and outdoor storages. Outdoor storages are only suitable for products which can handle relatively large temperature fluctuations. Temperature and vapour sensitive products are mainly stored in indoor storage facilities. In these facilities, controllers are involved to maintain an optimal climate for a high quality product storage.

Large amounts of agricultural products are stored in bulk storage systems, in which the product is stored at one large pile. This bulk is ventilated by fans in order to keep all physical conditions inside the bulk at the right level and uniformly distributed. The air is distributed through the bulk by air channels or by a fully gridded floor, as schematically presented in Figure 1-1. Compared to a design of a storage facility with air channels, a fully gridded floor results in higher building costs. However, a more uniform air distribution is reached by a fully gridded floor.
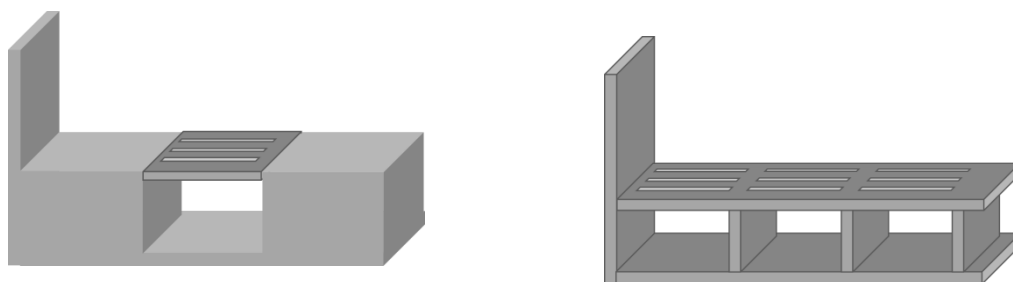
Figure 1-1 Air channel (left hand side) and fully gridded floor right hand side).

In addition to system fans, also other equipment can be placed in advanced storage facilities. Mechanical cooling units can be activated in order to cool down the air in the storage facility (and consequently the product temperature) when outdoor air conditions are unsuitable for ventilation or cooling purposes. Furthermore, a humidifier can be placed inside the storage facility. This equipment humidifies the air before flowing through the product to limit the dehydration process of the product during the ventilation process.

1.2 Problem formulation

The optimal storage scenario is to ends up with an optimal quality of the stored product combined with minimal storage costs, mainly due to energy usage and decreasing product quality over time. To attain a high quality of the stored product at the end of the storage period, the climate during the storage period is of great importance. Several climate factors, like temperature, relative humidity and CO_2 concentration, have large influence on the product quality. In order to control the climate during the storage period at low costs, advanced controllers are needed. However, to develop such controllers, it is necessary to investigate the dynamics and the spatial distribution of the climate factors in the storage facility at first.

Recently, Grubben (2013) developed a model and performed simulations on a potato bulk storage facility in order to investigate the dynamics and spatial distribution of the climate factors. However, this model took not all parts of a storage facility into account and consequently not all dynamics could be evaluated. Furthermore, air conditioning equipment, which is nowadays used in advanced storage facilities, are left out of consideration. In order to investigate the dynamics and spatial distribution of the climate factors in a complete storage facility, including air conditioning equipment, a more extensive model is needed.

1.3 Research goal

The goal of this research is to develop dynamic 2D and 3D simulation models of the climate and the product in bulk storages, where the climate is considered to be a function of temperature, relative humidity of the air, air velocity and pressure. The simulations will be used to evaluate the system behaviour under different circumstances. Additional to that, the simulations can be used to design advanced model predictive climate controllers and to improve the design of advanced storage facilities.

In order to reach this goal, the following research question is defined:

- ***How to set up a dynamic 2/3 D simulation of an advanced climate controlled bulk storage facility?***

Dynamic simulations are needed to evaluate the (dynamic) behaviour of the system for time dependent cases. Advanced storage facilities are defined as storage facilities in which the effects of cooling units and humidifiers on the air conditions are taken into account as well. A 3D simulation is preferred, since some dynamics are not uniform in the three dimensions. However, if 3D simulations are not feasible, a method has to be derived in which all physics of a 3D storage facility can be represented in 2D simulations. Using a 2D or 3D simulation model, the system behaviour will be further investigated in order to answer the following questions:

- What is the influence of the settings of the control input variables on the system behaviour?
- What is the effect of actuators (cooling unit and humidifier) on the system behaviour?
- What are the optimal settings with respect to the economic costs over a storage period?

1.4 Approach

First, a literature review will be performed in which the functioning of Computational Fluid Dynamics (CFD) is globally described. This review will also contain some information regarding the modelling of agricultural storage facilities.

Since the setup for a 2D simulation will be easier compared to a setup for 3D simulations, first the dynamics in 2D will be investigated. As a starting point, the study of Grubben (2013) will be used. In order to be able to evaluate the spatial distribution of the climate factors in three dimensions, also the possibilities for a 3D setup will be investigated.

In case 3D simulations cannot be realised, methods that are able evaluate all dynamics in a 3D storage facility on the basis of 2D simulations will be investigated.

The behaviour of the system with respect to the control variables (pressure drop over the fan and difference between potato temperature and ventilated air temperature) will also be evaluated in terms of needed ventilation time and dehydration rates of the product. Furthermore, the effect of air conditioning equipment on the system behaviour will be evaluated. Finally, cost analyses will be performed on different scenarios in order to find optimal control settings over a specific storage period.

1.5 Outline thesis

In chapter 2, a literature review concerning CFD-modelling is presented. The several phases in CFD-modelling are described. Furthermore, the functioning of different stabilization techniques incorporated in CFD software is described. Since our research focusses on dynamic simulations of climate and product quality in modern potato storage facilities, the modelling includes the description of air conditioning equipment as well. In addition to this, the pressure drop over the product is investigated. Finally, an overview is presented of the current level of CFD modelling of potato storages and the additions to that as result of this study.

The geometry of the storage facility and the corresponding dynamics (related to climate and product conditions) are described in chapter 3. Since the storage facility is divided into several domains, all boundary conditions for coupling these domains are presented. Next, the functioning of stabilization techniques needed to obtain stable solutions is further investigated. Finally, a relation between the pressure drop over the product and the amount of soil in the product is derived in order to be able to simulate also scenarios with soiled products.

The CFD implementation of the dynamics in the software package COMSOL Multiphysics 4.4 is presented in chapter 4. This chapter describes the used methods to include all dynamics of the system in 2D simulations.

In chapter 5, scenario studies are evaluated to obtain rules of thumb related to the system behaviour. First, scenarios are performed in December and April in which the effect of the control variables and the air conditioning equipment on the system behaviour is evaluated on ventilation time and dehydration rate of the potato. Furthermore, cost functions for ventilation, mechanical cooling, air humidifying and dehydration are defined in order to investigate how the total costs can be minimized.

Finally, discussion points related to this research are presented in the chapter 6, the research questions are answered in chapter 7 and some recommendations are mentioned in chapter 8.

2   Theory

2.1 CFD-modelling

CFD stands for Computational Fluid Dynamics, which means that the related physics of a system (fluid flow, heat or mass transfer or chemical reactions) are analysed by computer-based simulations. These physics are described by partial differential equations (PDE's) in 1, 2 or 3 dimensions, depending on type of application and the corresponding research or design questions. Analytical solutions of PDE's are mostly preferred, since this result in exact solutions. However, analytical solutions can only be found for relatively simple systems. Therefore, more complex systems are solved numerically.

Although the underlying physics for CFD modelling was already known in the nineteenth century, CFD modelling is only applied since approximately 50 years. This has to do with the introduction of the digital computer at that time, which is needed to solve the physics of complex systems numerically. Nowadays, CFD-modelling is applied in a large range of fields, as environmental engineering, chemical engineering, mechanical engineering, climate engineering and so on. The fast increase of the application of CFD-modelling in all kind of fields is related to the following advantages of CFD-modelling:

- Significant reduction of production time and costs of new design, compared to experimental-based design
- Ability to analyse systems where controlled experiments are difficult or impossible to perform due to scales of the system or safety conditions
- High level of detail of results can be realised

2.1.1   Procedure of CFD-modelling

According to Versteeg (2007), the process to simulate the physics in a system can be divided into three steps. First, a pre-processor step, followed by the step in which the solver is defined and finally an analysing step of the results.

Pre-processing

In this phase, the physics of the system has to be transformed into a suitable form for the solver. In order to do that, the following steps need to be taken:

- Defining the geometry of the system. This geometry can be divided into several computational domains
- Creating a grid of the geometry, such the domains of the geometry are covered by a finite number of elements. The density of the grid (mesh) depends on the geometry and the physics of the system.
- Defining the physical phenomena that need to be modelled in the form of partial differential equations (PDE's).
- Defining the fluid properties
- Specifying all boundary conditions and initial conditions of each domain of the system.

The provided solution in the next step is defined at the nodes of the elements defined by the grid. Therefore, defining a proper mesh is important to obtain a stable solution, since too coarse meshes will result in inaccurate solutions or are even unsolvable. On the other hand, a very dense mesh entails long computational time and high memory usage, which is also not preferred. As a rule of thumb, the mesh size should be at maximum one third of the smallest dimension of the corresponding domain. Optimal meshes are often non-uniform; they are dense in domains with small dimensions and large spatial variations in the simulated physics and less dense in domains with relatively large dimensions and small spatial variation in the physics. Nowadays, some commercial software packages include automatic remeshing possibilities in order to create an optimal mesh.

Solver

To simulate the physics of a system, several numerical solution techniques can be used, for example the Finite Element Method (FEM), Finite Volume Method (FVM) or Finite Difference Method (FDM). According to Versteeg (2007), all techniques are based on performing the following steps:

- Approximate the unknown physical variables in each node by using simple shaped functions.
- Discretization process, in which the approximations of the previous steps are substituted into the governing physic equations.
- Solution of a set of algebraic equations.

The main differences between the several numerical solution techniques can be traced back to the approximation of the unknown variables and the discretization process. The three steps mentioned above, will be explained in a bit more detail for the FEM technique.

For each node in the mesh, all unknown variables are approximated by defining a shape function with a finite number of parameters. The mathematical representation is given in equation (2-1).

$$u(x) = \sum_i U_i \varphi_i \qquad \text{(2-1)}$$

Here, $u(x)$ represents piecewise polynomials of degree p, U_i represents the degree of freedom and φ_i represents the shape function. The approximations of the unknown variables are substituted into the equations which covers the physics. These equations are precisely satisfied by the exact solution. A residual term, which represents the difference between the exact solution and the approximations, is defined. This residual term is minimised, which result in a set of algebraic equations for the unknown coefficients of the approximation function. During the numerical solving process, instabilities in the solution can easily arise. To prevent unstable solutions, several stabilization techniques can be applied (see section 2.1.2).

Post processing

The solution obtained from the previous step, has to be analysed in the so-called post processing stage. Nowadays, several commercial software packages include fancy visualization tools in which vector plots, 2D or 3D surface plots and even animations of dynamic systems can be created in order to analyse the physics. Since the solution is found numerically, it always includes a certain error. Therefore, it is important to validate the found results, for example with measurements.

2.1.2   Stabilization techniques in CFD-modelling

Numerically solving partial differential equations that describe convection-diffusion phenomena can result in an oscillatory behaviour of the solution. This can already occur for very simple convection-diffusion problems, even when there exist a smooth analytical solution. This spurious oscillatory behaviour is caused by numerical instabilities. A general representation of a convection-diffusion equation is given by:

$$\frac{\partial u}{\partial t} + \beta \cdot \nabla u = \nabla \cdot (c \, \nabla u) + F \qquad (2\text{-}2)$$

Here, β is the convective velocity vector, c is the diffusion coefficient, u is the transported state and F is a source term. For stabilization issues, the relation between the convection and diffusion term and the mesh size is important. This relation is known as the Péclet number. This number is presented in equation (2-3). As a rule of thumb, a maximum mesh size of one third of the smallest dimension of the system is often used.

$$Pe = \frac{\|\beta\| \, h}{2c} \qquad (2\text{-}3)$$

Here, β is the convective velocity vector, c is the diffusion coefficient and h represents the mesh size. In discretization processes, as described above, solutions becomes unstable if the Péclet number exceeds 1, in combination with one of the following conditions:

- Steep gradients near boundaries, caused by Dirichlet boundaries.
- Local disturbance caused by space-dependent initial conditions which are not resolved by the mesh. This leads to local initial disturbances which finally propagates through (part of) the configuration.
- Local disturbance caused by small diffusion term in combination with a non-constant source term or a non-constant Dirichlet boundary.

For problems in which diffusion is present, a solution with a Péclet number smaller than 1 can theoretically be obtained by an infinite small mesh size. This means that spurious oscillating behaviour can be prevented by refining the mesh. However, in most cases is this not feasible in practice, since a very fine grid is needed, which leads to very long computational time. Therefore, stabilization techniques are applied in order to enforce stable solutions.

Several stabilization techniques are used, but all techniques boil down to adding an artificial (numerical) diffusion term to the transport term in equation (2-2). The stabilization techniques can be classified as:

- Inconsistent stabilization
  - Isotropic diffusion
- Consistent stabilization
  - Streamline diffusion
  - Crosswind diffusion

First, there exists a difference between inconsistent and consistent stabilization techniques. Inconsistent stabilization techniques add artificial diffusion independently on how close the numerical solution is to the exact solution. On the contrary, consistent stabilization techniques add artificial diffusion to equation (2-2) such that if there exist an exact solution of u, this also is the solution from the problem in which artificial diffusion is applied. So, less artificial diffusion is applied when the numerical solution comes close to the exact solution.

Isotropic diffusion
The simplest way of stabilizing is by adding isotropic diffusion (c_{art}) to equation (2-2) such that the Péclet number becomes smaller than one. The amount of isotropic diffusion is defined as:

$$c_{art} = \delta_{id} \|\beta\| \, h \tag{2-4}$$

Here, δ_{id} is a tuning parameter. This means that instead of equation (2-4), now the modified $O(h)$ perturbed problem must be solved, as presented in equation (2-5).

$$\frac{\partial u}{\partial t} + \beta \cdot \nabla u = \nabla \cdot \left((c + c_{art}) \, \nabla u \right) + F \tag{2-5}$$

If δ_{id} is fixed at 0.5, the Péclet number never exceeds one (as presented in equation (2-6)) and the solution becomes stable.

$$Pe = \frac{\|\beta\| \, h}{2(c + c_{art})} = \frac{\|\beta\| \, h}{2c + \|\beta\| \, h} < 1 \tag{2-6}$$

Since the Péclet number is smaller than one by adding this amount of artificial diffusion, the spurious oscillations are damped. However, using this stabilization method, artificial diffusion is added independently on how close the numeric solution is to the exact solution. Therefore, the solution is less accurate compared to consistent stabilization techniques.

8

Streamline diffusion

Alternatively, artificial diffusion can be added in the streamline direction of the flow. This can be done by the Streamline Upwind Petrov-Galerkin (SUPG) method or by the Galerkin least-squares (GLS) method.

The SUPG method is very complicated, a detailed explanation is given by Zienkiewicz et al. (2005). This method results in a better accuracy, since the accuracy using SUPG is at least $O(h^{p+0.5})$, compared to $O(h)$ by using isotropic diffusion. In this relation p stands for the order of the polynomial functions.

The Galerkin least-squares (GLS) method is similar to the SUPG method and result in the same order of accuracy. However, instead of adding artificial diffusion, this method adds artificial production ($s > 0$) or absorption ($s < 0$), as presented in equation (2-7).

$$\frac{\partial u}{\partial t} + \beta \cdot \nabla u = \nabla \cdot (c \, \nabla u) + su + F \qquad (2\text{-}7)$$

If $s \neq 0$, stability is related to the Péclet number (see equation (2-3)) and the element Damköhler number:

$$Da = \frac{|s|h}{\|\beta\|} \qquad (2\text{-}8)$$

According to Hauke (2002), the solution becomes stable if the combined Péclet-Damköhler relation is smaller than one:

$$2DaPe = \frac{|s|h^2}{c} < 1 \qquad (2\text{-}9)$$

If this is the case, the production or absorption effects dominate the convective effects.

Crosswind diffusion

For most problems, only adding artificial diffusion in streamline direction is sufficient to perform a stable solution. However in some problems steep gradients, perpendicular on the streamline direction, are present, caused by boundary conditions. In these cases, still spurious oscillations can occur. This can be resolved by also adding artificial diffusion in crosswind direction. Also for adding crosswind diffusion, several methods exist, which are explained by John and Knobloch (2007). Which method has to be used depends on the physics involved in the problem.

2.2 Modelling advanced storage facilities

In modelling storage facilities for agricultural products, choices have to be made regarding the topology and the process dynamics of a physical model. This mainly determines the complexity of the model. The more realistic the topology and process dynamics are incorporated in the model, the more realistic the output of the model. However, taking all process dynamics and the real topology into account results in a very complex model, which has disadvantages with respect to the computational time of the simulation. Furthermore, by taking all process dynamics into account, the system can be over-parameterised, leading to identifiability problems. According to Grubben (2013), modelling of a physical system can be defined in three steps:

- Process definition
- Model boundaries
- Model structure

2.2.1 Process definition

In the process definition phase, a choice has to be made between stationary or dynamic modelling. Since the physics involved in storage facilities are time dependent, these systems are usually considered as dynamical processes. With respect to modelling, a storage facility for agricultural products consists out of several components, namely the agricultural product, the air between the product, air in remaining part of the storage facility and the environment. Each of these components has their own influence on the system behaviour and the related control of the system (Verdijck, 2003). These relations are visualized by Grubben (2013), as presented in Figure 2-1.
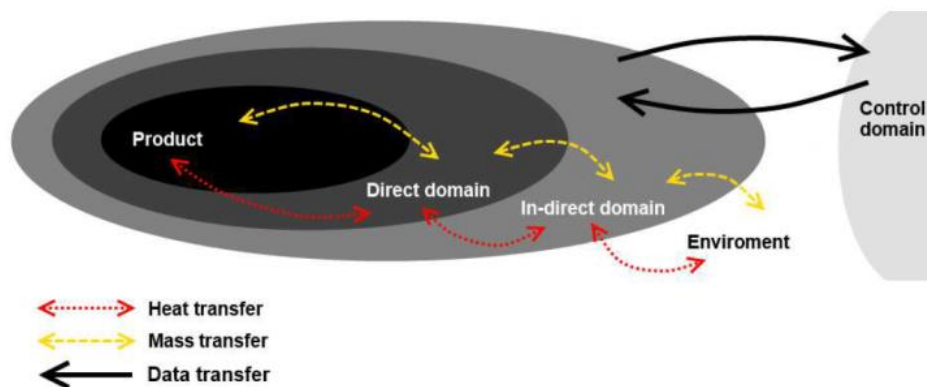

Figure 2-1. The four domains related to an agricultural storage facility and the control domain. The arrows represents the interaction between the different domains (Grubben, 2013).

Figure 2-1 shows that interactions takes place between the physical domains in terms of heat and mass. Heat and mass flows forms the base of the physical model of an agricultural storage facility (Ofoli and Burgess, 1986). The interactions between the different domains can be represented in the model by mass, energy and momentum equations. Since the agricultural product is a living mechanism, several biological processes take place inside the product, which affects the air between the product. Most important processes related to the product are evaporation and respiration (Beukema et al. (1982), Verdijck (2003)). As stated above, the indirect domain represents the air in the remaining part of the storage facility. In this domain, sensors and actuators can be placed for controlling purposes.

By controlling the physical properties as temperature, relative humidity and CO_2 concentration in this domain, the product quality can be controlled indirectly. The environment is a very large domain in which all kind of processes occur. However, usually only temperature and moisture interactions with the indoor climate are taken into account.

2.2.2   Model boundaries

Several configurations are used for storing agricultural products. The physics involved in these configurations are more or less similar to each other, only boundary conditions can be different. A total model consists out of several domains, as presented in Figure 2-2. The outside air enters the storage facility in the air room, where the air is mixed with the indoor air and forced to move into an air channel by a fan. Due to forced convection, the air flows through the product. At the top of the storage, the air leaves the storage facility and/or is used for internal ventilation. For modelling bulk storage facilities, the product can be represented by only one product domain.
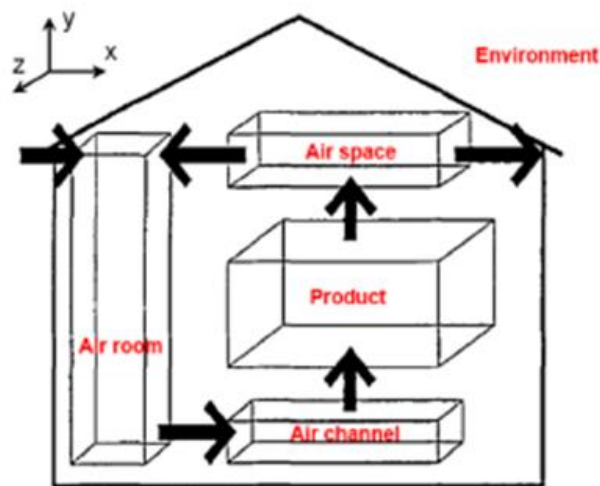

Figure 2-2. A conventional configuration for agricultural bulk storage.

2.2.3   Model structure

The complexity of a model mainly depends of the number of states, the processed included in the model and the spatial configuration of the model. Three main approaches for defining the model structure are commonly used, namely lumped parameter models, fully spatial distributed models and data-based models (Amos, 1995).

Lumped parameter models consist out of one or more layer(s) in which all states are assumed to be ideally mixed. In every layer, the states are represented by ordinary differential equations. The more layers are involved, the more realistic the model becomes, since the assumption of ideal mixing is more consistent with the reality.

When defining an infinite number of layers, which represents infinite small spaces, the lumped parameter model becomes a fully spatial distributed model. These models are more realistic and more complex compared to lumped parameter models.

The behaviour of the states is described by partial differential equations. These kinds of models are able to represent phenomena in 1D, 2D or 3D.

Data-based models are, opposite to lumped parameter models and fully spatial distributed models, based on black box modelling. This kind of models merely relies on real time data instead of the involved physics.

2.2.4   Modelling of the physics in potato storage facilities

Several physical and biological processes take places in potato storage facilities. In order to end up with a realistic model, the most relevant processes have to be taken into account in the model. These processes can be described by the corresponding physical laws and empirical expressions. In this research, a spatially distributed model of a storage facility is proposed and described by a set of partial differential equations (PDE). Therefore, the processes and the general PDE's included in this model will be explained in this section.

In a model of a storage facility, the transport of momentum, mass and energy plays an important role. Using laws of conservation, these transport phenomena are taken into account. These laws of conservation are very general expressions in which the change of a certain state is equal to a transport term and a production term, see equation(2-10).

$$accumulation\ of\ X = flux(X_{in} - X_{out}) \pm reaction\ of\ X \tag{2-10}$$

Using PDE's in a spatial distribution model, small volume elements are defined in which the change of X depends on the flux densities is x, y and z direction and a production or reaction term, as presented in equation (2-11).

$$\frac{\partial X}{\partial t} = -\frac{\partial \phi_x''}{\partial x} - \frac{\partial \phi_y''}{\partial y} - \frac{\partial \phi_z''}{\partial z} + r_X \tag{2-11}$$

The flux densities in the three dimensions are given by:

$$\phi_n'' = v_n X - c\frac{\partial X}{\partial n} \tag{2-12}$$

Here, n represents the x, y and z direction, v_n represents the velocity in the corresponding directions and c is a constant. Equations (2-11) and (2-12) can be combined and put into a compact vector notation:

$$\frac{\partial X}{\partial t} = -\vec{v} \cdot \nabla X + c \cdot \Delta X + r_X \tag{2-13}$$

Here, $\vec{v} = \begin{bmatrix} v_x & v_y & v_z \end{bmatrix}^T$, the gradient operator $\nabla = \begin{bmatrix} \frac{\partial}{\partial x} & \frac{\partial}{\partial y} & \frac{\partial}{\partial z} \end{bmatrix}^T$ and the Laplacian operator $\Delta = \begin{bmatrix} \frac{\partial^2}{\partial x^2} & \frac{\partial^2}{\partial y^2} & \frac{\partial^2}{\partial z^2} \end{bmatrix}^T$.

According to Grubben (2013), the heat, mass and momentum balances are defined as:

$$\rho_m C_{p,m} \frac{\partial T}{\partial t} = -\rho_m C_{p,m} \vec{v} \cdot \nabla T + \lambda \cdot \Delta T + r_T \tag{2-14}$$

$$\rho_m \frac{\partial X}{\partial t} = -\rho_m \, \vec{v} \cdot \nabla X + \rho_m \, \mathbb{D} \cdot \Delta X + r_X \tag{2-15}$$

$$\rho_m \frac{\partial v_i}{\partial t} = -\rho_m \vec{v} \cdot \nabla v_n + \rho_m v \cdot \Delta v_i + \frac{\partial p}{\partial i} + \sum F_i \tag{2-16}$$

Here, ρ_m represents the density of the material, $C_{p,m}$ represents the specific heat capacity of the material and λ represents the thermal conductivity of the material. These partial differential equations are analogue to each other and derived from the general vector notation as given in equation (2-10). In the heat balance, mass balance and momentum balance, the constant c is replaced by respectively the thermal conductivity λ, the diffusion coefficient $\mathbb{D}$ and the kinetic viscosity v. For the momentum balance, the time derivative is taken to a specific direction i ($i = [x\ y\ z]$), so three momentum balance equations are obtained. The production term in the momentum balance is divided into two parts. The first term represents the derivative of the pressure in direction i $\left(\frac{\partial P}{\partial i}\right)$ and the second term represents the sum of forces in the i direction.

In storage facilities, two different phases can be distinguished, namely a moving gas phase and a solid phase. The air in the storage facility can be represented by the moving gas phase, while the agricultural product can be represented by the solid phase. As mentioned in section 2.2.2, the storage facility is divided in several domains. In the air room, air channel and air space domains, only the physics of the moving air has to be modelled. For these domains, a one-phase model description is sufficient. However, in the product domain, both the physics of the moving air and the solid product have to be modelled. Therefore, a so called two-phase model description is introduced. The product domain is considered as a porous media. Two different balance equations for each state are defined, one for the solid fraction (X_s) and one for the moving gas fraction (X_g), as presented in the equations (2-17) and (2-18).

$$(1 - \epsilon)\frac{\partial X_s}{\partial t} = (1 - \epsilon)\lambda_s \cdot \Delta X_s + r_s + (1 - \epsilon)\, \xi A\big(X_s - X_g\big) \tag{2-17}$$

$$\epsilon \frac{\partial X_g}{\partial t} = -\vec{v} \cdot \nabla X_g + \epsilon \, \lambda_g \cdot \Delta X_g + r_g + (1 - \epsilon)\, \xi A\big(X_s - X_g\big) \tag{2-18}$$

Here, ϵ represents the porosity of the product. Compared to the one-phase model balances, an extra term is added to these equations, which represent the interaction between the solid and the moving phase. The contact surface between the two phases is given by A. The parameter ξ represents the transfer coefficient between the solid and the moving gas phase. For heat or mass transfer, this parameter is replaced by respectively the heat transfer coefficient or the mass transfer coefficient.

2.2.5   Models found in literature

In the past decades, quite some modelling work on storage facilities for agricultural products has been performed. Transport, heat and moisture production are important phenomena in storage facilities. Therefore, these phenomena are taken into account in most models. Some models also include a controller for controlling the climate in storage facility. Since airflow through bulk storage of agricultural products can be represented by airflow through porous media, most models are based on equations which describe transport through porous media. For this reason, models that describe phenomena in other fields of application, but which are also strongly related to transport through porous media, can be interesting as well.

Recently, Grubben (2013) performed a literature review on modelling of storage facilities. In this review, an extended model classification with respect to modelling of storage facilities was presented. The model structure, the involved physics, the states included in the model and the dimensions (1,2 or 3D) of each model was described. Furthermore, the models which may be interesting for further research were separated from the rest of the models. For these models, the aim of each model, and the underlying modes and assumptions were described. Since this review covers many aspects and presents an up to date overview of all models related to storage facilities for agricultural products, in this research no additional literature review on existing models is performed.

2.2.6   Additions to previous models

Grubben (2014) performed simulations of potato storage facilities. These simulations were a simplification of the real situation, since only the air channel, the bulk and the air space above the bulk are simulated. Also, frequently used equipment in potato storage facilities, as a fan, humidifier and a mechanical cooling unit were not taken into account. Therefore the applications of these simulations are limited, since for example the effect of the above mentioned equipment cannot be simulated using this model. In order to simulate a complete advanced storage facility, the remaining parts should be modelled as well. Figure 2-3 shows an advanced storage facility including the related equipment. The blue (dark coloured) elements of this storage facility were already modelled by Grubben (2014). The remaining parts and the advanced devices are modelled in this research.
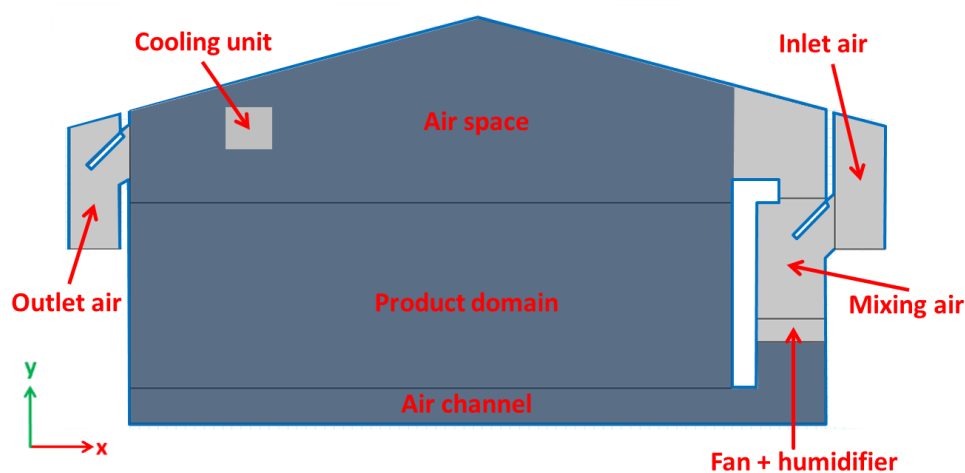

Figure 2-3. Overview of an advanced storage facility. The blue elements (dark coloured) was already modelled in the work of Grubben (2014). The remaining parts are included in this study taken into account as well.

14

2.2.6.1 System fan and humidifier

System fans are used to ventilate the storage facility. A picture of a system fan is presented in Figure 2-4. The capacity of the individual fans and the number of fans placed in a storage facility determines the maximum pressure drop over the fan and consequently the maximum feasible airflow through the bulk. The relation between the dynamic and static pressure created by the fan depends on the positioning and the number of blades of the fan.

Figure 2-4. System fan

A picture of a humidifier used in potato storages in presented in Figure 2-5. A humidifier can be placed directly after the fan in order to humidify the air before it enters the potato bulk. Since the humidity ratio of the ventilated air through the bulk is higher, moisture losses from the potatoes during the ventilation period will be limited. In the humidifier, the air flows through porous pads, which are continuously being saturated with water. Due to the evaporation of the water in the porous pads, the outgoing air contains more vapour compared to the ingoing air. The physical

Figure 2-5. Air humidifier

process in the humidifier is adiabatic, which means that the enthalpy of the air is not changed. Due to the evaporation of water and the adiabatic process, the temperature of the air will decrease. This is an extra advantage when ventilation is necessary for cooling purposes, because the temperature of the air at the inlet may be higher than the desired temperature for cooling. The cooling effect of a humidifier can be calculated using enthalpy expressions and the Magnus equation valid for temperatures below zero degree (Van't Ooster, 1999):

$$H_{fan} = C_{pa}T_{fan} + X_{fan}\big(C_{pw}\,T_{fan} + H_w\big)$$

$$H_{goal} = C_{pa}T_{goal} + X_{goal}\big(C_{pw}\,T_{goal} + H_w\big)$$

$$Ps_{goal} = 610.5 \cdot 10^{\frac{7.5*T_{goal}}{237.3+T_{goal}}} \qquad\qquad \text{for } T_{goal} > 0° C \qquad (2\text{-}19)$$

$$Xs_{goal} = 0.622\,\frac{Ps_{goal}}{P_{tot} - Ps_{goal}}$$

Here, H_{fan} and H_{goal} are respectively the enthalpy content of the air in the fan and of the desired air. C_{pa}, C_{pw} and H_w represents respectively the specific heat of dry air, the specific heat of vapour and the evaporation heat of water. Ps_{goal} and Xs_{goal} represents respectively the pressure and the water content of saturated air and P_{tot} represents the total air pressure.

15

The cooling effect is visualized in Figure 2-6 for a maximum desired air temperature in the bulk of 4 [$°C$] in case with and without humidifier for different fan temperatures and humidity ratios. In case of the humidifier, the humidity ratio of the outlet air is increased to 95%. The green area represents the feasible air conditions in the fan in order to reach the desired cooling temperature. Figure 2-6 shows that, in case of a humidifier, the fan temperature may be much higher than the desired cooling air temperature, especially for lower humidity ratios.
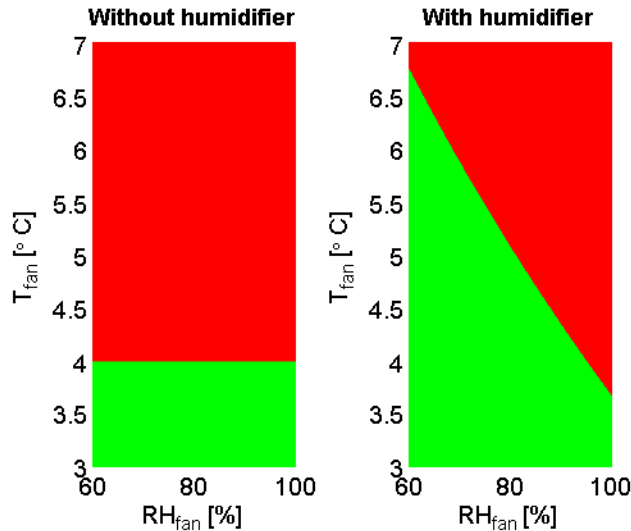
Figure 2-6. Effect of humidifier compared to situation without humidifier. The green area represents the conditions in which the desired cooling temperature of 4 $°C$ can be reached. Due to the cooling effect of the humdifier, the air temperature in the fan (just before the inlet of the humidifier) can be much higher than 4 $°C$, especially for low humidity ratios.

2.2.6.2 Cooling unit

The cooling unit consist out of several parts, namely a compressor, condenser and evaporator. The evaporator is placed in the storage facility and consequently directly influences the air conditions. In Figure 2-7, a picture of an evaporator which is placed above the potato bulk is presented. In the evaporator, the air flows along cold evaporation plates (with temperature T_c) and therefore, the air is cooling down. The air close to the evaporation plates is assumed to be saturated. The absolute water content on the cooling surfaces can be calculated using the Magnus equation (saturated vapour pressure) and Daltons law (absolute saturated water content):

Figure 2-7. Evaporator

$$P_s = 610.5 \cdot 10^{\left(\frac{9.5\,T_c}{265.5 + T_c}\right)} \qquad \text{for } T_c < 0° \, C$$

$$X_s = \frac{M_w}{M_{da}} \frac{P_s}{P_{tot} - P_s}$$

(2-20)

16

Here, P_s $[Pa]$, is the saturated vapour pressure, T_c $[°C]$ is the temperature of the evaporation surfaces, x_s $[kg/kg]$ is the absolute water content at saturation, M_w and M_{da} are respectively the molecular mass of water and dry air (respectively 18.01 $[kg/kmol]$ and 28.96 $[kg/kmol]$) and P_{tot} $[Pa]$ is the air pressure.

Knowing the airflow and the capacity of an evaporator, the enthalpy decrease per kilogram air $[kJ/kg]$ can be calculated by:

$$\Delta H_{cooling} = \frac{P_{evap}}{\phi_{fan\ evap} \cdot \rho_a} \tag{2-21}$$

Here, P_{evap} $[kW]$ is the capacity of the evaporator, $\phi_{fan\ evap}$ $[m^3/s]$ is the airflow along the cooling plates of the evaporator and ρ_a $[kg/m^3]$ is the density of the air.

Next, the enthalpy difference between the flowing air along the evaporation plates and the cooling surfaces can be calculated by:

$$\Delta H_{tot} = C_{pa}\ (T_{in} - T_c) + H_{v,0}\ (X_{in} - X_c) + C_{pw}\ (X_{in}T_{in} - X_cT_c) \tag{2-22}$$

Here, ΔH_{tot} $[kJ/kg]$ is the enthalpy difference between the conditions of the airflow at the inlet of the evaporator and the conditions at the cooling surfaces and C_{pa} and C_{pw} $[kJ/(kg\ K)]$ are respectively the specific heat of dry air and vapour.

Finally, the conditions of the airflow at the outlet of the evaporator (T_{out} and X_{out}) can be calculated by the conditions of the air at the inlet and on the cooling surfaces and the ratio between the total enthalpy difference (ΔH_{tot}) and the enthalpy decrease caused by the cooling process ($\Delta H_{cooling}$):

$$R_{enth} = \frac{\Delta H_{cooling}}{\Delta H_{tot}}$$

$$T_{out} = T_{in} - (T_{in} - T_c) \cdot R_{enth} \tag{2-23}$$

$$X_{out} = X_{in} - (X_{in} - X_c) \cdot R_{enth}$$

Calculations on the cooling process are performed and the results are visualized in a Mollier diagram, see Appendix A.

2.3 Air resistance in bulk storage

As stated in section 2.2.4, fluid flow through bulk storage can be represented by a flow through a porous medium in which the product represents the solid particles. Since the air movement is partly obstructed by these solid particles, a pressure drop over the bulk is created. The resistance factor of the product and the corresponding pressure drop depends on several factors:

- Size of the product
- Shape of the product
- Porosity of the bulk
- Path length of air movement through bulk

In literature, several expressions are found to approximate the pressure drop of a fluid flow in a porous media. Furthermore, specific research of airflow resistance through bulk potato is found. These findings are presented in the next subsections.

2.3.1   Resistance of fluid flow through porous media

A very general and widely used approximation of the pressure drop over a porous medium is Darcy's law. This law was derived by Henry Darcy based on experiments (Darcy, 1856). However, this law which is analogous to Fourier's law, Ohm's law and Fick's law, is mathematical derived from the Navier Stokes equations via homogenization (Whitaker, 1986). This law is given in equation (2-24), in which q represents the flux [m/s], κ represents the intrinsic permeability [m^2], μ represents the viscosity [Pa·s] and ∇p represents the pressure gradient vector [Pa/m].

$$q = -\frac{\kappa}{\mu} \nabla p \qquad (2\text{-}24)$$

Darcy's law is only valid for laminar, viscous fluid flow through porous media, since inertial forces by the kinetic energy of the fluid are neglected (Sen, 1995) . For non-viscous fluid flow, especially in the turbulent domain, inertial forces have a dominant effect. Forchheimer (1901) included an inertial term representing the kinetic energy of the fluid to Darcy's law. The Darcy-Forchheimer law is presented in equation (2-25).

$$\nabla p = -\frac{\mu}{\kappa} v_i - \beta \, \rho_a \bar{v} \, v_i \qquad (2\text{-}25)$$

Ergun (1952) determined an expression for the Forchheimer resistance coefficient β in the field of fluid flow through packed columns and fluidized beds as shown in equation (2-26). In this equation C_E represents the Ergun coefficient, which is strongly dependent on the flow regime.

$$\beta = \frac{C_E}{\sqrt{\kappa}} \qquad (2\text{-}26)$$

Hence, the equations (2-27), (2-28) and (2-29) describe the resistance of fluid flow through a porous media.

2.3.2 Airflow resistance in potato bulk storage

For airflow resistance in bulk potato storage, Chourasia and Goswami (2007) derived the following expressions for the intrinsic permeability (κ) and the Forchheimer resistance coefficient β:

$$\kappa = \frac{d_p^2 \, \epsilon_a^3}{150 \, \epsilon_p^2} \tag{2-27}$$

$$\beta = \frac{1.75 \, \epsilon_p}{d_p \, \epsilon_a^3} \tag{2-28}$$

Also, more empirical relations between the airflow rate and the pressure drop over the bulk were found. In the ASAE Standards (1997), the following expression based on measured data is found:

$$\frac{\Delta P}{l} = \frac{aQ^2}{\ln(1 + bQ)} \tag{2-29}$$

In this expression, Q represents the airflow rate [m^3/m^2/s], $\frac{\Delta P}{l}$ represents the pressure drop per length [Pa/m]. The constants a and b are empirically determined on respectively $2.18 \cdot 10^3$ and 824. This relation is valid in the range $0.030 \leq Q \leq 0.300$.

Also Rastovski et al. (1985), Irvine et al. (1993) and Huijsmans (1985) found empirical relations which can be described by the expression in equation (2-30).

$$\frac{\Delta P}{l} = K \cdot Q^B \tag{2-30}$$

In these researches, the values for K and B vary in the range of respectively $237 \leq K \leq 1676$ and $1.65 \leq B \leq 1.90$, depending on the potato variety, dimensions of the potatoes, the amount of sprouted potatoes and the soil content in the bulk.

In this study, the Forchheimer resistance is used for modelling the airflow resistance through a potato bulk. For the intrinsic permeability and the Forheimer resistance coefficient, the expressions derived by Chourasia and Goswami (2007) are used (section 3.2.2.4). Furthermore, an extension on the Forchheimer resistance is derived in order to estimate the airflow resistance in soiled potato bulks as well (section 3.5).

3   Dynamic simulation of potato bulk storage facilities

In a recent study, Grubben (2014) presented the equations which cover all physics involved in storage facilities. Also CFD-simulations of the product and the air were performed and presented. These simulations were validated with measurements. For these reasons, the study of Grubben (2014) is used as a starting point for the simulations of an advanced storage facility in this study.

Simulations were performed using the simulation software package COMSOL Multiphysics 4.4. This software package is based on the Finite Elements Methods (FEM). First, the configuration of the system is defined. COMSOL provides two ways of implementing the physics, using predefined interfaces or using the mathematical environment. Grubben (2014) investigated both methods and performed simulations using the predefined interfaces for fluid flow and the mathematical environment to define the temperature and moisture balances. Similarly, both methods are used in this research to implement all physics.

In this chapter, first the model assumptions are presented. Next, an overview of 2D bulk simulation of a potato storage facility is given in section 3.2. In this overview, the topology of system, the physics in form of PDE's and all domains with their boundaries are described. Besides dynamic 2D simulation of bulk storage facilities, also 3D simulations of dynamic bulk storage facilities are performed. The setup for 3D simulation is described in section 3.3. For 2D and 3D simulations, stabilization methods are necessary in order to obtain stable solutions. The implementation of stabilization methods is described in section 3.3. Furthermore, airflow resistance through soiled potatoes is further investigated and described in section 3.5.

3.1 Model assumptions
The following assumptions are made with respect to the model:
- Steady state region of storage period
  > *This means that no drying and wound healing of the potatoes are taken into account and the parameter values related to the potatoes are fixed.*
- Uniform distribution of uniform spherical potatoes
  > *Uniform distribution of uniform shaped potatoes makes that processes in the bulk are only temperature and moisture content dependent.*
- No difference in diffusion between interior of potato and potato skin
  > *A nominal diffusion rate at the skin of the potato is taken.*
- The individual potatoes are completely surrounded by air
  > *Since the contact surfaces between the potatoes is very small, interaction process between potatoes (conduction) is minimal and therefore neglected.*
- No condensation
  > *Condensation on the product or on surfaces of the storage facility is neglected, since the drying process is not taken into account and temperature and humidity changes in time are relatively small.*

21

3.2 Dynamic 2D bulk simulation

In this section, first the geometry of the 2D setup will be presented. Next, the physics and boundary conditions related to all domains are described.

3.2.1 Geometry

The 2D-geometry for the performed simulations is visualized in Figure 3-1.
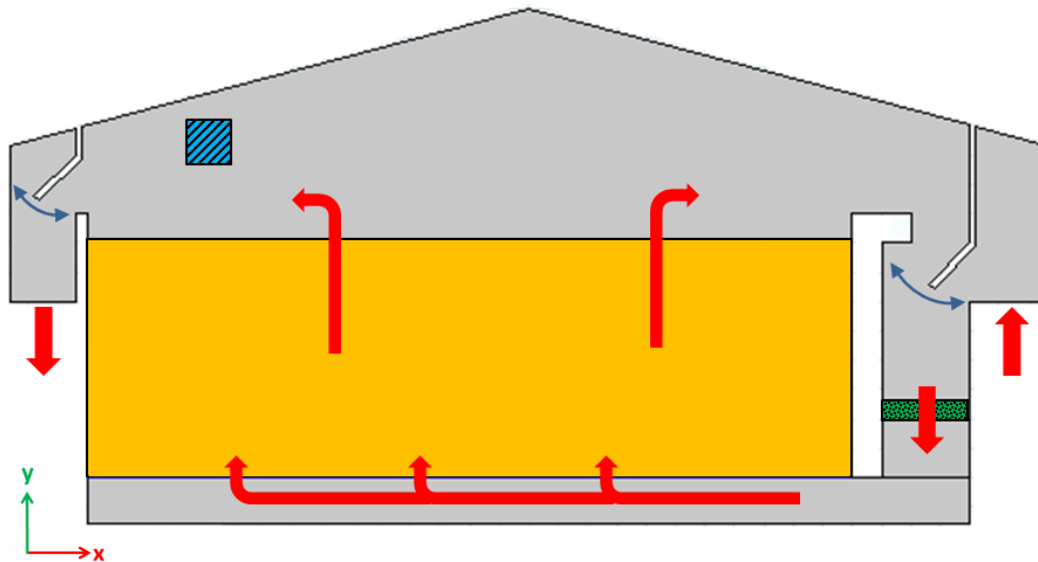
Figure 3-1. Schematic representation of the storage facility. The red arrows indicates the airflow through the facility. The blue arrows indicate the moving panels. The bulk, fan and cooling unit are represented by respectively the yellow, green (dottted) and blue (dashed) box.

The red arrows indicate the airflow through the storage facility. The air enters the facility on the right hand side of the facility. Next, the air is pressed into the air channel by the fan (represented by the green dotted box) and flows through the potato bulk (represented by the yellow box). After passing the potato bulk, the air can either leave the storage facility on the left hand side or the air is recirculated towards the fan. The amount of internal ventilation of the air is controlled by an inlet and outlet panel, which can be opened or closed (indicated by the blue arrows). Finally, a cooling unit is placed close to the ceiling in order to simulate the effect of mechanical cooling (represented by the blue dashed box).

An overview of all dimension of the simulated storage facility is presented in Table 3-1.

Table 3-1. Overview of dimensions 2D configuration

	Size	
	x	y
Total facility [1]	$21.1\ [m]$	$6.8\ [m]$
Bulk	$16.5\ [m]$	$4.0\ [m]$
Air channels	$17.0\ [m]$	$0.8\ [m]$
Fan	$1.5\ [m]$	$0.5\ [m]$

1. Maximum dimensions of the facility

Moving parts

As indicated in Figure 3-2, the inlet and outlet panels can be opened or closed by changing the angle α, which, in what follows, is considered as a control input variable. In order to simulate a real situation under feedback control, it should be possible to change the position of the panels during a time dependent simulation. However, changing the geometry within a time-dependent simulation causes changes in the mesh of the geometry. This not very well implemented in COMSOL and therefore, finding a solution is not straightforward.
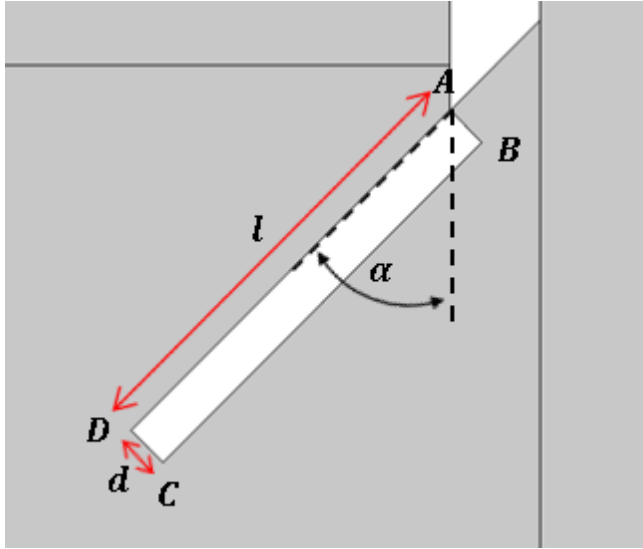
Figure 3-2. Overview of moving panel. The panel can be rotated by changing the angle α.

First, a quasi-steady state approach was investigated in order to simulate changing panel positions. Time-dependent simulations were divided into a number of discrete simulation steps. The opening angles α were changed in between the steps, but fixed during the simulation time of one step. Final results of the previous step (with initial opening angle α) were taken as initial conditions of the next step (with adapted opening angle α). A disadvantage of this approach is that some dynamics, due to the step-wise movement of the panels, are disregarded. A more practical problem was discovered by implementing this method for simulations in which the position of the panels changes more frequently. All steps have to be defined manually, which result in a very time consuming activity.

To solve these problems, another method was used to include the movements of the panels directly in a time dependent simulation. This was done using the 'Moving Mesh' interface of COMSOL. By this interface, forces and/or velocities can be applied on boundaries of the geometry, which results in a deformed mesh. In order to simulate the movement of the panels, velocities were defined on the line segments AB, BC, CD and DA, presented in Figure 3-2.

When the rotation point of the panel (A) is defined as the origin with coordinates $(0,0)$, the movements of the points B, C and D are described by:

$$
\begin{bmatrix} \dot{B}_x & \dot{B}_y \\ \dot{C}_x & \dot{C}_y \\ \dot{D}_x & \dot{D}_y \end{bmatrix} = \begin{bmatrix} \cos(\dot{\alpha}) \cdot d & -\sin(\dot{\alpha}) \cdot d \\ -\sin(\dot{\alpha}) \cdot l + \cos(\dot{\alpha}) \cdot d & -\cos(\dot{\alpha}) \cdot l - \sin(\dot{\alpha}) \cdot d \\ -\sin(\dot{\alpha}) \cdot l & -\cos(\dot{\alpha}) \cdot l \end{bmatrix} \quad (3\text{-}1)
$$

The velocity on a point on the line segments of the moving panel depends on the distance between that point and a reference corner of the line segment. Point A is chosen as reference corner for the line segments AB and AD, point B is chosen as reference corner for line segment BC and point D is chosen as reference corner for line segment CD. This results in the following distances:

$$r_{AB} = r_{AD} = \sqrt{x^2 + y^2}$$

$$r_{BC} = \sqrt{(x - B_x)^2 + (y - B_y)^2} = \sqrt{(x - \cos(\alpha) \cdot d)^2 + (y + \sin(\alpha) \cdot d\ )^2} \quad (3\text{-}2)$$

$$r_{CD} = \sqrt{(x - D_x)^2 + (y - D_y)^2} = \sqrt{(x + \sin(\alpha) \cdot l)^2 + (y\ + \cos(\alpha) \cdot l)^2}$$

in which $[x\ y]$ represents the coordinates of a specific point on the corresponding line segment. Using the velocities in the points A, B, C and D and the distances between a point on a line segment and their corresponding reference corner, the following velocities on the line segments are derived:

$$\begin{bmatrix} v_{AB_x} & v_{AB_y} \\ v_{AD_x} & v_{AD_y} \\ v_{BC_x} & v_{BC_y} \\ v_{CD_x} & v_{CD_y} \end{bmatrix} = \begin{bmatrix} \dot{B}_x \cdot \dfrac{r_{AB}}{d} & \dot{B}_y \cdot \dfrac{r_{AB}}{d} \\ \dot{D}_x \cdot \dfrac{r_{AD}}{d} & \dot{D}_y \cdot \dfrac{r_{AD}}{d} \\ \dot{B}_x - \sin(\dot{\alpha}) \cdot r_{BC} & \dot{B}_y - \cos(\dot{\alpha}) \cdot r_{BC} \\ \dot{D}_x + \cos(\dot{\alpha}) \cdot r_{CD} & \dot{D}_y - \sin(\dot{\alpha}) \cdot r_{CD} \end{bmatrix} \quad (3\text{-}3)$$

Applying these velocities on the corresponding line segments of the panels and defining a time dependent opening angle α, the positions of the panels will change within a time dependent simulation. However, this is only possible if the panels do not touch one of the walls of the facility. This is the case if the panels are completely closed (point C touch the wall) or if the panels are completely opened (point D touch the wall). Therefore, position change of the panels is only feasible for opening angles in the range of $0^o < \alpha < 90^o$ and not for 0° or 90° itself. Panel positions of 0° and 90° are approximate by panel positions nearby 0° and 90°, which causes small unwanted flows through the (fully opened or closed) panels. To avoid these flows, boundary conditions are defined, see section 3.2.3.4.

3.2.2 Physics

In order to simulate the system, the configuration as presented in Figure 3-1 is divided into several domains. These domains are visualised in Figure 3-3. For each domain, a set of PDE's is defined, which covers the air flow and the temperature and moisture balances. The blue dahsed lines in Figure 3-3 indicate zero flux boundary conditions, see also subsection 3.2.3.1. For the air domains ($\Omega_{a1} - \Omega_{a7}$), the predefined 'Turbulent Flow ($\kappa - \epsilon$)' interface is used for simulating the airflow. The area in which the potatoes are stored (Ω_p) is considered as porous media. For this domain, the predefined 'Brinkman Equation' interface is used.
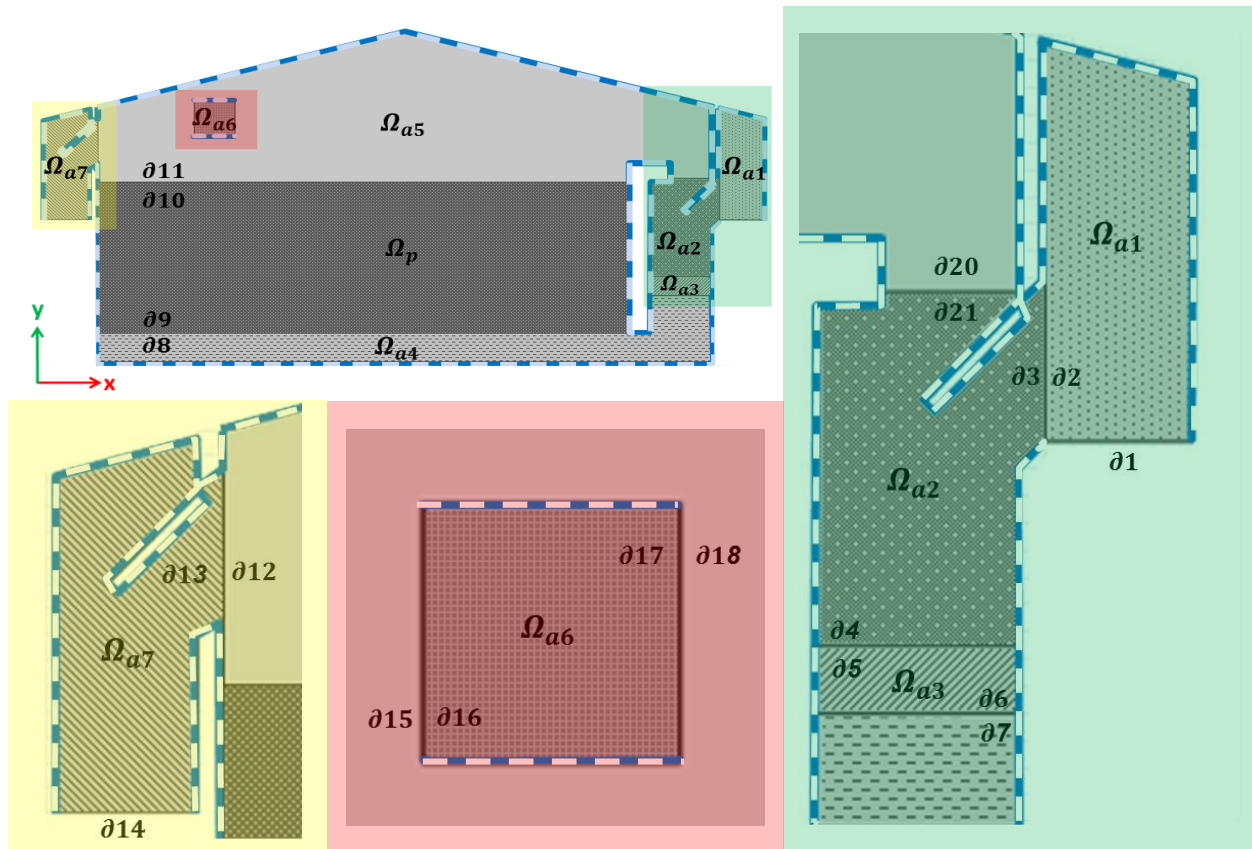
Figure 3-3. Overview of the configuration, divided into seven air domains (Ω_{a1-a7}) and one porous domain (Ω_p). Boundaries of the domains presented by blue dashed lines are considered as zero-flux boundaries. The remaining boundaries are indicated by $\partial 1 - \partial 21$.

Grubben (2014) presented partial differential equations that describe all physics related to airflow, temperature and moisture content in the air and the porous domains. These PDE's were used to perform simulations of the total storage facility and are presented below. States related to air in the air domains are denoted with subscript 'a_i', in which $i := (1,2 ...,7)$. States related to air in the porous domain are denoted with 'ap' and states related to the potato in the porous domain are denoted with 'pp'. All model parameters were taken from Grubben (2014). In this study, new domains are introduces, which causes changes in boundary conditions compared to Grubben (2014) and additional PDE's for the new domains.

First, the general partial differential equations for describing the airflow, temperature and moisture content are given for the air domains. In Ω_{a3}, an extra volume force is applied in the partial differential equations to simulate the effect of a fan. Also in the cooling unit,

some extra terms are included to simulate the effect of the cooling unit. These additions to the general partial differential equations are given and explained. Finally, the partial differential equations related to the porous domain is presented.

3.2.2.1 Air domains

In this section, the continuity and momentum equations of the air domains (excluding the fan domain Ω_{a3}, which is described in the next subsection) are given. These equations, which describe the airflow at each point in the air domains over a time $t \, \epsilon \, [0,T]$, are defined as:

$$\frac{\partial \rho_a}{\partial t} + \nabla(\rho_a \, v) \; = \; 0 \qquad\qquad \text{in } (0,T] \text{ x } \Omega_{a1,a2,a4-a7}$$

$$\rho_a \frac{\partial v_x}{\partial t} + \; \rho_a (v \cdot \nabla) v_x - \nabla \cdot \tau_x \; = \; -\frac{\partial P}{\partial x} \qquad\qquad \text{in } (0,T] \text{ x } \Omega_{a1,a2,a4-a7} \qquad (3\text{-}4)$$

$$\rho_a \frac{\partial v_y}{\partial t} + \; \rho_a (v \cdot \nabla) v_y - \nabla \cdot \tau_y \; = \; -\frac{\partial P}{\partial y} - \rho_a g \qquad\qquad \text{in } (0,T] \text{ x } \Omega_{a1,a2,a4-a7}$$

Here, τ_x and τ_y represent respectively the x and y components of the stress tensor τ. This stress tensor is the deviatoric stress component of the Cauchy stress tensor, which is defined as:

$$\tau = \left[(\nabla v + \nabla v^T) - \frac{2}{3}(\nabla \cdot v)I \right]$$

$$\nabla \cdot \tau_x = \frac{\partial}{\partial x} \, \mu \left(2\frac{\partial v_x}{\partial x} - \frac{2}{3}(\nabla \cdot v) \right) + \frac{\partial}{\partial y} \, \mu \left(\frac{\partial v_x}{\partial y} + \frac{\partial v_y}{\partial x} \right) \qquad (3\text{-}5)$$

$$\nabla \cdot \tau_y = \frac{\partial}{\partial x} \, \mu \left(\frac{\partial v_y}{\partial x} + \frac{\partial v_x}{\partial y} \right) + \frac{\partial}{\partial y} \, \mu \left(2\frac{\partial v_y}{\partial y} - \frac{2}{3}(\nabla \cdot v) \right)$$

Here, I is defined as the unit tensor and μ represents the material dependent dynamic viscosity.

The corresponding temperature and moisture balances for the air domains (excluding the cooling unit domain Ω_{a6}, which is described in section 3.2.2.3) are defined as:

$$\frac{\partial T_a}{\partial t} + v \cdot \nabla T_a - \nabla \left(\frac{\lambda_a}{(\rho_a C_{pa}} \, \nabla T_a \right) \; = \; 0 \qquad\qquad \text{in } (0,T] \text{ x } \Omega_{a1-a5,a7}$$

$$\frac{\partial X_a}{\partial t} + v \cdot \nabla X_a - \nabla(\, \mathbb{D}_a \nabla X_a) \; = \; 0 \qquad\qquad \text{in } (0,T] \text{ x } \Omega_{a1-a5,a7} \qquad (3\text{-}6)$$

3.2.2.2 Fan domain

As mentioned before, an extra volume force is added in Ω_{a3} to simulate the pressure drop created by the fan. This pressure drop is defined as:

$$\Delta P_{fan} = \overline{P_{out}} - \overline{P_{in}} \tag{3-7}$$

Here, $\overline{P_{out}}$ and $\overline{P_{in}}$ are respectively the average pressure on the outlet and the inlet of the fan. This pressure drop is added to the momentum equation in y-direction as source term, which result in the following continuity and momentum equations:

$$\frac{\partial \rho_a}{\partial t} + \nabla(\rho_a\, v) = 0 \qquad\qquad \text{in } (0, T] \text{ x } \Omega_{a3}$$

$$\rho_a \frac{\partial v_x}{\partial t} + \rho_a(v \cdot \nabla)v_x - \nabla \cdot \tau_x = -\frac{\partial P}{\partial x} - \Delta P_{fan} \qquad \text{in } (0, T] \text{ x } \Omega_{a3} \quad (3\text{-}8)$$

$$\rho_a \frac{\partial v_y}{\partial t} + \rho_a(v \cdot \nabla)v_y - \nabla \cdot \tau_y = -\frac{\partial P}{\partial y} - \rho_a g - \Delta P_{fan} \qquad \text{in } (0, T] \text{ x } \Omega_{a3}$$

3.2.2.3 Cooling unit domain

Specifications of a commonly applied cooling unit in agricultural storages are used in the simulations. The effect of the evaporator (Helpmann 26-7 230) on the air conditions is simulated. The specifications of this evaporator are given in Appendix B.

According to the specifications of the evaporator, the temperature of the cooling plates (T_c) is $7°\,C$ lower than the air temperature at the inlet of the evaporator. Furthermore, it is assumed that air at the cooling surfaces is saturated, so a relative humidity of 100%. Using the equations presented in section 2.2.6.2, the cooling effect on the air conditions can be calculated.

To simulate these effects, the partial differential equations related to temperature and water content of the air are split up in x and y direction. In the direction of the airflow through the cooling unit (x direction), source terms are added resulting in a decrease of the temperature and water content in this direction.

$$\frac{\partial T_{a_x}}{\partial t} + v_x \cdot \nabla T_{a_x} - \nabla\left(\frac{\lambda_a}{(\rho_a C_{pa}}\, \nabla T_{a_x}\right) = \frac{v_x \cdot \left(T_{a_x} - T_{a_{in}}\right)}{l} \qquad \text{in } (0, T] \text{ x } \Omega_{a6}$$

$$\frac{\partial T_{a_y}}{\partial t} + v_y \cdot \nabla T_{a_y} - \nabla\left(\frac{\lambda_a}{(\rho_a C_{pa}}\, \nabla T_{a_y}\right) = 0$$

$$\qquad\qquad\qquad (3\text{-}9)$$

$$\frac{\partial X_{a_x}}{\partial t} + v_x \cdot \nabla X_{a_x} - \nabla\left(\mathbb{D}_a \nabla X_{a_x}\right) = \frac{v_x \cdot \left(X_{a_x} - X_{a_{in}}\right)}{l} \qquad \text{in } (0, T] \text{ x } \Omega_{a6}$$

$$\frac{\partial X_{a_y}}{\partial t} + v_y \cdot \nabla X_{a_y} - \nabla\left(\mathbb{D}_a \nabla X_{a_y}\right) = 0$$

3.2.2.4 Porous domain

The continuity and momentum equations related to the porous domain are presented in (3-10). These are almost similar to the equations related to the air domains, presented in (3-4). The main difference in the balances related to the porous domain is that a source term is added. For the continuity equation, this source term represents the increase in air density due to the evaporation process in the bulk. In the momentum equations, the extra terms represent the Forchheimer resistance in the bulk (F) and, in y-direction, the gravity force.

$$\frac{\partial \rho_a}{\partial t} + \frac{1}{\epsilon_a} \nabla(\rho_a\, v) \;=\; K_{evap} \frac{F_m}{\epsilon_a} \left(X_s - X_{ap}\right) \qquad \text{in } (0,T] \text{ x } \Omega_p$$

$$\rho_a \frac{\partial v_x}{\partial t} + \rho_a(v \cdot \nabla)v_x - \nabla \cdot \tau_x \;=\; -\frac{\partial P}{\partial x} - F \qquad \text{in } (0,T] \text{ x } \Omega_p \quad \text{(3-10)}$$

$$\rho_a \frac{\partial v_y}{\partial t} + \rho_a(v \cdot \nabla)v_y - \nabla \cdot \tau_y \;=\; -\frac{\partial P}{\partial y} - F - \rho_a g \qquad \text{in } (0,T] \text{ x } \Omega_p$$

The corresponding air temperature and moisture content of the air in the porous domain can be described by:

$$\frac{\partial T_{ap}}{\partial t} + \frac{1}{\epsilon_a} v \cdot \nabla T_{ap} - \nabla\left(\frac{\lambda_a}{(\rho_a C_{pa}} \nabla T_{ap}\right) = \frac{\alpha_C F_m}{(\rho_a C_{pa}\epsilon_a)} \left(T_{pp} - T_{ap}\right) \qquad \text{in } (0,T] \text{ x } \Omega_p$$

$$\text{(3-11)}$$

$$\frac{\partial X_{ap}}{\partial t} + \frac{1}{\epsilon_a} v \cdot \nabla X_{ap} - \nabla\left(\mathbb{D}_a \nabla X_{ap}\right) \;=\; K_{evap} \frac{F_m}{\rho_a \epsilon_a} \left(X_s - X_{ap}\right) \qquad \text{in } (0,T] \text{ x } \Omega_p$$

The potatoes in the storage facility are represented by the solid fraction of the porous media. Temperature and moisture content of the potatoes are described by:

$$\frac{\partial T_{pp}}{\partial t} - \nabla\left(\frac{\lambda_p}{(\rho_p C_{pp}} \nabla T_{pp}\right) = -\frac{\alpha_C F_m}{\left(\rho_p C_{pp}\epsilon_p\right)} \left(T_{pp} - T_{ap}\right) + \frac{R}{C_{pp}\epsilon_p} - h_{fg} K_{evap} \frac{F_m}{\rho_p C_{pp}\epsilon_p} \left(X_s - X_{ap}\right) \qquad \text{in } (0,T] \text{ x } \Omega_p$$

$$\frac{\partial X_{pp}}{\partial t} - \nabla\left(\mathbb{D}_p \nabla X_{pp}\right) \;=\; -E_{resp} \frac{R}{\epsilon_p} - K_{evap} \frac{F_m}{\rho_p \epsilon_a} \left(X_s - X_{ap}\right) \qquad \text{in } (0,T] \text{ x } \Omega_p$$

$$\text{(3-12)}$$

3.2.3   Boundary conditions

In order to simulate a total storage facility, all adjacent domains has to be coupled to each other. This is done by defining the boundary conditions for pressure, velocity, temperature and moisture content of the domains. In this section, the following groups of boundary conditions are described:

- Zero flux boundary conditions
- Open boundary conditions
- Dirichlet boundary conditions (related to coupling domains)
- Switching boundary conditions (related to the moving panels)
- Dirichlet and Neumann boundary conditions related to fan and cooling unit domain

3.2.3.1 Zero flux boundary conditions

All boundaries visualized in Figure 3-3 with a blue dashed line (∂s) are considered as zero-flux boundaries. This means that no exchange of pressure, velocity, temperature and moisture content will occur. These boundary conditions (except for the boundaries on the roof of the storage facility) can be mathematically described by:

$$\frac{\partial T_a}{\partial n} = \frac{\partial T_{ap}}{\partial n} = \frac{\partial T_{pp}}{\partial n} = 0 \qquad \text{on } (0,T] \text{ x } \partial s$$

$$\frac{\partial X_a}{\partial n} = \frac{\partial X_{ap}}{\partial n} = \frac{\partial X_{pp}}{\partial n} = 0 \qquad \text{on } (0,T] \text{ x } \partial s \qquad (3\text{-}13)$$

$$v^T\, n = 0 \qquad \text{on } (0,T] \text{ x } \partial s$$

$$(-PI + \tau)^T\, n = 0 \qquad \text{on } (0,T] \text{ x } \partial s$$

Here, $v := [v_x\ v_y]$ and n represents the direction perpendicular on the related boundary condition.

Since the orientation of the boundaries on the roof is not similar to the coordinate frame, the zero flux boundary conditions of the roof are described by:

$$\sin(\alpha_{roof}) \, \frac{\partial T_{aa}}{\partial x} \; = \; 0 \qquad \text{on } (0, T] \, \text{x} \, \partial_{roof}$$

$$\cos(\alpha_{roof}) \, \frac{\partial T_{aa}}{\partial y} \; = \; 0 \qquad \text{on } (0, T] \, \text{x} \, \partial_{roof}$$

$$\sin(\alpha_{roof}) \frac{\partial X_{aa}}{\partial x} \; = \; 0 \qquad \text{on } (0, T] \, \text{x} \, \partial_{roof}$$

$$\cos(\alpha_{roof}) \frac{\partial X_{aa}}{\partial y} \; = \; 0$$

(3-14)

$$\sin(\alpha_{roof}) \, v_x^{\ T} \; = \; 0 \qquad \text{on } (0, T] \, \text{x} \, \partial_{roof}$$

$$\cos(\alpha_{roof}) \, v_y^{\ T} \; = \; 0 \qquad \text{on } (0, T] \, \text{x} \, \partial_{roof}$$

$$\sin(\alpha_{roof}) \, (-PI + \tau_x)^T \; = \; 0 \qquad \text{on } (0, T] \, \text{x} \, \partial_{roof}$$

$$\cos(\alpha_{roof}) \, \left(-PI + \tau_y\right)^T \; = \; 0 \qquad \text{on } (0, T] \, \text{x} \, \partial_{roof}$$

Here, α_{roof} equals to $12°$ represents the inclination angle of the roof.

Besides the zero flux boundary conditions mentioned in (2-12), some boundaries related to temperature and moisture content are also defined as zero flux boundary conditions:

$$\frac{\partial T_a}{\partial n} = 0 \qquad \text{on } (0,T] \times \partial s^*$$

$$\frac{\partial T_{ap}}{\partial n} = 0 \qquad \text{on } (0,T] \times \partial 10$$

$$\frac{\partial T_{pp}}{\partial n} = 0 \qquad \text{on } (0,T] \times \partial 9, \partial 10$$

$$(3\text{-}15)$$

$$\frac{\partial X_a}{\partial n} = 0 \qquad \text{on } (0,T] \times \partial s^*$$

$$\frac{\partial X_{ap}}{\partial n} = 0 \qquad \text{on } (0,T] \times \partial 10$$

$$\frac{\partial X_{pp}}{\partial n} = 0 \qquad \text{on } (0,T] \times \partial 9, \partial 10$$

Here $\partial s^* \coloneqq \partial 2, \partial 4, \partial 6, \partial 8, \partial 10, \partial 12, \partial 15, \partial 17, \partial 20$ and n represents the direction perpendicular on the related boundary condition.

3.2.3.2 Open boundary conditions

Boundaries $\partial 1$ and $\partial 14$ are connected to the environment. Open boundaries conditions, which means that the normal stress component over these boundaries are equal zero, are used to describe the airflow on these boundaries. Temperature and moisture content on the inlet side of the facility depends on the outdoor conditions. The mathematical expressions for these boundary conditions are:

$$(-PI + \tau)^T n = 0 \qquad \text{on } [0,T] \times \partial 1, \partial 14$$

$$T_{a1} = T_{in} \qquad \text{on } [0,T] \times \partial 1 \qquad (3\text{-}16)$$

$$X_{a1} = X_{in} \qquad \text{on } [0,T] \times \partial 1$$

3.2.3.3 Dirichlet boundary conditions for coupling domains
In order to couple the domains to each other, the following boundary conditions are applied:

$$P_{\Omega i} = P_{\Omega j} \qquad \text{on } (0,T] \times \partial(k)$$

$$\tau^T n = 0 \qquad \text{on } (0,T] \times \partial(k)$$

$$v_{\Omega j} = v_{\Omega i} \qquad \text{on } (0,T] \times \partial(l)$$

$$i = [a1, a4, p, a5, a5]$$

$$j = [a2, p, a5, a7, a2]$$

$$k = [2, 8, 10, 12, 20]$$

$$l = [3, 9, 11, 13, 21] \qquad\qquad\qquad (3\text{-}17)$$

$$T_a = T_{\Omega j} \qquad \text{on } (0,T] \times \partial(k)$$

$$X_{\Omega i} = X_{\Omega j} \qquad \text{on } (0,T] \times \partial(k)$$

$$i = [p, a5]$$

$$j = [4, ap]$$

$$k = [9, 11]$$

NOTE 1: In the coupling boundary conditions presented in 2-12, boundaries related to the domains Ω_{a3} and Ω_{a6} are not included. This is because these domains are considered to be ideally mixed resulting in different boundary conditions. For these boundary conditions, see section 3.2.3.5.

NOTE 2: In the coupling boundary conditions presented in 2-12, boundary conditions related to temperature and moisture content of the boundary pairs $\partial 2/\partial 3$, $\partial 12/\partial 13$ and $\partial 20/\partial 21$ are not included. This is related to the movement of the panels, which result in periodic boundary conditions. For these boundary conditions, see section 3.2.3.4.

3.2.3.4 Switching boundary conditions
As described in section 3.2.1, position changing of the panels are only feasible in the range of $0^o < \alpha < 90^o$. In order to simulate also the effect of fully opened and closed panels, switching boundary conditions for temperature and moisture content on the boundary pairs $\partial 2/\partial 3$, $\partial 12/\partial 13$ and $\partial 20/\partial 21$ are defined. These boundary conditions imply that there is no exchange of temperature and moisture content in case of fully closed panels ($\alpha = 0^o$) between Ω_{a1} and Ω_{a2} and between Ω_{a5} and Ω_{a7}. In case of fully opened panels ($\alpha = 90^o$), there is no exchange of temperature and moisture content between Ω_{a5} and Ω_{a6}.

To describe these switching boundary conditions mathematically, the total simulation time $t \in [0, T]$ is divided in the following time domains:

$$t_1 \in [T_{\angle\alpha 1}, T'_{\angle\alpha 1}] \qquad \text{for } \alpha > 1°$$

$$t_2 \in [T_{\angle\alpha 2}, T'_{\angle\alpha 2}] \qquad \text{for } \alpha < 1°$$

$$t_3 \in [T_{\angle\alpha 3}, T'_{\angle\alpha 3}] \qquad \text{for } \alpha < 89°$$

$$t_4 \in [T_{\angle\alpha 4}, T'_{\angle\alpha 4}] \qquad \text{for } \alpha > 89°$$

(3-18)

For (partly) opened panels, the following boundary conditions holds:

$$T_{a2} = T_{a1} \qquad \text{on } [T_{\angle\alpha 1}, T_{\angle\alpha 1}'] \times \partial 3$$

$$X_{a2} = X_{a1} \qquad \text{on } [T_{\angle\alpha 1}, T_{\angle\alpha 1}'] \times \partial 3$$

$$T_{a7} = T_{a5} \qquad \text{on } [T_{\angle\alpha 1}, T_{\angle\alpha 1}'] \times \partial 13$$

$$X_{a7} = X_{a5} \qquad \text{on } [T_{\angle\alpha 1}, T_{\angle\alpha 1}'] \times \partial 13$$

(3-19)

For completely closed panels, the boundary conditions mentioned in (3-19) change into zero flux boundaries:

$$\frac{\partial T_a}{\partial n} = 0 \qquad \text{on } [T_{\angle\alpha 2}, T_{\angle\alpha 2}'] \times \partial 3, \partial 13$$

$$\frac{\partial X_a}{\partial n} = 0 \qquad \text{on } [T_{\angle\alpha 2}, T_{\angle\alpha 2}'] \times \partial 3, \partial 13$$

(3-20)

For (partly) closed panels, the following boundary conditions holds:

$$T_{a2} = T_{a5} \qquad \text{on } [T_{\angle\alpha 3}, T_{\angle\alpha 3}'] \times \partial 21$$

$$X_{a2} = X_{a5} \qquad \text{on } [T_{\angle\alpha 3}, T_{\angle\alpha 3}'] \times \partial 21$$

(3-21)

For completely opened panels, the boundary conditions mentioned in (3-21) change into zero flux boundaries:

$$\frac{\partial T_a}{\partial n} = 0 \qquad \text{on } [T_{\angle\alpha 4}, T_{\angle\alpha 4}'] \times \partial 21$$

$$\frac{\partial X_a}{\partial n} = 0 \qquad \text{on } [T_{\angle\alpha 4}, T_{\angle\alpha 4}'] \times \partial 21$$

(3-22)

3.2.3.5 Boundary conditions related to fan and cooling unit

The domains Ω_{a3} and Ω_{a6} represent respectively the fan and the cooling unit. Both domains are considered as ideally mixed areas. Therefore, the air velocity, temperature and moisture content at the outlet are defined as the average of the air velocity, temperature and moisture content at the inlet of these domains. Furthermore, a pressure drop $\left(\Delta P_{fan}\right)$ is created over domain Ω_{a3} and an air velocity $\left(v_{evap}\right)$ is applied on domain Ω_{a6}.

The following boundary conditions are defined for the boundaries related to domain Ω_{a3}:

$$
\begin{aligned}
P_{\Omega a2} &= \overline{P_{\partial 7}} - \Delta P_{fan} && \text{on } (0,T] \text{ x } \partial 4 \\
P_{\Omega a3} &= P_{\Omega a2} && \text{on } (0,T] \text{ x } \partial 5 \\
\tau^T n &= 0 && \text{on } (0,T] \text{ x } \partial 4, \partial 5 \\
v_{\Omega a3} &= v_{\Omega a4} && \text{on } (0,T] \text{ x } \partial 6 \\
v_{\Omega a4} &= \overline{v_{\partial 4}} && \text{on } (0,T] \text{ x } \partial 7 \\
\\
T_{\Omega a3} &= T_{\Omega a2} && \text{on } (0,T] \text{ x } \partial 5 \\
T_{\Omega a4} &= \overline{T_{\partial 4}} && \text{on } (0,T] \text{ x } \partial 7 \\
X_{\Omega a3} &= X_{\Omega a2} && \text{on } (0,T] \text{ x } \partial 5 \\
X_{\Omega a4} &= \overline{X_{\partial 4}} && \text{on } (0,T] \text{ x } \partial 7
\end{aligned}
$$

(3-23)

Here, ΔP_{fan} is the user defined pressure drop over the fan and $\overline{U_{\Omega\iota-\partial J}}$ is the average value of state U in domain Ω_i on boundary ∂_j. Since the air in the fan is considered to be ideally mixed, both temperature and water content on the outlet of the fan ($\partial 7$) are defined as the average conditions of the air on the inlet of the fan.

The following boundary conditions are defined for the boundaries related to domain Ω_{a6}:

$$
\begin{aligned}
v_{\Omega 5} &= v_{evap} && \text{on } (0,T] \text{ x } \partial 15, \partial 16 \\
P_{\Omega 6} &= P_{\Omega 5} && \text{on } (0,T] \text{ x } \partial 15, \partial 16 \\
\tau^T n &= 0 && \text{on } (0,T] \text{ x } \partial 15, \partial 16 \\
\\
T_{\Omega 6} &= T_{\Omega 5} && \text{on } (0,T] \text{ x } \partial 16 \\
T_{\Omega 5} &= \overline{T_{\Omega 5}} && \text{on } (0,T] \text{ x } \partial 18 \\
X_{\Omega 6} &= X_{\Omega 5} && \text{on } (0,T] \text{ x } \partial 16 \\
X_{\Omega 5} &= \overline{X_{\Omega 5}} && \text{on } (0,T] \text{ x } \partial 18
\end{aligned}
$$

(3-24)

in which v_{evap} is the air velocity caused by the evaporator fans, which can be found in the specifications of the evaporator. Furthermore, it is assumed that the air is perfectly mixed, resulting in average temperature and water content of the air on $\partial 18$.

34

3.3 Dynamic 3D bulk simulation

In this section, the dynamic simulation of a 3D storage facility is described. In Figure 3-4, the topology of the facility is presented. The yellow box represents the bulk of potatoes and the green box represents the fan.
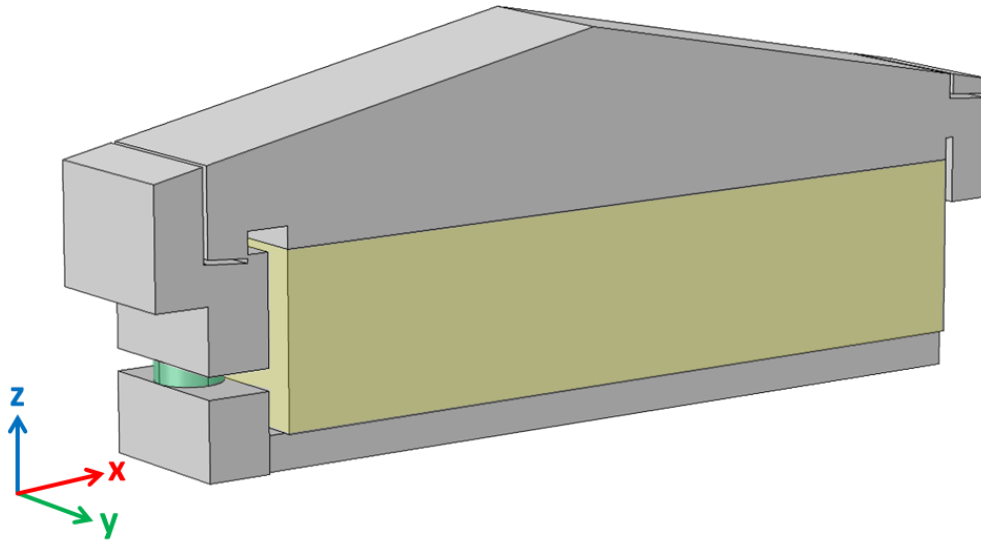

Figure 3-4. Graphical representation of 3D configuration. The bulk and the fan are represented by respectively the yellow and the green objects.

Compared to 2D simulation, the main difference is that in this case three instead of two dimensions are taken into account. Due to the third dimension, the mesh contains much more elements ($\pm$ 130 000) than in case of 2D simulation ($\pm$ 5 000 elements). Also, the physics and the boundary conditions involved in the storage facility has to be evaluated in three instead of two dimensions. This results in a strong increase in computation time. In order to limit the computation time, only a representative piece in y-direction of the storage facility is taken into account. This piece includes one fan and two air channels, as visualized in Figure 3-5, in which the bulk is made invisible.
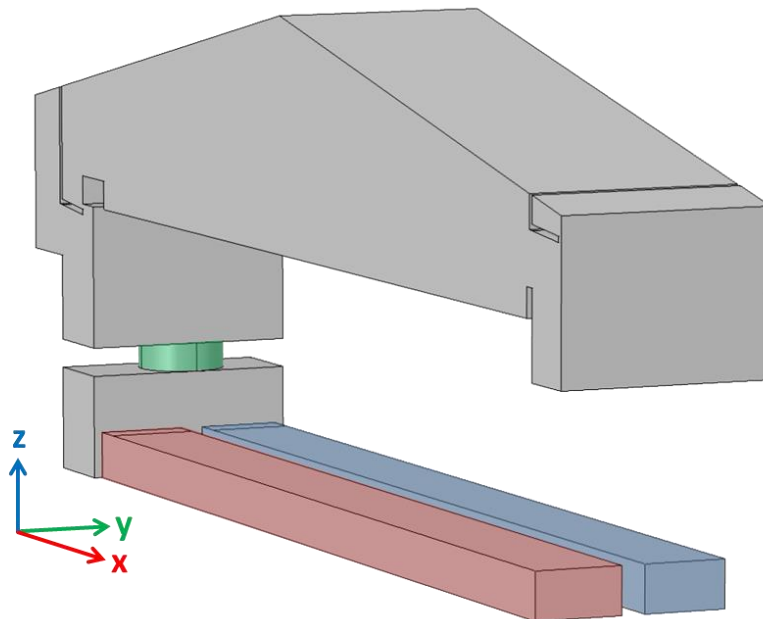
Figure 3-5. Graphical representation of the 3D configuration without the bulk. The two air channels are represented by the blue and red objects.

In Table 3-2, an overview of the dimensions of the facility is presented.

Table 3-2. Overview of dimensions of the simulated 3D storage facility.

	Size		
	x	y	z
Total facility [1]	21.1 $[m]$	4.6 $[m]$	6.0 $[m]$
Bulk	16.5 $[m]$	4.6 $[m]$	4.0 $[m]$
Air channels	17.0 $[m]$	2.0$[m]$	0.8 $[m]$
Fan	$\emptyset: 1.5\ [m]$		

[1]. Maximum dimensions of the facility

All physics and boundary conditions involved in the 3D model setup has a similar structure as the physics and boundary conditions related to the 2D model, described in section 3.2.1 and 3.2.3. The physics in the 2D model applied on a plane, are in the 3D model applied on a volume and boundary conditions in the 2D model applied on a line, are in the 3D model applied on a plane. As mentioned before, the computational time of a 3D-simulation is much longer. For this reason, the cooling unit is not taken into account in the 3D-model.

3.4 Stabilization issues

As described in section 3.2, the predefined interfaces are used for simulating the airflow while related temperature and moisture balances are simulated in the mathematical environment of COMSOL. In these predefined interfaces, both consistent (streamline and crosswind diffusion) and inconsistent (isotropic diffusion) stabilization techniques were applied in order to stabilize the fluid flow. Also, in the temperature and moisture balances artificial diffusion is necessary, because otherwise the solver does not converge and no solution is obtained. Since it is not possible to apply consistent stabilization techniques in the mathematical environment in COMSOL, isotropic diffusion is added to stabilize the temperature and moisture balances.

According to the theory described in section 2.1.2, the amount of artificial diffusion is calculated in such a way that the Péclet number never exceeds one. Since the convective term (velocity), the diffusion term and the mesh size are space dependent, the artificial diffusion is chosen space dependent, as well. This is visualized in Figure 3-6.
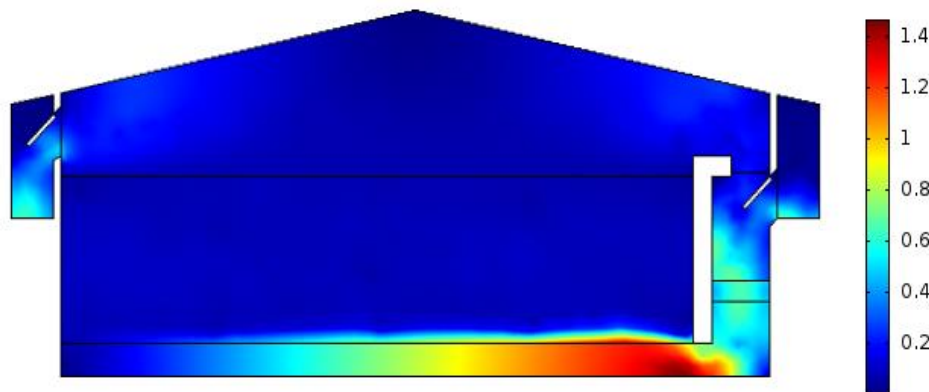
Figure 3-6. Spatial distribution of the necessary artificial diffusion in order to perform a stable simulation according the Péclet number.

Figure 3-6 shows that the needed artificial diffusion is in the range of $(0:1.45)$ $[m^2/s]$. However, stable simulations are performed with a space independent artificial diffusion of only 0.05 $[m^2/s]$. This supposes that the system is stable if the Péclet number is smaller than one, but systems might still be stable with higher Péclet numbers.

This presumption is further investigated with a few simple simulations. Three 2D simulations were performed on airflow through a pipe. In Figure 3-7, the used configurations with their meshes are visualized. Simulation 1 (S1) and 2 (S2) are performed using the left configuration of Figure 3-7, simulation 3 (S3) is based on the right configuration of Figure 3-7. The corresponding boundary conditions for each simulation are given in Table 3-3.

Table 3-3. Boundary conditions for the three test simulations (S1, S2 and S3).

	$v = v_{in}$	on [0,T] x $\delta 1$
S1	$T = T_{in}$	on [0,T] x $\delta 1$
	$P = P_{out}$	on [0,T] x $\delta 6$
	$v = v_{in}$	on [0,T] x $\delta 1,3$
S2	$T = T_{in}$	on [0,T] x $\delta 1,3$
	$P = P_{out}$	on [0,T] x $\delta 6$
	$v = v_{in}$	on [0,T] x $\delta 1$
S3	$T = T_{in}$	on [0,T] x $\delta 1$
	$P = P_{out}$	on [0,T] x $\delta 5$
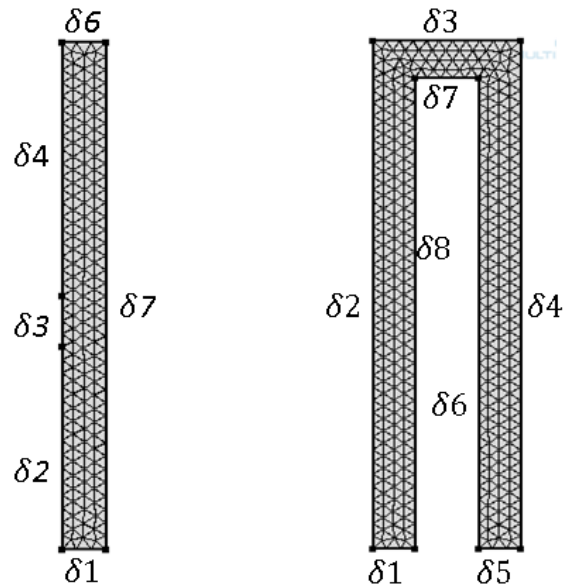
Figure 3-7. Two configurations for testing stability in simple configuration (left) and more complex configuration (right).

For boundaries not mentioned in Table 3-3, the following conditions hold:

$$n \cdot \nabla T = 0$$
$$v^T n = 0 \tag{3-25}$$
$$(-PI + \tau)^T n = 0$$

Here, $\nabla = \left[\frac{\partial}{\partial x}, \frac{\partial}{\partial y}\right]$.

For all simulations, $T(t_0) = 279.15\ K$, $P(t_0) = 101325\ Pa$, $T_{in} = 278.15\ K$ and $P_{out} = 101325\ Pa$. The inlet velocity (v_{in}) is varied in the range of $10^{-3} < v < 10\ [m/s]$. Taking into account the involved physics and the different configurations, S1 is the most simple system. Since S2 and S3 are more complex systems (either due to the physics or the configuration), high inlet velocities result in unstable and therefore unsolvable solutions for these simulations. This is visualized in Figure 3-8, in which the avarage Péclet number of the system is plotted against the inlet velocity.
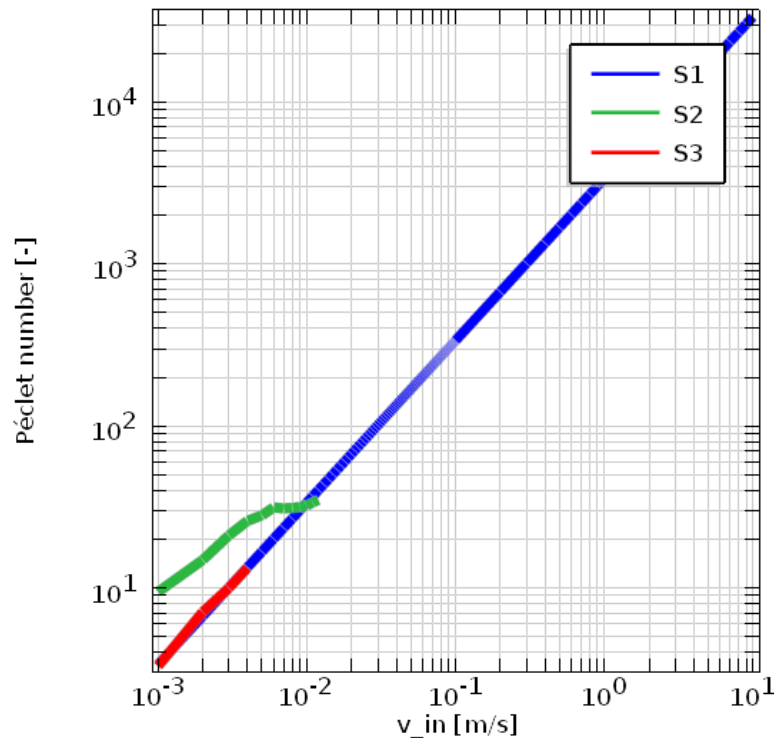
Figure 3-8. Relation between the inlet velocity and the Péclet number for each simulation in the range for which stable solutions were found. For S1, stable solutions were found until inlet velocity of 10 m/s, while for more complex systems (S2 and S3) the maximum inlet velocity for stable solution are respectively 0.1 m/s and 0.05 m/s.

Figure 3-8 shows that system S1 is stable for all evaluated inlet velocities. System S2 starts at a higher average Péclet number, which is caused by the extra inlet velocity on $\delta 3$. This system is stable for inlet velocities up to 0.01 [m/s], related to an average Péclet number equals 3. System 3 is only stable for inlet velocities up to 0.004 [m/s], which result in the lowest average Péclet number at which stable solutions are obtained.

This analysis shows that for systems with relatively simple physics and a simple configuration, the solutions can still be stable, even if the Péclet number is very high. However, if the systems are more complex, the maximum Péclet number for which a stable solution is feasible is reduced.

This analysis is performed in order to investigate the relation between stable solutions and the Péclet number. In the following simulations, artificial diffusion is not based on the Péclet number, but the artifical diffusion is minimized to the level at which stable solutions are feasible.

3.5 Airflow resistance in a soiled potatoes bulk

As stated in section 02.3, airflow resistance in clean and soiled potatoes bulks have been investigated several times. In this research, an extension on the Darcy-Forchheimer law is determined. In this extended equation, also the influence on the resistance of the amount of soil in the bulk is taken into account. This is done for airflow rates in the range of $0.01 \leq Q \leq 0.1 \ [m^3/m^2/s]$. Since Irvine et al. (1993) performed measurements on pressure drops in potato bulk for several potato varieties and several amount of soil in the bulk, this research is used to derive the extended Darcy-Forchheimer equation. The dimensions of the potatoes and the estimators of K and B in equation (2-30), estimated by Irvine et al. (1993), are presented in Table 3-4.

Table 3-4. Properties of potato cultivars and results from Irvine et al. (1993).

Potato variety	Soil content (% vol.)	Diameter (mm)				Constants equation		
		largest	*middle*	*smallest*	*ESD*	K	B	$\bar{B}$
Norchip	0	84	65	54	66.56	379.67	1.8522	1.8505
	2.5					646.32	1.8856	
	4					976.66	1.8280	
	6					1290.63	1.8364	
Russet Burbank	0	114	57	47	67.34	374.50	1.8346	1.7843
	2.5					630.23	1.8641	
	4					627.30	1.6462	
	6					1097.21	1.7921	

Irvine et al. (1993) measured the average dimensions (length, width and height) of the used potatoes. From these diameters, the equivalent spherical diameter (ESD) is calculated, see Table 3-4. For clean potatoes, the volume ratios of the potatoes and air are estimated. The results are presented in Table 3-5.

Table 3-5. Estimated volume ratios of the air (ϵ_a) and potatoes (ϵ_p).

	Norchip	Russet Burbank
$\epsilon_a(0)$	0.3519	0.3489
$\epsilon_p(0)$	0.6481	0.6511

Since only three soil percentages were investigated in Irvine et al. (1993), the data is extrapolated for soil percentages in the range of 0-10%. This is done by fixing parameter B to the average of the values found for B (see $\bar{B}$ in Table 3-5, last column) and then calculating the corresponding K values which result in the same pressure drop. After that, an exponential relation is found between the new K values and the soil percentage *(m)* for both potatoes varieties, as presented in the equations (3-26) and (3-27).

$$K_{Norchip} = 375 \, e^{0.2196 \, m} \tag{3-26}$$

$$K_{Russet\ Burbank} = 335\ e^{0.2043\ m} \tag{3-27}$$

Using these K-values and the average B-values, pressure drops can be calculated for soil percentages in the range of 0-10%. The amount of soil in the potato bulk influences two physical properties of the Darcy-Forchheimer law, namely the intrinsic permeability (κ) and the Forchheimer resistance coefficient (β). Therefore, the derived expressions for these properties by Chourasia and Goswami (2007) are adapted to:

$$\kappa_{new} = \frac{d_{eff}(m)^2\ \epsilon_a(m)^3}{150\big(\epsilon_p(m) + \epsilon_s(m)\big)^2} \tag{3-28}$$

$$\beta_{new} = \frac{1.75\ \big(\epsilon_p(m) + \epsilon_s(m)\big)^2}{d_{eff}(m)\epsilon_a(m)^3} \tag{3-29}$$

In these expressions, d_{eff} represents the effective diameter, which represents both the potato diameter and soil diameter. The effective diameter and the volume fraction of the air, the potatoes and the soil depend on the soil content percentage (m). In order to determine the volume fractions of these components, the relations as presented in equations (3-30), (3-31) and (3-32) are derived.

$$\epsilon_s(m) = m \tag{3-30}$$

$$\epsilon_p(m) = \epsilon_p(0) - f \cdot \epsilon_s(m) \tag{3-31}$$

$$\epsilon_a(m) = \epsilon_a(0) - (1 - f) \cdot \epsilon_s(m) \tag{3-32}$$

In these relations, f determines how the volume fraction of the air and potatoes changes by the volume fraction of the soil, compared to zero soil content percentage. Using nonlinear parameter estimation techniques, the parameters f and d_{eff} were estimated based on the extrapolated data of Irvine et al. (1993) for the potato variety Norchip. The results are visualized in Figure 3-9.
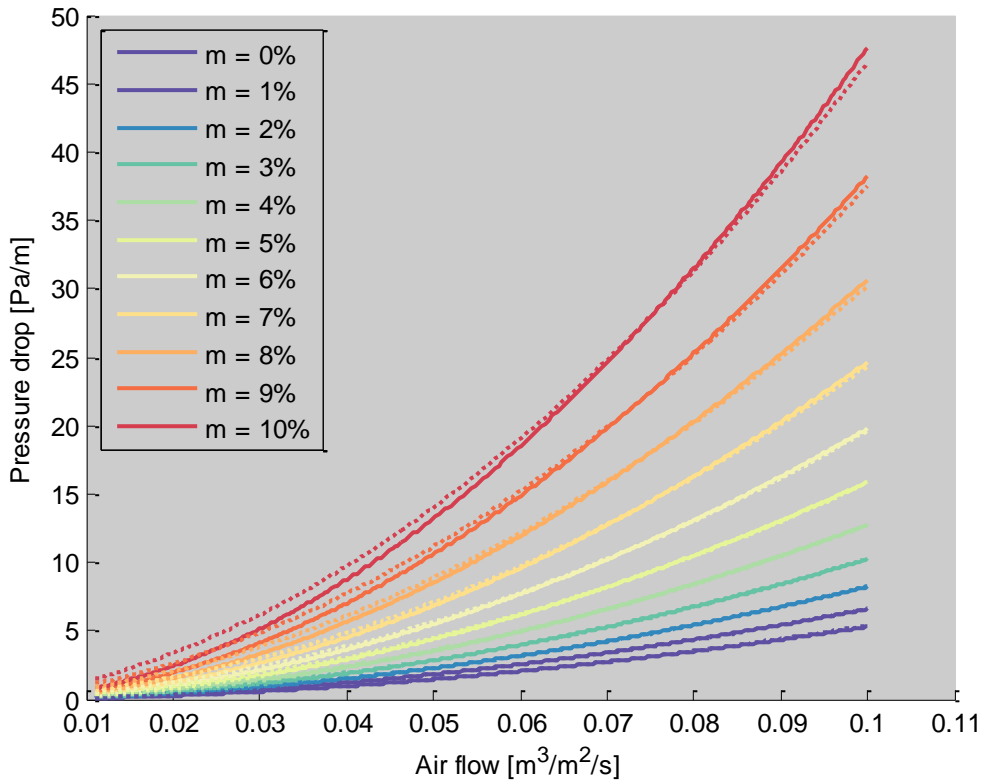
Figure 3-9. Pressure drops according to extrapolated data of Irvine et al. (1993)   (solid lines) and according to the extended Forchheimer law (dashed lines) for soil percentages in range of 0-10% for the potato cultivar Norchip.

The volume ratios of the potatoes, air and soil are visualized in Figure 3-10. This figure shows that the volume fraction of the potatoes ϵ_p remains almost the same regardless the soil content percentage. Only for 1% soil content, the volume fraction of the soil is slightly reduced. This implies that the parameter f in the equations (3-31) and (3-32) is equal to zero, except for 1% soil content.
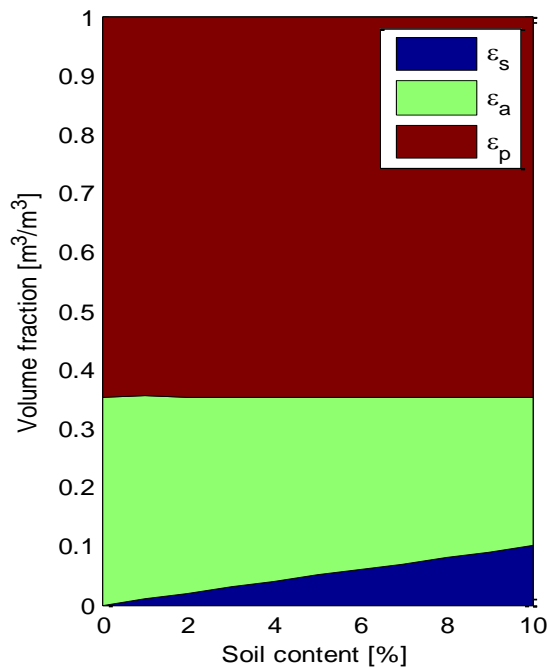
Figure 3-10. Volume fractions of air, potato and soil by increasing soil percentages.

Next, the relation between the soil content percentage and the parameter d_{eff} is investigated, as shown in Figure 3-11.
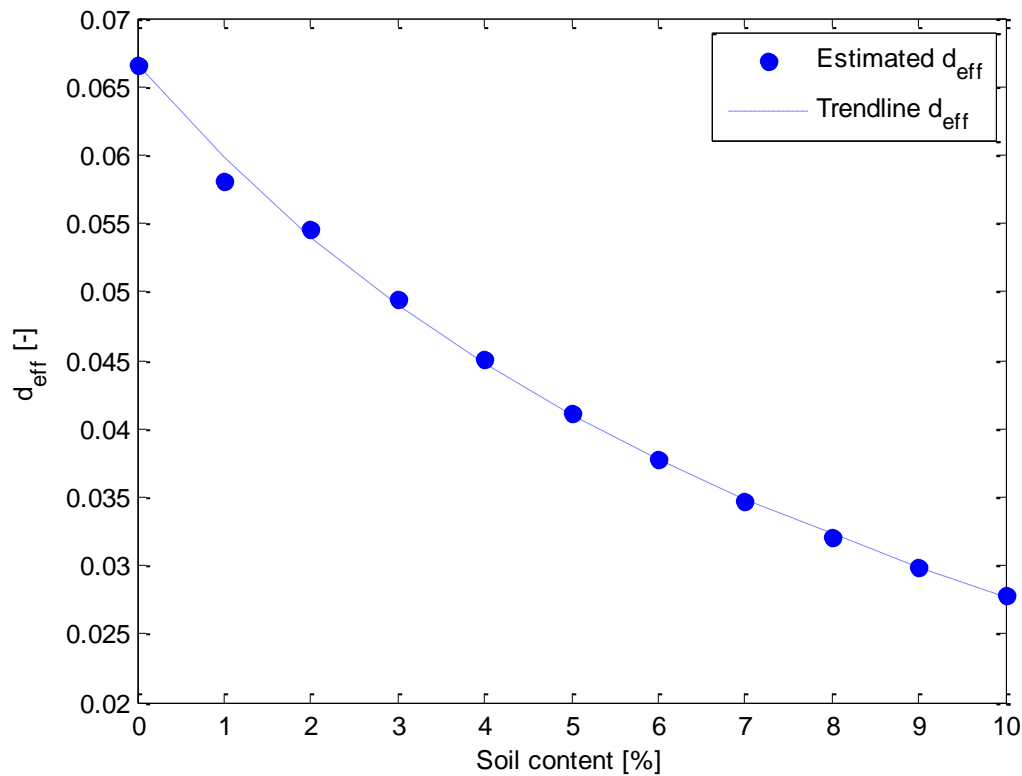
Figure 3-11. Relation between estimated effective diameter $\left(d_{eff}\right)$ and the soil content.

A third order polynomial is derived to approximate d_{eff}. This polynomial is given in equation (3-33).

$$d_{eff} = -16.8 \, m^3 \, + \, 5.0 \, m^2 \, - \, 0.72 \, m + d_p \qquad\qquad (3\text{-}33)$$

The derived third order polynomial is validated by the extrapolated data of Irvine(1996) of the potato variety Russet Burbank. The pressure drops for soil content up to 10% are approximated using the extended Darcy-Forchheimer law, with f equals zero and d_{eff} according to the polynomial in equation (3-33). The results are shown in Figure 3-12.
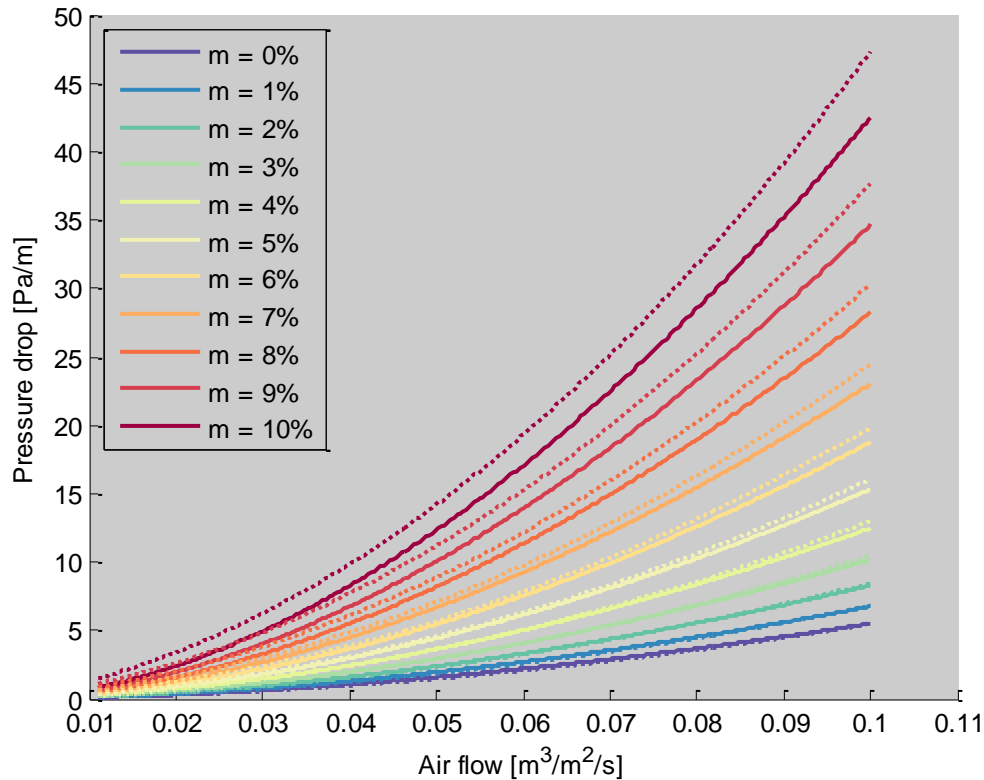
Figure 3-12. Pressure drops according to extrapolated data of Irvine et al. (1993) (solid lines) and according to the extended Forchheimer law (dashed lines) for soil percentages in range of 0-10% for the potato cultivar Russet Burbank.

In the performed simulations, an effective diameter of 7 $[cm]$ is used, so the effect of soiled potatoes is not further investigated in the following simulations.

4   Dynamic simulation analysis

Both the 2D and 3D setup, described in chapter 0, are implemented in the software package COMSOL Multiphysics 4.4. First, a validation related to the system resistance and the corresponding air velocity through the bulk is performed, which is described in section 4.1. Air flow through the storage facility caused by free convection and the effect of the cooling unit are analysed in the 3D model. Furthermore, 2D simulations with and without controller are analysed.

4.1   Validation of system resistance

A first validation step is performed by visual inspection of the results. The air pressure, air velocity, air temperature and air humidity ranges over time and space are evaluated. All these ranges are in a feasible region.

In order to define the accuracy of the simulations, measurements from measuring equipment placed in a storage facility are used. The total pressure on several places in the storage facility is analysed to evaluate the pressure drops over the fan, in the air channels and over the bulk. However, by analysing the data retrieved from a pressure difference sensor, it was found that the data was highly fluctuating and consequently very inaccurate. This was probably caused by the turbulence character of the airflow.

Instead of validating the simulations by measurements, values from literature are used for the validation. Rastovski et al. (1985) stated that the overall pressure drop over a potato bulk storage facility is approximately 150 $[Pa]$. The overall pressure drop depends mainly on the pressure drop over the bulk, caused by the airflow resistance through the bulk. As described in section 1.4, the Darcy-Forchheimer law is used for modelling this airflow resistance. However, this law is based pressure drops on perfect spherical objects. Therefore, it is necessary to perform a correction on this law in order to calculate the pressure drop over a potato bulk, by adding a correction factor to the Darcy-Forchheimer law:

$$\nabla p = C \left(-\frac{\mu}{\kappa} v_i - \beta \rho_a \bar{v} v_i \right) \qquad (4\text{-}1)$$

in which C represents the correction factor and κ and β represent respectively the intrinsic permeability of the bulk and the Forchheimer coefficient. In order to estimate the value C, the following assumptions are made:

- Pressure drop over the fan equals to 150 $[Pa]$ (according to Rastovski et al. (1985))
- Average air velocity through the bulk equals 0.3 $[m/s]$ (equal to 100 $[m^3/m^3/h]$, a commonly used air flux through potato bulks)

In Figure 4-1, the average air velocity through the bulk is plotted against values of C in the range of (0.3-0.6). From this figure, it can be concluded that C equals 0.38 results in an average air velocity through the bulk of 0.3 $[m/s]$.
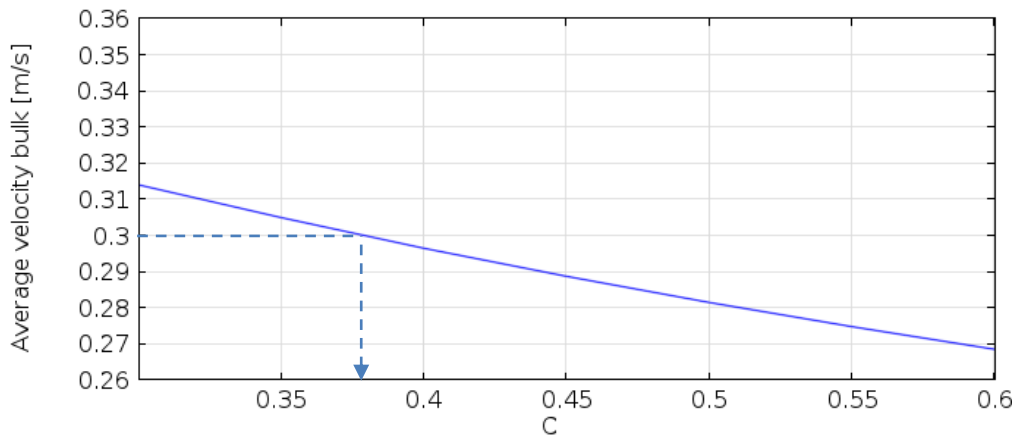

Figure 4-1. Average air velocity through the potato bulk for C values in the range of (0.3-0.6).

4.2 Free convection

As a starting point for the simulations, the simplest scenario is taken. In this scenario, all equipment (the fan, the humidifier and the cooling unit) is turned off and the panels are fully opened. For these settings, there is no forced airflow in the storage facility and consequently the effect of free convection can be investigated. This is done using the 3D setup and with the following conditions:

$$T_{aa}(t_0), T_{ap}(t_0), T_{pp}(t_0) = 7.5\ °C$$
$$X_{aa}(t_0), X_{ap}(t_0), X_{pp}(t_0) = 6.11\ g/kg\ (RH = 95\%)$$

$$T_{out} = 5.5\ °C$$
$$X_{out} = 5.03\ g/kg\ (RH = 90\%)$$

(4-2)

The temperature variation and the velocity profile in the storage facility after 6 hours are visualised in Figure 4-2. This figure shows that air enters the facility at the right hand side and flows through the bulk in upwards direction.
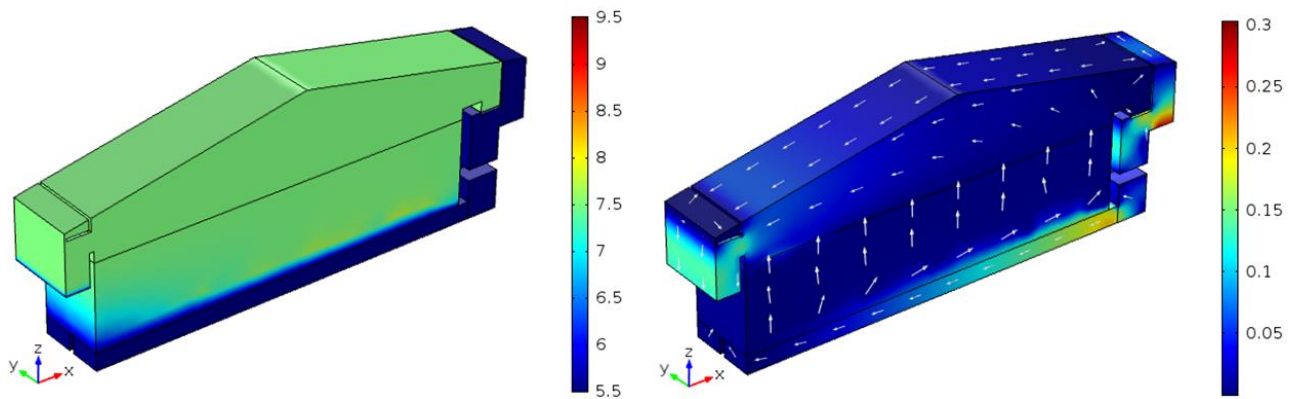

Figure 4-2. Temperature variation (left hand side) and velocity profile (right hand side) in storage facility after 6 hours with lower outside temperature and humidity compared to initial indoor conditions.

Airflow through the facility is caused by density differences between the indoor and outdoor air. Since the density of the outdoor air is higher (due to lower temperature and humidity), the outdoor air flows in a downwards direction. This is only possible at the opening of the storage facility at the right hand side. This results in a velocity profile as visualized in Figure 4-2.

However, the density differences and the corresponding air velocity rates are very low. Therefore, small numerical errors caused by the integration steps in solving the partial differential equations may have a relatively large impact on the result. To investigate whether the results visualized in Figure 4-2 are caused by the underlying physics or by numerical errors, a second simulation is performed. In this simulation, the temperature and the humidity of the outdoor air are higher compared to the initial indoor conditions, which should result in an opposite temperature and velocity profile. This simulation is performed with the following conditions:

$$T_{aa}(t_0), T_{ap}(t_0), T_{pp}(t_0) = 7.5\,°C$$
$$X_{aa}(t_0), X_{ap}(t_0), X_{pp}(t_0) = 6.11\,g/kg\,(RH = 95\%)$$

$$(4\text{-}3)$$

$$T_{out} = 9.5\,°C$$
$$X_{out} = 7.23\,g/kg\,(RH = 98\%)$$

The temperature variation and the velocity profile in the storage facility after 1 hour are visualised in Figure 4-2. This figure shows an opposite air flow direction compared to Figure 4-2, as expected.
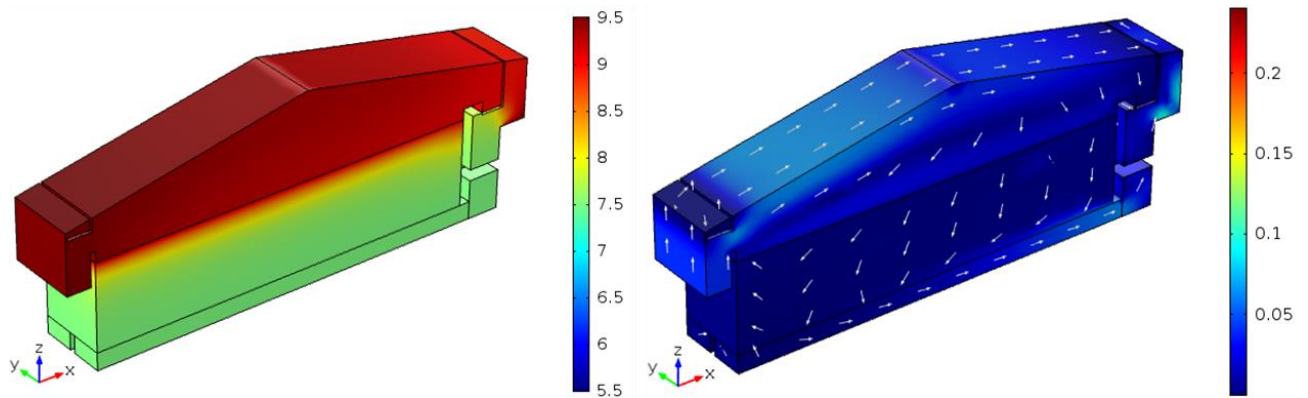
Figure 4-3. Temperature variation (left hand side) and velocity profile (right hand side) in storage facility after 6 hours with higher outside temperature and humidity compared to initial indoor conditions.

4.3 Cooling performance

In the previous subsection, the effect of free convection is described. From the perspective of a numerically solving procedure, this is a rather simple system, since all physics related to the equipment in the storage facility were not taken into account. When these physics are taken into account as well, the system becomes much more complicated, resulting in very large computational times.

In order to be able to perform simulations within a reasonable time span, the 2D setup is used. However, this leads to problems with respect to the cooling unit, since the cooling effect takes place in 3D. Therefore, first the performance of the cooling unit is evaluated in the 3D setup, as presented in Figure 4-4.
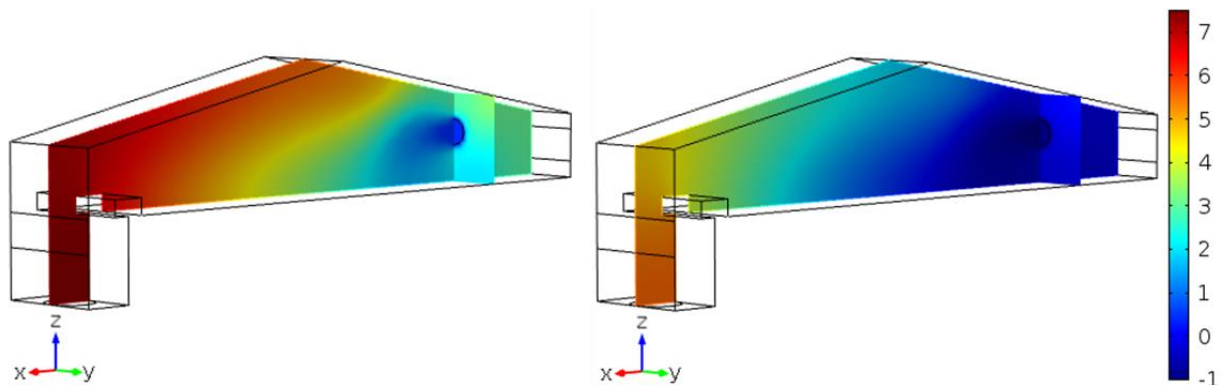
Figure 4-4.Temperature profile after 2 minutes (left hand side) and after 5 minutes (right hand side). Initial temperature is 7.5° C.

Next, the average decrease in temperature and humidity of the air domain above the bulk is calculated. The derivatives of the temperature and humidity content of the air are above the bulk are presented in Figure 4-5.
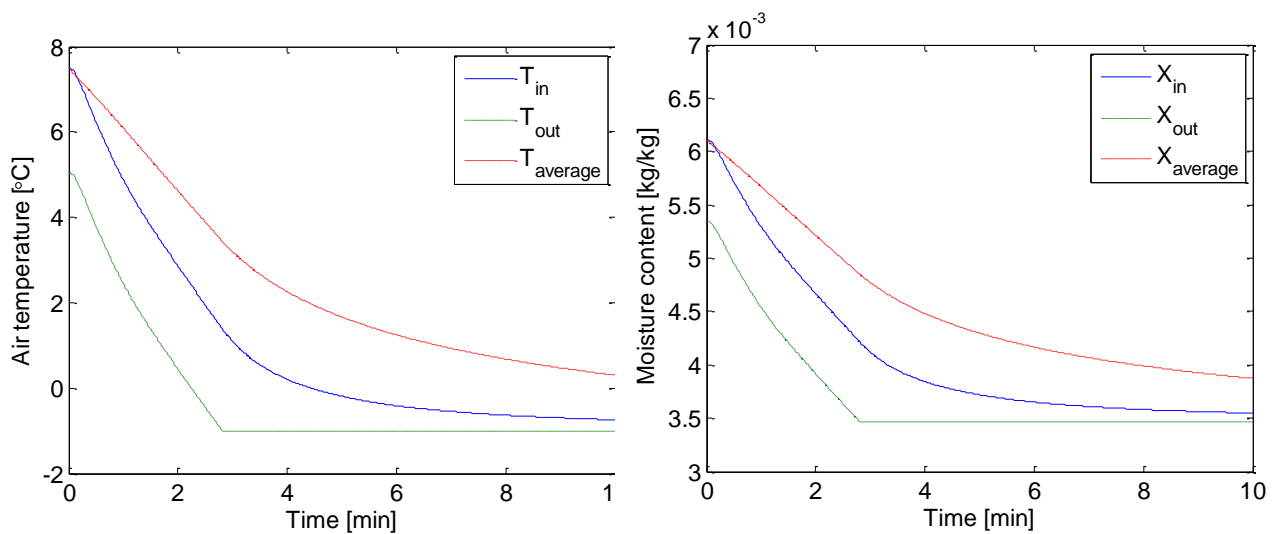
Figure 4-5. Inlet and outlet temperature of the evaporator and average temperature of the air above the bulk evaluated in 3D (left hand side). Inlet and outlet humidity content of the evaporator and average humidity content of the air above the bulk evaluated in 3D (right hand side).

Figure 4-5 shows a linear decrease of both the average temperature and humidity content in the first three minutes. Since a cooling unit is mostly activated for short time periods (a few minutes), the average decrease in temperature and humidity content of the air above the bulk are assumed to be constant. The rates for average temperature and humidity content decrease are respectively:

$$r_T = \frac{dT_{aa}}{dt} = -0.0245 \; [°C/s]$$

$$r_X = \frac{dX_{aa}}{dt} = -0.76 \cdot 10^{-5} \; [kg/kg/s]$$

(4-4)

These rates are applied in the 2D setup in order to simulate the average decrease in temperature and humidity content caused by the cooling unit.

4.4 2D simulations without control

First, a simulation is performed in which the outdoor conditions are assumed to be time independent. The humidifier and cooling unit are in this simulation not taken into account. This 2D simulation of the total storage facility is performed to evaluate the behaviour of the system. This is done using the following settings:

$$T_{aa}(t_0), \; T_{ap}(t_0), \; T_{pp}(t_0) = 7.5 \; °C$$

$$X_{aa}(t_0), \; X_{ap}(t_0), \; X_{pp}(t_0) = 6.11 \; g/kg \; (RH = 95\%)$$

$$T_{out} = 5.5 \; °C$$

$$X_{out} = 4.75 \; g/kg \; (RH = 85\%)$$

$$\alpha = 60°$$

$$\Delta P = 150 \; Pa$$

(4-5)

The results of this simulation, containing velocity, pressure, temperature and humidity profiles are presented in Figure 4-6. From the temperature profiles, it can be concluded that the horizontal distribution of the temperature is not uniform. This is because the ventilation rate at the left hand side of the bulk is slightly higher compared to the right hand side of the bulk. For control purposes, which are included in the next sections, a reference point for the temperature and water content of the potatoes have to be chosen. This reference point is chosen in the middle of the bulk (see whit dot in Figure 4-6), since it is assumed that the conditions at this point are equal to the (uniformly distributed) conditions at the end of a ventilation period.

So control of the system is based on the conditions $(T_{pp\,ref}, X_{pp\,ref})$ in the middle of the bulk.

Velocity profile

Pressure profile

Temperature profile [6 hours]

Temperature profile [12 hours]

Humidity profile [6 hours]

Humidity profile [12 hours]
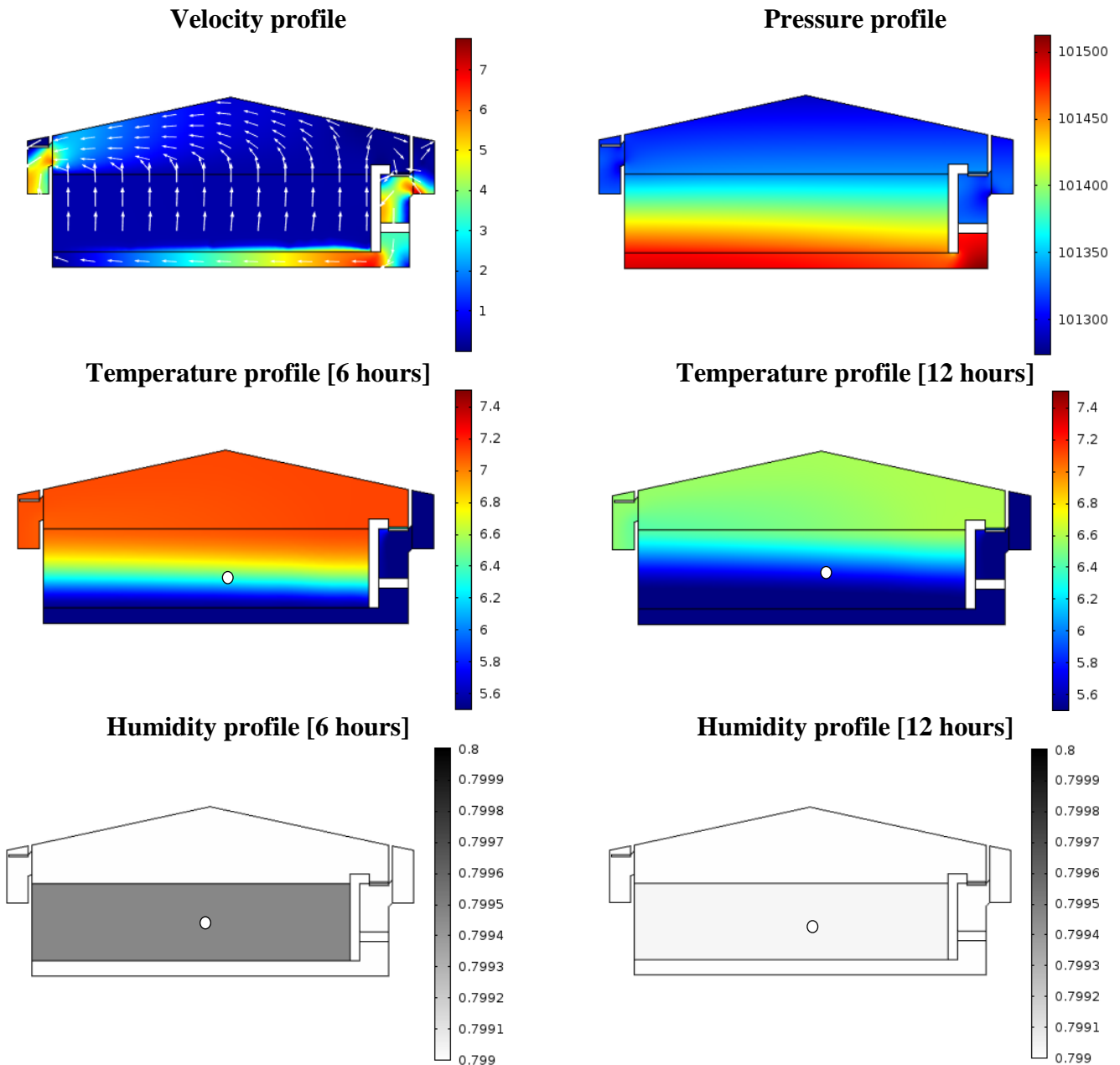
Figure 4-6. Results of simulation without controller and without real outdoor conditions. The white dot represents the reference point for control purposes (located in the middle of the bulk).

Another 2D simulation of the total storage facility is performed using real outdoor conditions of 1 April 2010, retrieved from the Royal Netherlands Meteorological Institute (KNMI). Furthermore, in this simulation all equipment is taken into account. In this simulation, the control input variables are fixed. Therefore, control of the system is not yet included; however, this simulation was performed to check if all equipment works properly.

The results of this simulation regarding the temperature and humidity profile after 1 hour are presented in Figure 4-7. This figure shows clearly the effect of the mixing air flows, the cooling effect of the humidifier (lower temperature behind the fan) and the effect of the cooling unit (air near the roof is cooled down, while warm air flows out the bulk). The effects of the equipment on the humidity content are not visible in the plot, since these differences are too small compared with the difference between the indoor and outdoor humidity.
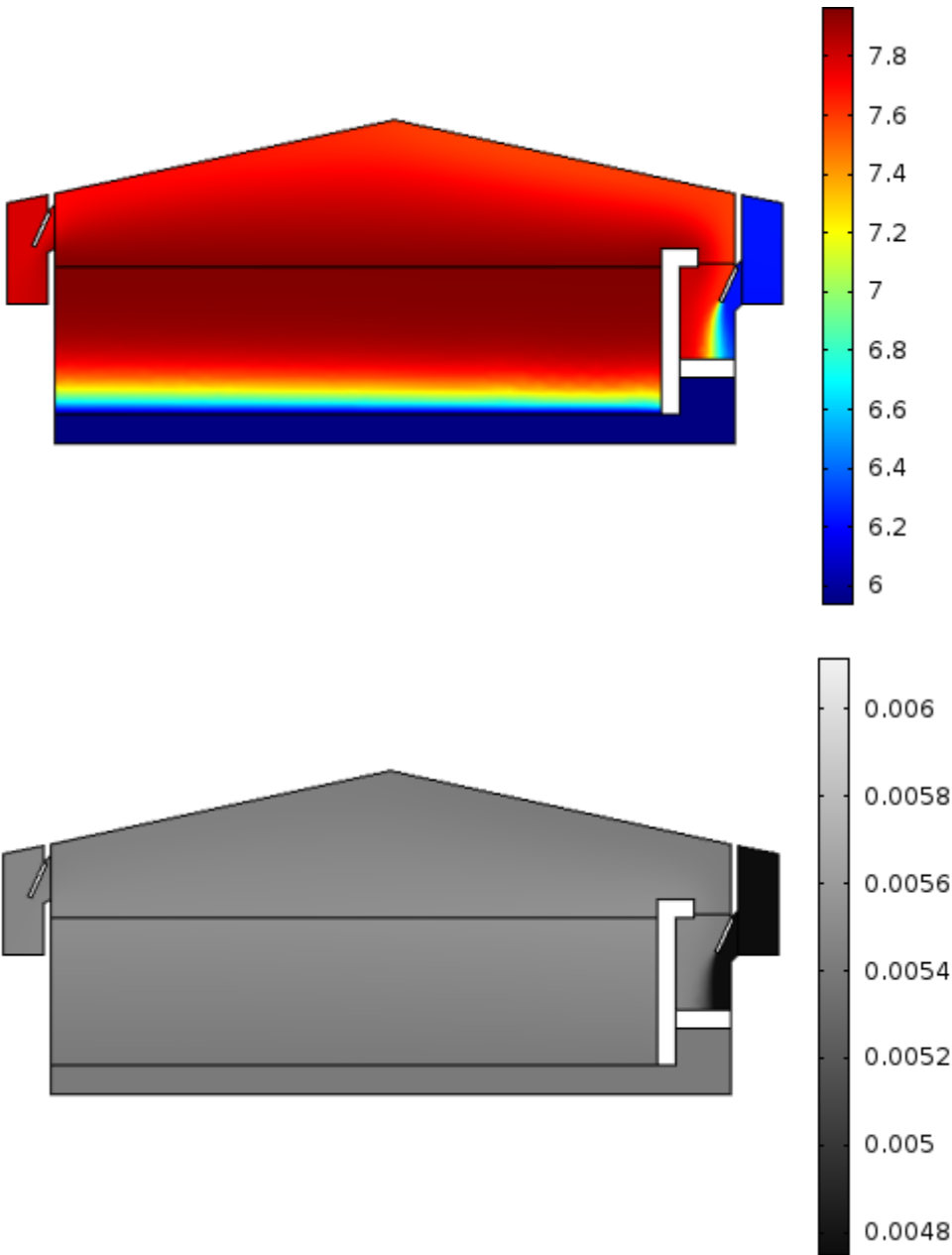
Figure 4-7. Temperature profile (upper plot) and humidity profile (lower plot) after 1 hour.

4.5 2D simulations with control

In order to be able to evaluate the behaviour of a controlled potato storage facility, also the control elements should be activated in the model. An overview of all control variables in an advanced potato storage facility is presented in Table 4-1.

Table 4-1. Overview control variables of an advanced storage facility.

Control variable	Range		Description
α	$(0-90)$	[°]	Opening angle panels
ΔP_{fan}	$(50-350)$	[Pa]	Pressure drop fan
Humidifier	$\{0,1\}$	[-]	Turn on/off humidifier
Cooling unit	$\{0,1\}$	[-]	Turn on/off cooling unit

However, implementing a real controller in COMSOL is not possible, since COMSOL is not able to evaluate all states and directly control the system during a dynamic simulation. Besides that, it turns out that opening or closing the panels within a time dependent simulation results in large convergence rates of the solver and consequently large computational times. For this reason, the following aspects are first investigated:

- Relation between the opening angle of the panels and conditions of the mixed air
- Relation between the mechanical cooling period and ventilation period

When these relations are known, these phenomena can be implemented in the model in a more straightforward way, resulting in feasible computation times for the simulations.

4.5.1   Relation opening angle panels and conditions of the mixed air

The opening angle α determines the mixing ratio between the internal airflow and the external airflow and consequently the conditions of the mixed air, as presented in Figure 4-8.
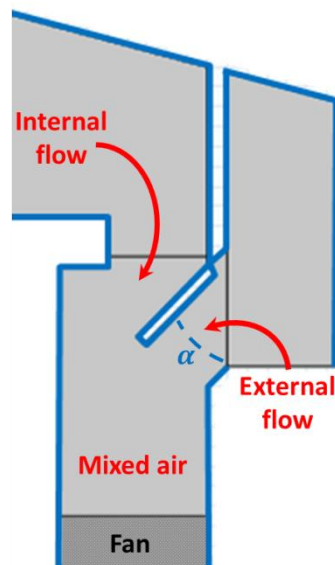
Figure 4-8. Schematic overview of internal and external airflows, depending on the opening angle α.

A simulation is performed in which the opening angle of the panels is stepwise changed and the internal and external air flows are evaluated (see Figure 4-9, left hand side plot). For each opening angle α, the outdoor air ratio $\left(r_1 = \frac{\phi_{external}}{\phi_{total}}\right)$ is calculated for each angle position. Finally, an expression is found for the opening angle α, depending on the fraction r_1 (see Figure 4-9, right hand side plot).
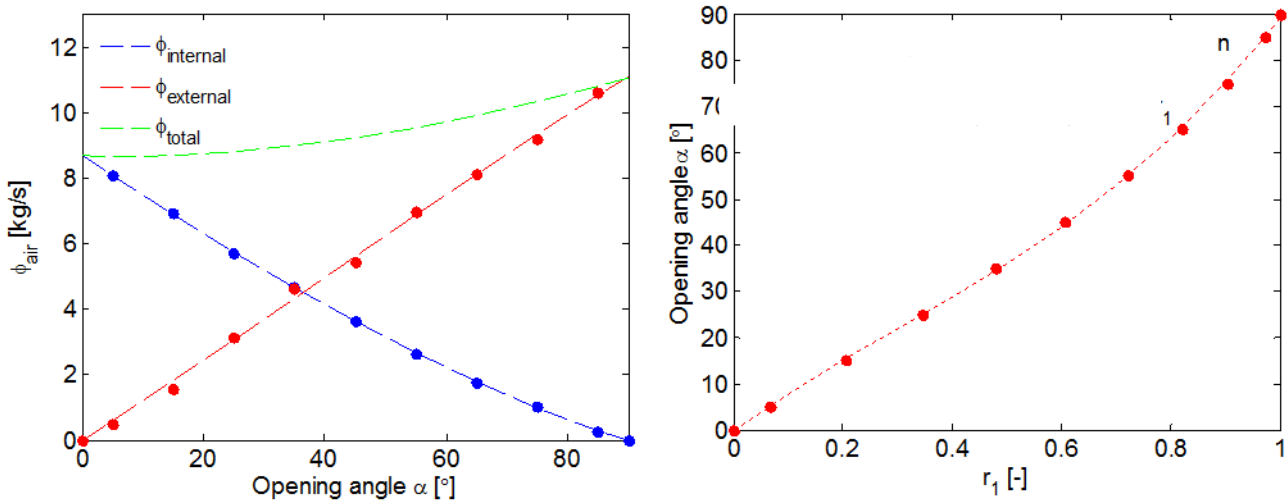

Figure 4-9. Internal, external and total air fluxes (left hand side) and derived relation between outdoor air fraction and opening angle α.

The relation between the ratio r_1 and the opening angle α is derived using a least squared error technique and is approximate by the polynomial:

$$\alpha(r_1) = 55.5\, r_1^3 - 48.8\, r_1^2 + 82.4\, r_1 \tag{4-6}$$

The enthalpy content of the several air fluxes are given by:

$$H_{out} = C_{pa}T_{out} + X_{out}\left(C_{pw}T_{out} + H_w\right)$$
$$H_{aa} = C_{pa}T_{aa} + X_{aa}\left(C_{pw}T_{aa} + H_w\right) \tag{4-7}$$
$$H_{fan} = r_1 H_{out} + (1 - r_1) H_{aa}$$

Here, H_{out}, H_{aa} and H_{fan} are respectively the enthalpy content of the outside air, the enthalpy content of the air above the bulk and the enthalpy content of the ventilated air in the fan. C_{pa}, C_{pw} and H_w represents respectively the specific heat of dry air, the specific heat of vapour and the evaporation heat of water. From the enthalpy expression of the air in the fan, the air temperature in the fan can be derived:

$$T_{fan} = \frac{H_{fan} - H_w X_{fan}}{C_{pa} + C_{pw} X_{fan}} \tag{4-8}$$

Furthermore, the water content of the air in the fan can be described by the ratio r_1:

$$X_{fan} = r_1 X_{out} + (1 - r_1)X_{aa} \tag{4-9}$$

53

For a storage facility without humidifier, a set point controller is designed, which means that a desired ventilated air temperature (T^*) is defined. Since this temperature is equal to the air temperature in the fan $(T^* = T_{fan})$, the ratio r_1 can be expressed as:

$$r_1 = \frac{(C_{pa} + C_{pw} X_{aa})(T_{aa} - T^*)}{C_{pa}(T_{aa} - T_{out}) + C_{pw} (T_{aa} X_{aa} + T^* X_{out} - T^* X_{aa} - T_{out} X_{out})} \quad (4\text{-}10)$$

A humidifier, located directly after the fan, will cool the air further down by the evaporation process. Therefore, the temperature in the fan is not equal to the desired temperature and consequently the ratio r_1 is changed. However, the enthalpy content of the air is not changed during the evaporation process in the humidifier. Using the following expression for the enthalpy content of all air fluxes, also a ratio for cases in which a humidifier is present can be derived:

$$H_{out} = C_{pa}T_{out} + X_{out}\left(C_{pw} T_{out} + H_w\right)$$

$$H_{aa} = C_{pa}T_{aa} + X_{aa}\left(C_{pw} T_{aa} + H_w\right)$$

$$H_{fan} = r_1 H_{out} + (1 - r_1) H_{aa}$$

$$H^* = C_{pa}T^* + X^*\left(C_{pw} T^* + H_w\right) \quad (4\text{-}11)$$

$$P_{sat}^* = 610.5 \cdot 10^{\frac{7.5 \cdot T^*}{237.3 + T^*}}$$

$$X^* = RH^* \cdot \left(0.622 \frac{P_{sat}^*}{P_{tot} - P_{sat}^*}\right)$$

Here, H^* represents the enthalpy content of the desired ventilated air, T^* represents the desired ventilated air temperature, P_{sat}^* represents the saturated vapour pressure of the desired ventilated air conditions, X^* represents the moisture content of the desired ventilated air and RH^* represents the desired relative humidity ratio of the air after passing the humidifier.

The ratio of outdoor air for situations in which a humidifier is applied $(r_{1\,hum})$ is equal to:

$$r_{1\,hum} = \frac{\left(H_w X_{aa} + C_{pa}(T_{aa} - T^*) + C_{pw}T_{aa}X_{aa} - 379731 \cdot 10^{\left(\frac{15\,T^*}{2(T^*+237.3)}\right)} RH_{goal}\left(H_w + C_{pw}T^*\right)\right)}{1000\left(P_{tot} - \left(610.5 \cdot 10^{\left(\frac{15\,T^*}{2(T^*+237.3)}\right)}\right)\right)}$$
$$\overline{H_w(X_{aa} - X_{out}) + C_{pa}(T_{aa} - T_{out}) + C_{pw}(T_{aa} X_{aa} - T_{out}X_{out})}$$

$$(4\text{-}12)$$

By implementing the derived ratios $(r_1$ and $r_{1hum})$ in COMSOL, it is possible to ventilate the potato bulk with a desired air temperature (T_{goal}). Furthermore, the implementation of the moving panels can be omitted, since the opening angle α can be calculated afterwards using the polynomial presented in (4-6). This results in a strong decrease in computational time.

4.5.2 Relation mechanical cooling periods and ventilation periods

Using a mechanical cooling unit, the air above the bulk is cooled down towards a user defined minimum temperature $(T_{aa_{min}})$. Then, the fans are activated and the cold air is blown into the potato bulk until the air above the bulk is heated up towards a user defined maximum temperature $(T_{aa_{max}})$. This cycle, which is visualized in Figure 4-10, is repeated until the desired situation is reached.
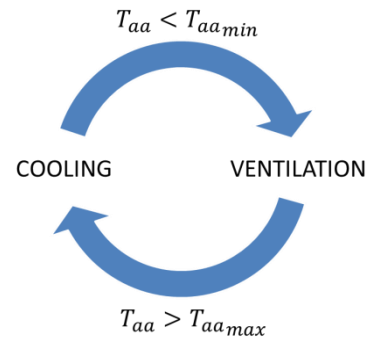

Figure 4-10. Mechanical cooling process (cooling and ventilation).

The cycle can be represented by the following simple if-statements, which can be implemented in COMSOL:

$$
\begin{aligned}
T_{aa} > T_{aa_{max}} & & & \rightarrow & Cool \\
T_{aa} > T_{aa_{min}} & \wedge & \frac{dT_{aa}}{dt} < 0 & \rightarrow & Cool \\
T_{aa} < T_{aa_{min}} & & & \rightarrow & Vent. \\
T_{aa} < T_{aa_{max}} & \wedge & \frac{dT_{aa}}{dt} > 0 & \rightarrow & Vent.
\end{aligned}
\tag{4-13}
$$

These rules are implemented in a non-spatial model in Matlab in order to evaluate the system behaviour. The cooling effect on the potato and air temperature and the cooling and ventilation periods are presented in Figure 4-11.
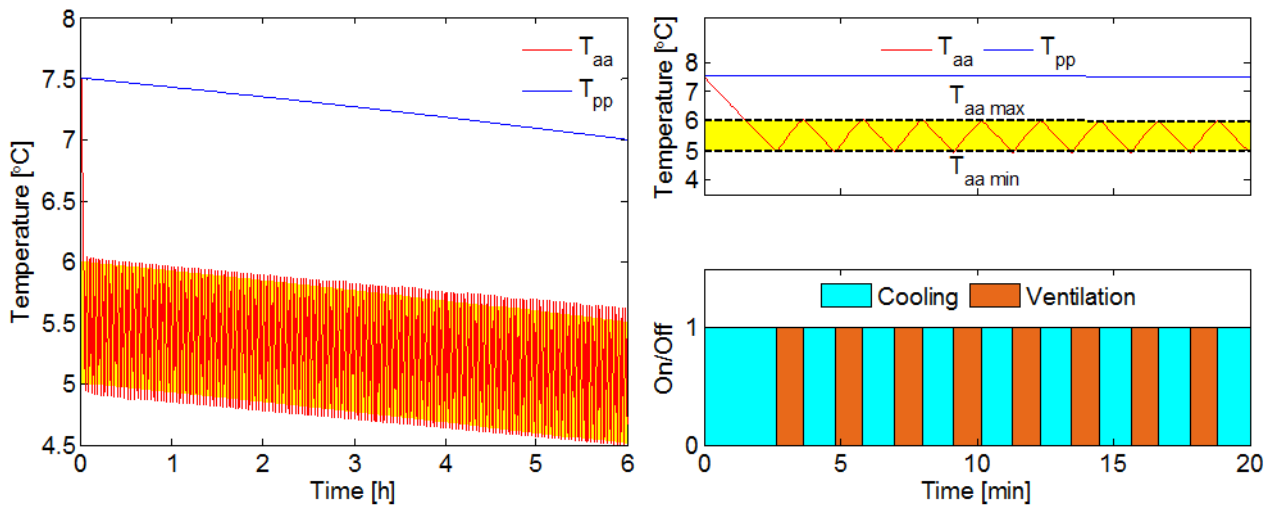
Figure 4-11. The potato temperature and the air temperature during the cooling process of 6 hours (left hand side). Zoomed in on the first 20 minutes of the cooling process (top right plot). The air temperature is varying between $T_{aa_{max}}$ and $T_{aa_{min}}$. The switching between cooling and ventilation is visualized in the bottom right plot. Note that either the cooling unit or the fan is activated at the same moment.

However, implementing these rules in COMSOL results in oscillatory behaviour of the system and finally the solver is not able to converge, so no solution is found. This is caused by:

- The switching conditions of the fan and cooling unit. No intermediate points between on and off can be defined, which results in steep gradients at the boundaries of the fan and cooling unit domain.
- Evaluating the temperature of the air above the bulk (T_{aa}). Since the switching between cooling and ventilation very frequently occur (every few minutes), T_{aa} have to be evaluated very frequently as well. This implies that the integration time step of the solver should be very small in order to evaluate T_{aa} accurately. This results in very large computational times.

This problem is solved by activating both the cooling and the fan simultaneously. However, activating both devices simultaneously is not does not correspond to the cooling process in reality. To correct for activating both devices simultaneously, the time fraction f in which the cooling unit is activated a real situation $t_{cool\,real}$ is defined. This fraction is expressed as:

$$f = \frac{t_{cool\,real}}{t_{cool\,real} + t_{vent\,real}}$$

$$t_{cool\,real} = \frac{T_{aa_{min}} - T_{aa_{max}}}{r_T}$$

$$t_{vent\,real} = \frac{T_{aa_{max}} - T_{aa_{min}}}{\frac{\phi_{bulk}}{V} \cdot (T_{ap} - T_{aa})}$$

(4-14)

Here, $t_{cool\,real}$ and $t_{vent\,real}$ represents respectively the cooling and ventilation time in a real situation.

The air above the bulk is represented by an ordinary differential equation in which the effect of simultaneously cooling and ventilation are corrected by the fraction f:

$$V\rho_a C_{pa} \cdot \frac{dT_{aa}}{dt} = \left(\rho_a C_{pa}\,\phi_{bulk}(T_{ap} - T_{aa})\right) \cdot (1 - f) + \left(V\rho_a C_{pa} \cdot r_T\right) \cdot f \qquad (4\text{-}15)$$

Here, V represents the volume of T_{aa}, ϕ_{bulk} represents the air flux out of the bulk and r_T represents the decrease in air temperature due to cooling unit (see equation (4-4)). Since r_T is defined as a negative value, this term is added to the differential equation. Similar to equation (4-15), an ordinary differential equation is derived for the water content of the air above the bulk:

$$V\frac{dX_{aa}}{dt} = \left(\frac{\phi_{bulk}}{V} \cdot (T_{ap} - T_{aa})\right) \cdot (1 - f) + (r_X) \cdot f \qquad (4\text{-}16)$$

Here, r_X represents the decrease in water content of the air due to cooling unit (see equation (4-4)).

Since the ventilation period is defined by $(1 - f)$, the pressure drop over the fan is corrected with this fraction as well. Combining the ordinary differential equations for the air condition above the bulk and the derived ratios for the opening panels (see previous section) with the remaining part of the model results in the model presented in Figure 4-12.


$$\frac{dT_{air}}{dt} \quad \frac{dX_{air}}{dt}$$

r_1

Fully spatially distributed

r_1
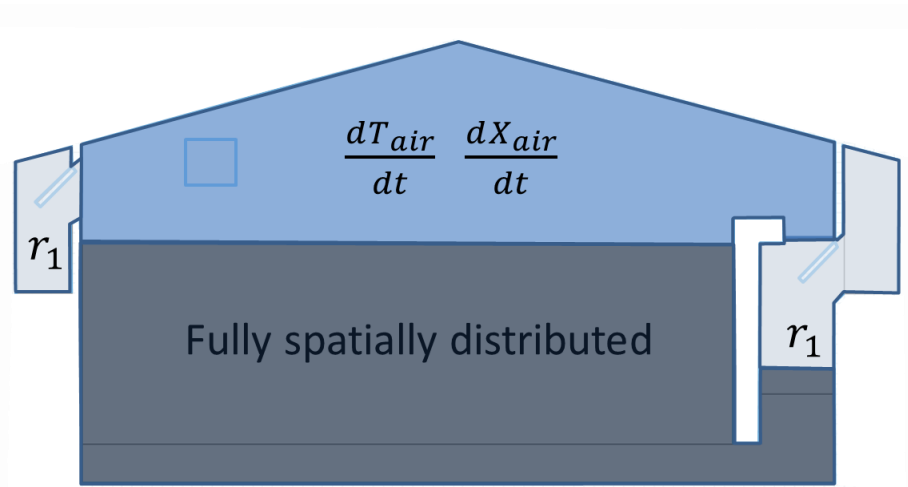
Figure 4-12. Schematic representation of the model. The gray part is fully spatially distributed. The blue part is modelled by ordinary differential equations for air temperature and water content. The light blue part is represented by the derived ratio r_1 (which is replaced with $r_{1\,hum}$ when the humidifier is taken into account.

In Figure 4-12, the gray part represents the fully spatially distributed model. The blue part is covered by ordinary differential equations for the state variables air temperature and water content. The light blue part of the figure is covered by the derived ratio of the opening panels r_1. This ratio is replaced by $r_{1\,hum}$ in cases in which a humidifier is taken into account. Using this modelling approach, the solver is able to converge rather fast, while the effect of mixing internal and external air and the effect of a cooling unit is taken into account. Therefore, this modelling approach is used for the scenario studies, as presented in the next chapter.

5 Scenario studies

In this chapter several scenario studies are presented based on the 2D model, in which different settings of the control input variables are applied for the month December and the month April. The outdoor air conditions of these months were retrieved from the Royal Netherlands Meteorological Institute (KNMI). First long time period simulations on the months December and April are performed in order to evaluate the number of ventilation periods. Next, sensitivity analyses on different scenarios are performed. Finally, cost functions are defined to evaluate the total costs of all scenarios.

5.1 Long-time period simulations

First, simulations over the months December and April are performed to investigate the number of ventilation periods in these months. In order to take the effect of the outdoor temperature on the indoor air temperature through the roof into account as well, a source term is added to the differential equation of the air temperature:

$$V\rho_a C_{pa} \cdot \frac{dT_{aa}}{dt} = \left(\rho_a C_{pa}\, \phi_{bulk}(T_{ap} - T_{aa})\right) \cdot (1-f) + \left(V\rho_a C_{pa} \cdot Cool_T\right) \cdot f \qquad (5\text{-}1)$$
$$+ A_{roof}\, R_{roof}\, (T_{out} - T_{aa})$$

in which A_{roof} represents the roof area and R_{roof} represents the insulation value of the roof, which is equal to $0.28\,[W/m^2/K]$. The simulations are performed according to the settings and initial conditions presented in Table 5-1.

Table 5-1. Overview of settings of the control variables and the initial conditions.

Control variables			Initial conditions	
$\Delta P_{fan} = 150$	$[Pa]$		$T_{aa}(t_0) = T_{ap}(t_0) = T_{pp}(t_0) = 7.5$	$[°C]$
$\Delta T = 2$	$[°C]$		$X_{aa}(t_0) = X_{ap}(t_0) = 6.11$	$[g/kg]$
$T_{pp_{max}} = 7.25$	$[°C]$		$X_{pp}(t_0) = 800$	$[g/kg]$
$T_{pp_{min}} = 6.75$	$[°C]$			

In Table 5-1, ΔP_{fan} represents the pressure drop over the fan, which is related to the fan capacity and ΔT represents the maximum difference between the air temperature during the ventilation periods and the reference product temperature. As mentioned in subsection 4.4, the reference point is located in the middle of the bulk (see Figure 4-6). The desired ventilation temperature can be defined as:

$$T(t)^* = T_{pp\,ref}(t) - \Delta T \qquad (5\text{-}2)$$

If this desired air temperature is restricted by the outdoor air temperature, the following condition hold:

$$if\ T_{pp\,ref} > T_{out} > T^* \rightarrow T^* = T_{out} \qquad (5\text{-}3)$$

The results of the simulations of the months December and April are presented in Figure 5-1. The upper plots present the air and potato temperatures. The yellow band in these plots represents the allowable potato temperature range, which is between $T_{pp_{min}}$ and $T_{pp_{max}}$. The plots in the middle presents the outdoor air temperature and the lower plots shows the ventilation periods.
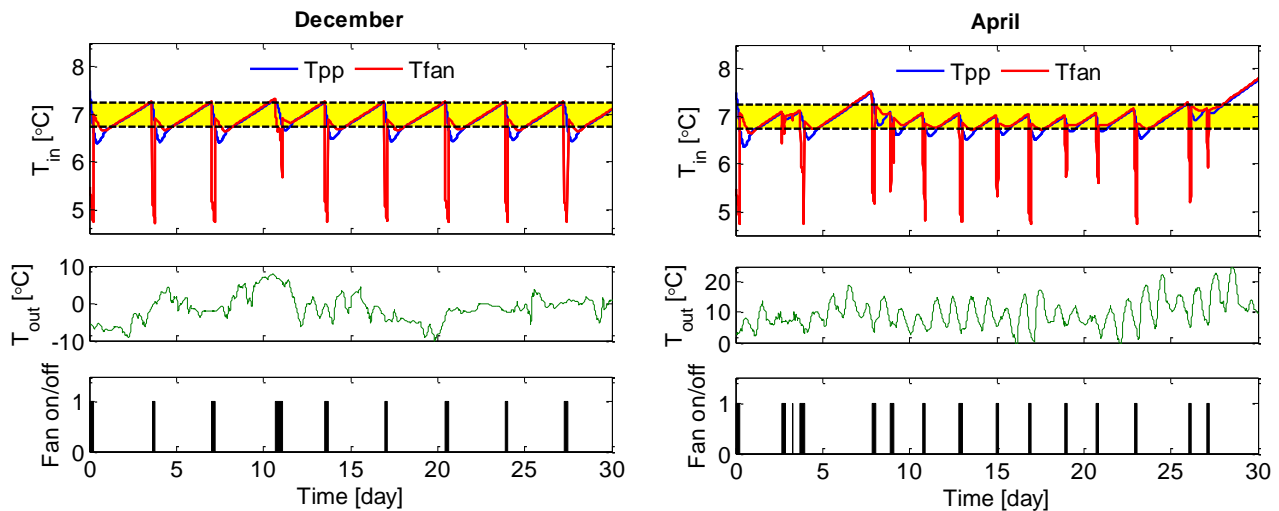

Figure 5-1. Simulations of December (left hand side) and April (right hand side). Upper plots presents the air and potato temperatures, middle plots presents the outdoor air temperature and lower plots presents the ventilation periods.

Figure 5-1 shows that the number of ventilation periods in December and in April are respectively 9 and 15. In April, the air temperature in the fan is often restricted by the outdoor temperature, and therefore more ventilation periods are necessary. Furthermore, the outdoor air temperature is sometimes even above the potato temperature for a longer period and consequently ventilation is not possible. This results in potato temperatures above the allowable yellow range at 8 April and at the end of April. Finally, also a simulation in April is performed in which a mechanical cooling unit is activated. The results of this simulation are presented in Figure 5-2.
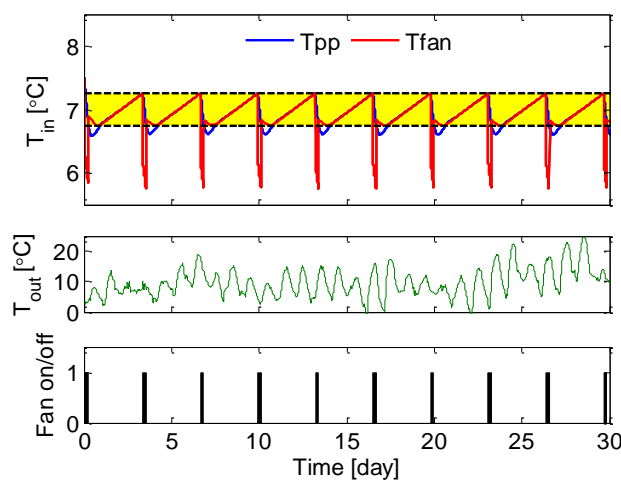
Figure 5-2. Simulation of cooling with mechanical cooling unit in April.

Figure 5-2 shows that 10 ventilation periods are needed in April using a mechanical cooling unit. Since in December, the outdoor air is cold enough, there is no difference in the number of ventilation periods between cooling with outdoor air and cooling with a cooling unit. Table 5-2 presents the number of ventilation periods for April and December, cooling with outdoor air or cooling with a cooling unit.

Table 5-2. Number of ventilation periods per month for several scenarios.

Month	Cooling with	Number of ventilation periods
December	Outdoor air	9
	Cooling unit	9
April	Outdoor air	15
	Cooling unit	10

5.2 Sensitivity analysis of control variables

A sensitivity analysis on the two control variables of the system $\left(\Delta P_{fan}, \ \Delta T, \ \text{see Table 5-1}\right)$ is performed in order to evaluate the behaviour of the system. The control input variables are evaluated in the range of:

$$50 < \Delta P_{fan} < 350 \ [Pa]$$
$$-2 < \Delta T < -0.5 \quad [°C] \tag{5-4}$$

First, the relation between the pressure drop over the fan and the average air velocity through the bulk is evaluated, as presented in Figure 5-3.
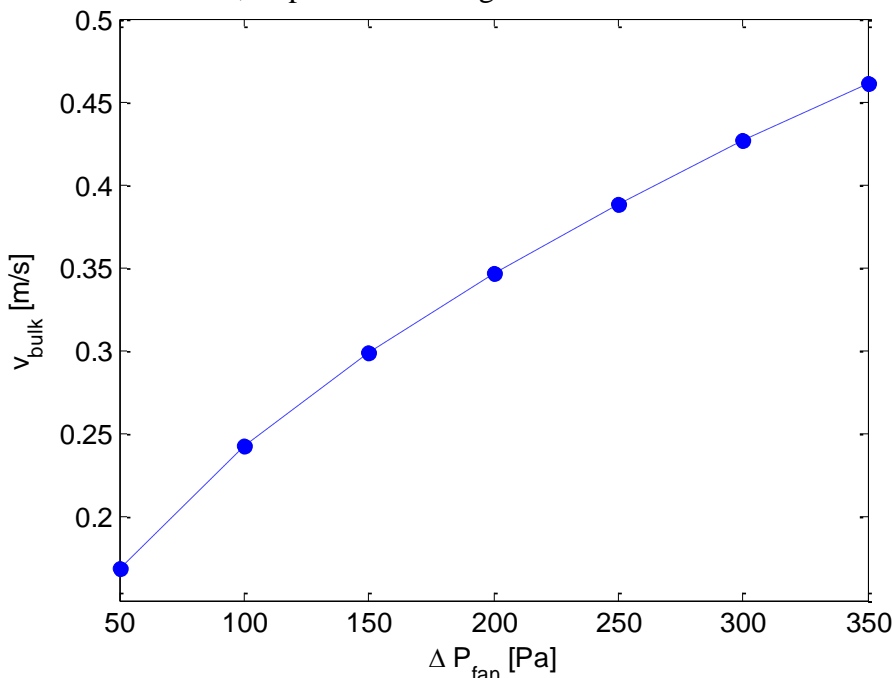
Figure 5-3. Relation ΔP_{fan} and average air velocity through the bulk.

This relation is mainly determined by the modelled airflow resistance through the bulk (see sections 2.3 and 3.2.2.4). In section 4.1, a validation of the system resistance was performed by fitting the correction factor C in the Darcy-Forchheimer law.

61

This validation was based on literature reference values of $\Delta P_{fan} = 150\ [Pa]$ and $v_{bulk} = 0.3\ [m/s]$. This relation may change when the pressure drop over the fan is adjusted. However, since no data of the average air velocity through the bulk is available for other pressure drops, a constant correction factor (C) equals 0.38 is used in the sensitivity analysis.

The average air velocity through the bulk correspond to an air flux through the bulk in the range of $50 < \phi_{air} < 150\ [m^3 air/m^3 product/hour]$.

The simulations are performed using outdoor air conditions of the first of December 2010. The aim was to cool down the potato temperature with $0.5\ ^\circ C$ at initial conditions for the potato temperature and water content of respectively $T(t_0) = 7.5\ [^\circ C]$ and $X(t_0) = 0.8\ [kg/kg]$. This is done for the following scenarios:

- Cooling with outdoor air
- Cooling with outdoor air and humidifier
- Cooling with mechanical cooling unit

These scenarios are evaluated on the ventilation time that is needed to cool down the potato temperature with $0.5\ ^\circ C$ and the corresponding moisture losses from the potatoes.

5.2.1 Cooling with outdoor air
In this set of simulations, the product is cooled down using outdoor air. Figure 5-4 presents the results concerning the time period of ventilation (left hand side) and the related moisture losses from the potatoes (right hand side).
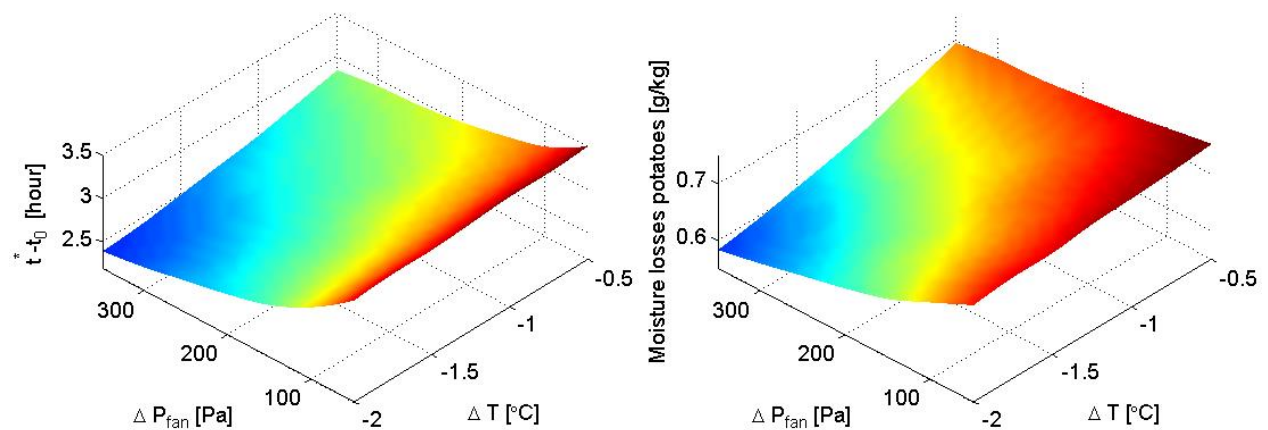

Figure 5-4. Ventilation period (left hand side) and moisture losses from the potatoes (right hand side) for cooling down the potatoes with $0.5\ ^\circ C$ using outdoor air.

Figure 5-4 shows that the ventilation period is shortest (nearly 2.5 hours) at the maximum pressure drop over the fan and the maximum ΔT between the air temperature in the fan and the potato temperature at the reference point. The moisture losses are also lowest at maximum pressure drop and ΔT. Furthermore, an increase of ΔP_{fan} from $150\ [Pa]$ to $300\ [Pa]$ and $\Delta T = -1.25\ ^\circ C$ results in:

- Decrease in ventilation time of approximately 10%
- Decrease in moisture losses of approximately 7%

These results can be explained by the fact that a higher pressure drop over the fan results in a higher (cold) airflow through the bulk. Consequently, the product is cooled down faster and the desired cooling of $0.5\,°C$ is reached earlier. Similar explanation holds for a large ΔT, since by large difference between the potato reference temperature and the ventilated air temperature, the cooling process is also faster. Due to a shorter ventilation period, less moisture is lost from the potatoes. This explains why minimal moisture losses from the potatoes is reached at maximum pressure drop over the fan and maximum ΔT.

5.2.2   Cooling with outdoor air and humidifier

In this set of simulations, the product is cooled down with outdoor air. Furthermore, a humidifier is activated, which cool down and humidifies the air. Due to the humidifier, the system resistance is increased by $100\,[Pa]$. Therefore, the pressure drop over the fan is evaluated in the range of $150 < \Delta P < 450\,[Pa]$. Figure 5-5 presents the results concerning the time period of ventilation (left hand side) and the related moisture losses from the potatoes (right hand side).
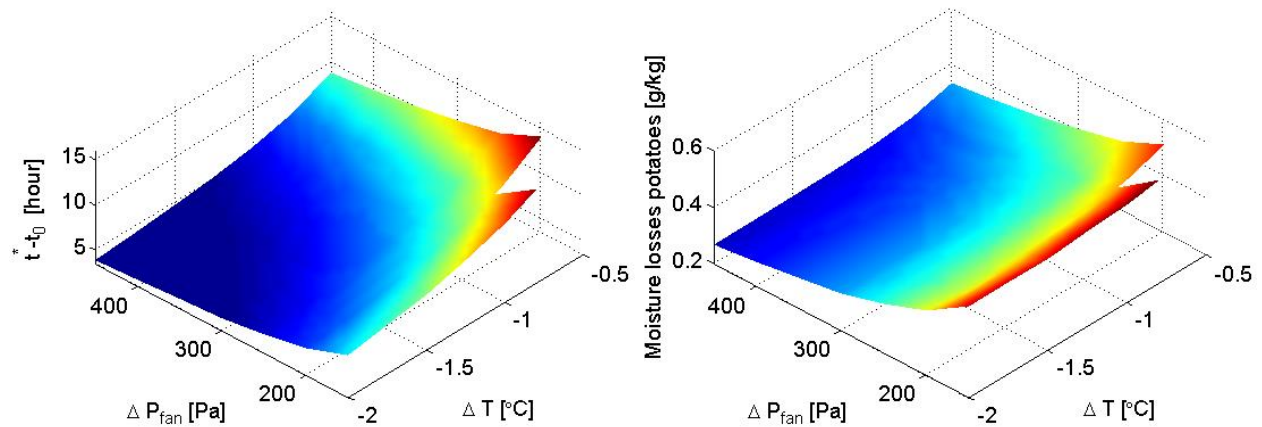

Figure 5-5. Ventilation period (left hand side) and moisture losses from the potatoes (right hand side) for cooling down the potatoes with $0.5\,°C$ using outdoor air and humidifier.

In Figure 5-5, one data point is missing (at $\Delta P_{fan} = 150\,[Pa]$ and $\Delta T = 0.5\,[°C]$). This is caused by the fact that using these control settings, the desired cooling of $0.5\,°C$ was not reached within the simulation time. This phenomena will also be seen in the following analyses. Figure 5-5 shows shortest ventilation period and lowest moisture losses at maximum ΔP_{fan} and maximum ΔT. In this scenario, an increase of ΔP_{fan} from $200\,[Pa]$ to $400\,[Pa]$ and $\Delta T = -1.25\,°C$ results in:

- Decrease in ventilation time of approximately 35%
- Decrease in moisture losses of approximately 30%

The same reasoning as stated in the previous subsection explains the shortest ventilation period and lowest moisture losses at maximum ΔP_{fan} and maximum ΔT.

5.2.3   Cooling with mechanical cooling unit

In this simulation, a mechanical cooling unit is activated in order to cool down the potatoes. The panels are completely closed, so only internal air is used for ventilation. Figure 5-6 presents the results concerning the time period of ventilation (left hand side) and the related moisture losses from the potatoes (right hand side).
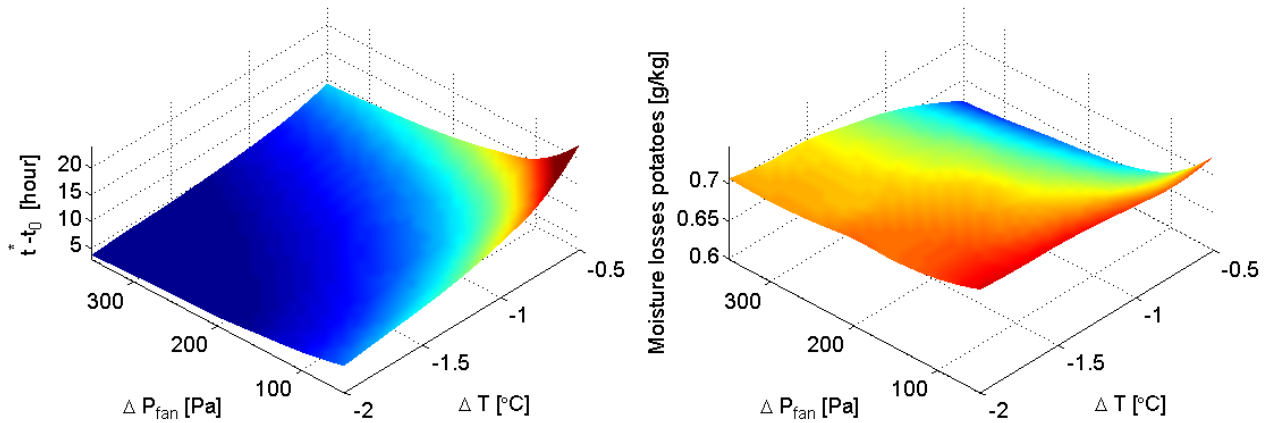
Figure 5-6. Ventilation period (left hand side) and moisture losses from the potatoes (right hand side) for cooling down the potatoes with $0.5\,°C$ using a mechanical cooling unit.

Figure 5-6 shows shortest ventilation period at maximum ΔP and maximum ΔT. The moisture losses from the potatoes are lowest at maximum ΔP and minimum ΔT. In this scenario, an increase of ΔP_{fan} from $150\,[Pa]$ to $300\,[Pa]$ and $\Delta T = -1.25\,°C$ results in:

- Decrease in ventilation time of approximately 25%
- Decrease in moisture losses of approximately 3%

The same reasoning as stated in the previous subsections explains the shortest ventilation period, which is reached at maximum ΔP_{fan} and maximum ΔT. However, the moisture losses from the potatoes are lowest at maximum ΔP and minimum ΔT (see Figure 5-6, right panel). This is caused by the functioning of the mechanical cooling unit. Cooling down the air temperature above the bulk by the mechanical cooling unit results in a decrease of the absolute water content of the air as well (with rate r_X, see section 4.3). This decrease in absolute water content is smaller at smaller ΔT, so cooling with a smaller ΔT results in higher absolute water content of the ventilated air and therefore less moisture losses.

5.2.4 Comparing scenarios

In order to compare the three scenarios presented above, the needed ventilation time and the moisture losses are presented in Figure 5 6, in which all surface plots have similar axes.
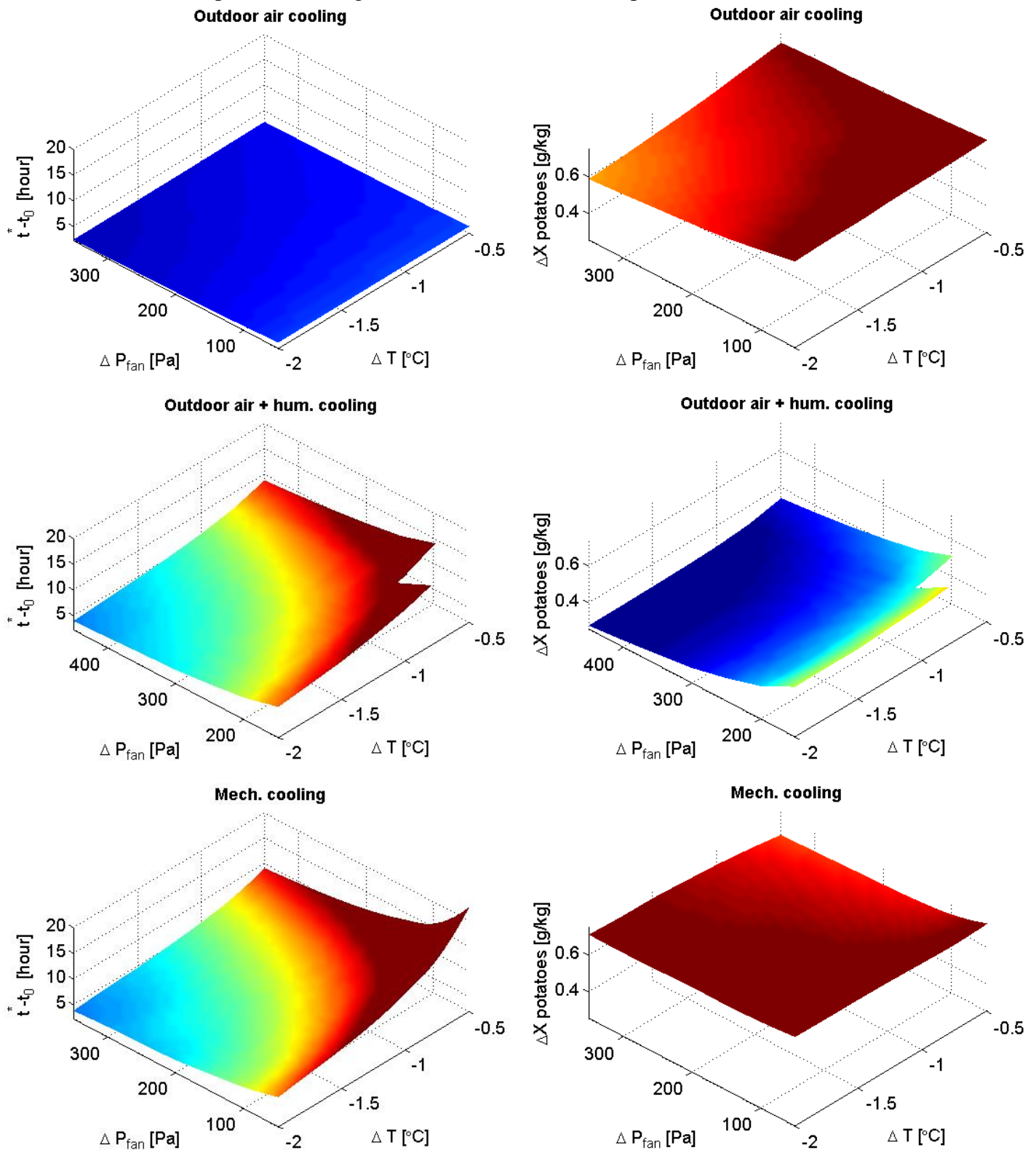
Figure 5-7. Comparing ventilation time and moisture losses from potatoes between the scenarios.

65

Comparing the scenario of outdoor air cooling in combination with a humidifier with the scenario of only outdoor air cooling results with respect to ventilation time and moisture losses:

- Increase in ventilation time in range of 70 – 480 % (depending on settings control variables; the larger ΔP_{fan} and ΔT, the smaller the increase in ventilation time)
- Decrease in moisture losses in range of 40 – 55 % (depending on settings control variables; the larger ΔP_{fan} and ΔT, the larger the decrease in moisture losses)

The needed ventilation time increases significantly by using a humidifier. This is caused by the high humidity of the ventilated air. Due to this high humidity, cooling of the potatoes by evaporation is limited and only sensible cooling occurs, which slows down the cooling process. Due to the limited evaporation process in the bulk, the moisture losses from the potatoes are limited as well.

Comparing the scenario of mechanical cooling with the scenario of only outdoor air cooling results with respect to ventilation time and moisture losses:

- Increase in ventilation time in range of 58 – 550 % (depending on settings control variables; the larger ΔP_{fan} and ΔT, the smaller the increase in ventilation time)
- Change in moisture losses in range of +21 – -10 %
  (depending on settings control variables;
    - largest increase in moisture losses at maximum ΔP_{fan} and ΔT
    - largest decrease in moisture losses at maximum ΔP_{fan} and minimum ΔT)

The needed ventilation time is increases significantly by using a mechanical cooling unit. This is caused by the functioning of a cooling unit. Two processes are involved by mechanical cooling, namely cooling down the air above the bulk and ventilation of the cold air (as explained in subsection 4.5.2.). Therefore the total time needed for cooling and ventilation is increased. The moisture losses from the potatoes are higher or lower compared to the scenario with outdoor air cooling, depending on the settings of the control variables. On the one hand, the moisture losses increase due to the longer ventilation time but on the other hand the moisture losses decrease due to a higher humidity of the ventilated air.

These scenarios are also performed for the first day of April. The results for mechanical cooling are similar to the one of December. Due to higher outdoor air temperature, not all control settings are feasible to cool down the reference potato temperature with outdoor air. Furthermore, the relative humidity on the evaluated data of the first day of April is relatively high and therefore the effect of the humidifier is limited. The results of the scenario studies on the first day of April are presented in Appendix C.

5.3 Economic evaluation

In order to perform an economic evaluation for the scenarios presented in section 5.2, cost functions with respect to ventilation, weight loss of the potatoes, the humidifier and the mechanical cooling are derived.

5.3.1 Cost functions

Ventilation costs
The ventilation costs consist of energy consumption of the system fans and are influenced by the time period, the fan capacity and the electricity price. The following cost function is derived to approximate the ventilation costs:

$$C_{sys\,fan} = \frac{\Delta P_{fan} \cdot \phi_{fan} \cdot t \cdot p_{elec}}{n_{ton}} \tag{5-5}$$

Here, p_{elec} [€/Ws] represents the electricity price and t [s] represents the ventilation time. The fan capacity is covered by ΔP_{fan} [Pa] (pressure drop over the fan) and ϕ_{fan} [m^3/s] (airflow through the fan). In order to express the cost per ton, the total costs are divided by the total weight of the potatoes (n_{ton} [ton]).

Costs moisture loss potatoes
The moisture losses from the potatoes results in a lower total weight of the potatoes at the end of the season and consequently reduce the earnings from selling the potatoes. The following cost function is derived to evaluate the costs related to moisture losses from the potatoes:

$$C_{weight\,loss} = \Delta X \cdot p_{potatoes} \tag{5-6}$$

Here, ΔX [kg/kg] represents the weight loss of the potatoes and $p_{potatoes}$ [€/kg] represents the potato selling price.

Costs mechanical cooling
The costs related to the mechanical cooling consist of energy consumption by the cooling unit, which is related to the capacity of the cooling unit. The energy usage of the cooling unit can be derived using the fan capacity, the energy efficiency ratio of the cooling unit and the cooling period. The following cost function is derived to evaluate the energy costs of the cooling unit:

$$C_{cooling\,unit} = \frac{E_{cooling\,unit} \cdot p_{elec}}{n_{ton}}$$
$$E_{cooling\,unit} = \frac{P_{cool} \cdot t}{EER} \tag{5-7}$$

Here, $E_{cooling\,unit}$ [Ws] is the energy consumption by the cooling unit, P_{cool} [W] is the capacity of the cooling unit and EER [−] is the energy efficiency ratio.

Costs humidifier

The costs related to the humidifier consist out of the water usage by the humidifier, the energy consumption related to pumping the water through the humidifier and extra energy consumption of the fans, since a humidifier increases the system resistance by $100 \, [Pa]$, which has to be overcome by the system fans. However, the costs related to the water usage are really small (0.1 %) compared to the total costs. Therefore, these costs are not taken into account. The following cost function is derived in order to evaluate the cost related to the humidifier:

$$C_{humidifier} = C_{pump} + C_{sys\,fan}^{\,*}$$

$$C_{pump} = \frac{P_{pump} \cdot t \cdot p_{elec}}{n_{ton}}$$

(5-8)

* *Extra costs for ventilation can be calculated using equation* (5-5)

Here, $P_{pump}[W]$ is the capacity of the pump.

For the evaluation of the total costs of each scenario, parameter values presented in Table 5-3 are used.

Table 5-3. Overview parameter values for cost evaluation.

Parameter				Description
P_{elec}	=	0.10	$[€/kWh]$	Electricity price
$P_{potatoes}$	=	0.12	$[€/kg]$	Potato price
n_{ton}	=	235 000	$[kg]$	Weight of potatoes
	=			$\left(= l_{bulk} \cdot w_{bulk} \cdot h_{bulk}\rho_{pot} = 16.5 \cdot 4 \cdot 3.5 \cdot 1.080 = 235\,ton \right)$
EER	=	3.18	$[-]$	Energy efficiency ratio
P_{pump}	=	300	$[W]$	Pump capacity

5.3.2   Costs evaluation scenarios

Using the cost functions presented in the subsection 5.3.1 and the number of ventilation periods (section 5.1), the total costs per month of each scenario is evaluated, where total costs are defined as the costs for cooling down with 0.5 °C multiplied by the number of ventilation periods. The surface plots resulting from the individual scenarios are presented in
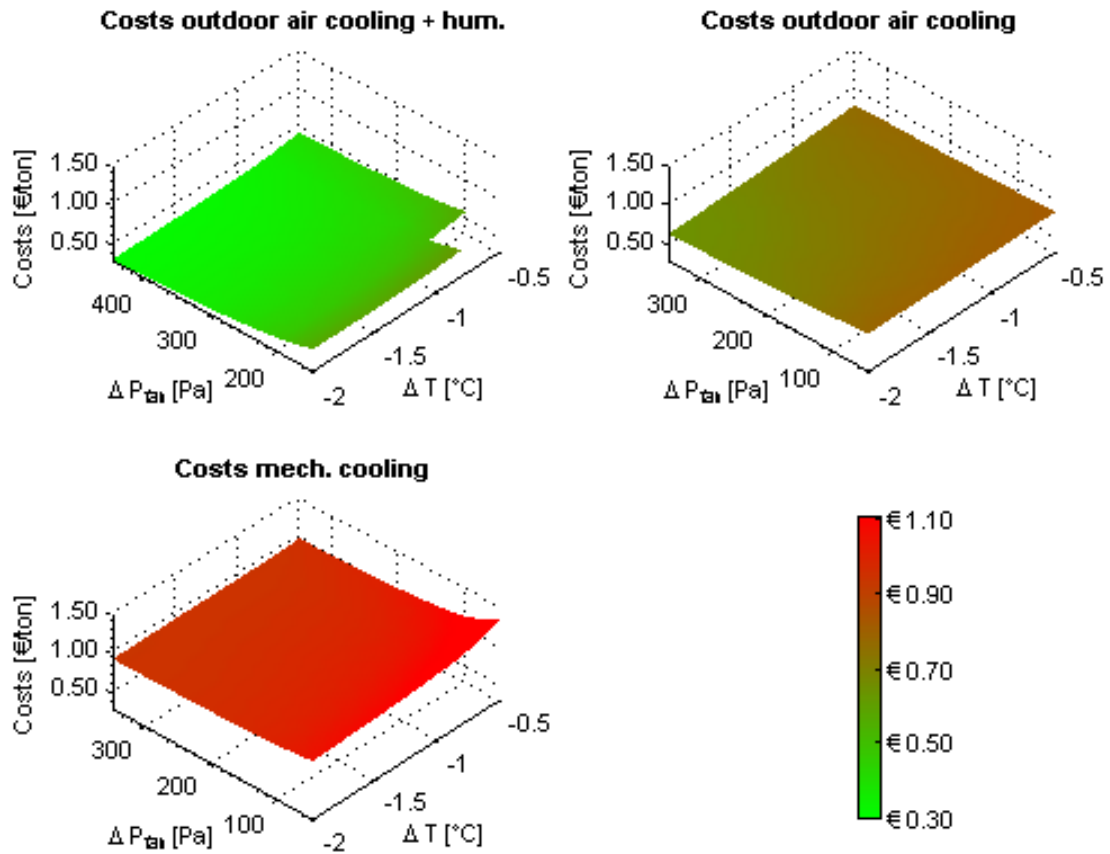
Figure 5-8. Total costs for several scenarios in December for cooling down the potato temperature with 0.5 °C.

Appendix D. In order to compare all scenarios based on outdoor air conditions of December, the surface plots containing the total costs of each scenario are presented in Figure 5-8.

Figure 5-8 shows that lowest total costs can be obtained by cooling with outdoor air in combination with a humidifier. The total costs in the scenario in which cooling is done by outdoor air only are approximately doubled compared to the scenario with a humidifier. The costs of the scenario in which the cooling unit is applied are approximately three times higher compared to the lowest cost scenario.

The lowest total costs in the scenario of cooling with outdoor air in combination with a humidifier can be explained by the significant reduction in moisture losses of the potatoes compared to the scenario without humidifier. Since the total costs mainly depends on the selling price of the potatoes, the extra costs due to the higher system resistance of the humidifier are minor compared with the decreasing costs of the moisture losses.

The highest costs are obtained in the scenario of cooling with a mechanical cooling unit. This is because extra energy costs, due to the energy usage of the mechanical cooling unit, have to be taken into account. Since cooling with a mechanical cooling unit reduces neither the total ventilation time nor the moisture losses, these extra energy costs are not compensated and therefore the total costs are highest compared to the other scenarios.

Similar to Figure 5-8, a comparison between the total costs of all scenarios in April is performed. These results are presented in Figure 5-9. For several combinations of the control variables in the scenarios in which outdoor air was involved, the goal of cooling down the potatoes with $0.5\,°C$ was never reached. Therefore, these combinations of control variables were not feasible and consequently, total costs could not be calculated for these settings. This explains the fragmented surface plots of the scenarios in which outdoor air is involved.
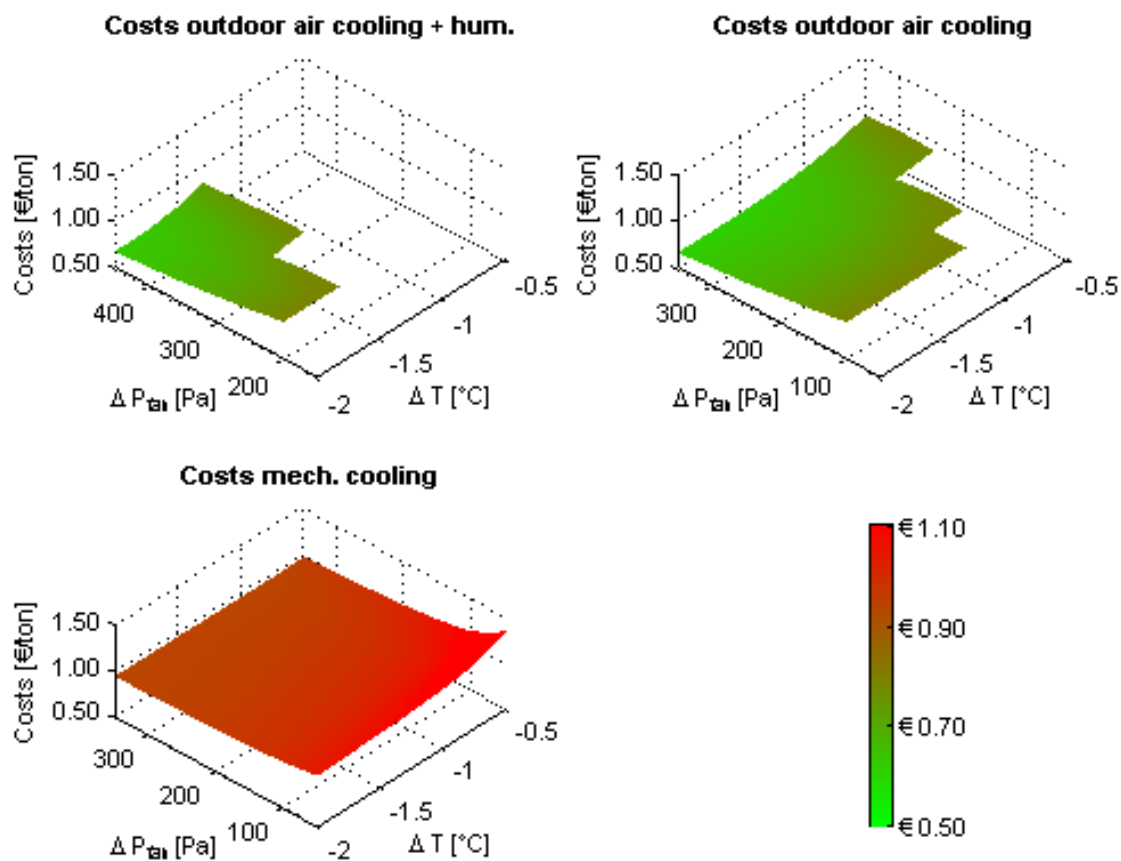
Figure 5-9. Total costs for several scenarios in April for cooling down the potato temperature with $0.5\,°C$.

Comparing the scenarios performed in April shows that the total costs of the two scenarios in which outdoor air is involved are approximately equal to each other. The relative humidity of outdoor air on the first day of April was already between 93-97%, so the effect of the humidifier is limited. Therefore, nearly no reduction in moisture losses are obtained using a humidifier and therefore the total costs of the two scenarios with cooling with outdoor air are approximately equal. The total costs for the scenario in which the cooling unit is applied are approximately 1.5 as high. This can be explained by the extra energy costs of the cooling unit.

5.3.3   Sensitivity analysis on prices

The economic evaluations of the several scenarios presented in the previous section are based on an average potato and electricity price. In order to investigate the sensitivity of the total costs with respect to other prices, a sensitivity analysis is performed. In this analysis, the total costs of all scenarios are evaluated for the following prices:

$$p_{potatoes} = € 0.20 \land p_{electricity} = € 0.06$$

$$p_{potatoes} = € 0.06 \land p_{electricity} = € 0.14$$

(5-9)

These prices are based on the real potato and electricity prices over the last years.

The shape of the surface plots regarding the total costs is not changed for cooling with outdoor air (with or without humidifier). However, for the scenario in which the mechanical cooling unit is activated, the shape of the total costs surface plot is slightly changed, as presented in Figure 5-10.
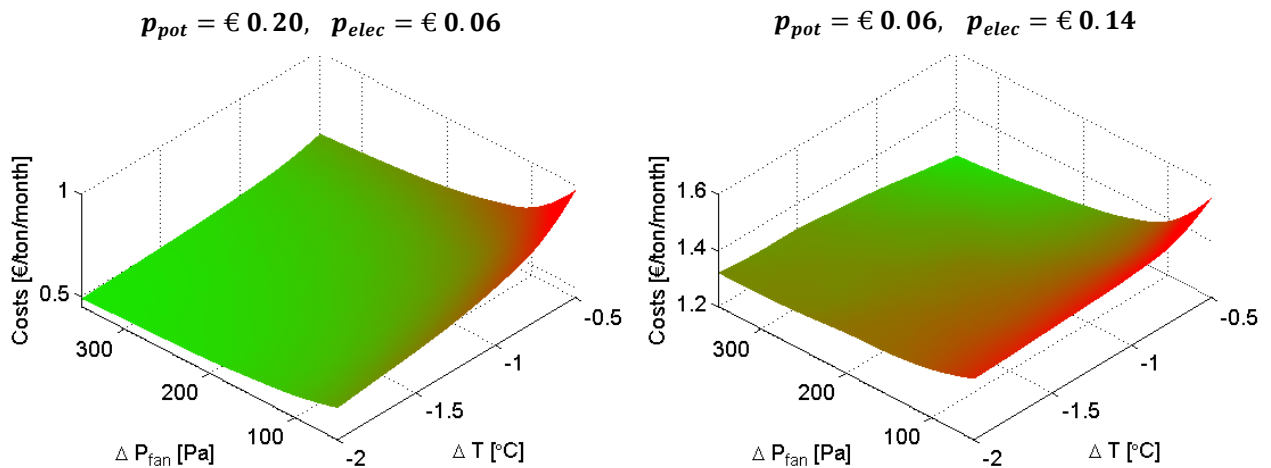
Figure 5-10. Total costs for cooling with mechanical cooling in December for high potato and low electricity prices (right hand side) and for low potato and high electricity prices (left hand side).

For high potato and low electricity prices, the minimal total costs can be obtained by a maximum ΔT, while for low potato and high electricity prices, the minimal total costs is obtained at minimum ΔT. The surface plots regarding the sensitivity analysis of all other scenarios are presented in Appendix E.

As mentioned before, only the shape of the total costs surface is slightly changed for the scenario of mechanical cooling. This can be explained that due to the mechanical cooling, the total costs are sensitive to both the potato and the electricity price, while the total costs of the other scenarios are mainly determined by only the potato price.

72

5.3.4   Optimal cooling strategy over a total storage period

As presented in the previous subsection, the lowest costs can be obtained by cooling with outdoor air in combination with a humidifier, followed by cooling with outdoor air only. The evaluations show that cooling using a mechanical cooling unit is the most expensive option. Therefore, the following heuristic cooling strategy over a storage period is defined as optimal:

- Cooling with outdoor air and humidifier
- Cooling with outdoor air without humidifier if the outdoor air is already saturated
- Cooling with mechanical cooling unit if outdoor conditions are insufficient to cool down the potato temperature

Finally, an evaluation is done to investigate for which outdoor air conditions cooling with outdoor air is feasible. The result of this simulation is presented in Figure 5-11.
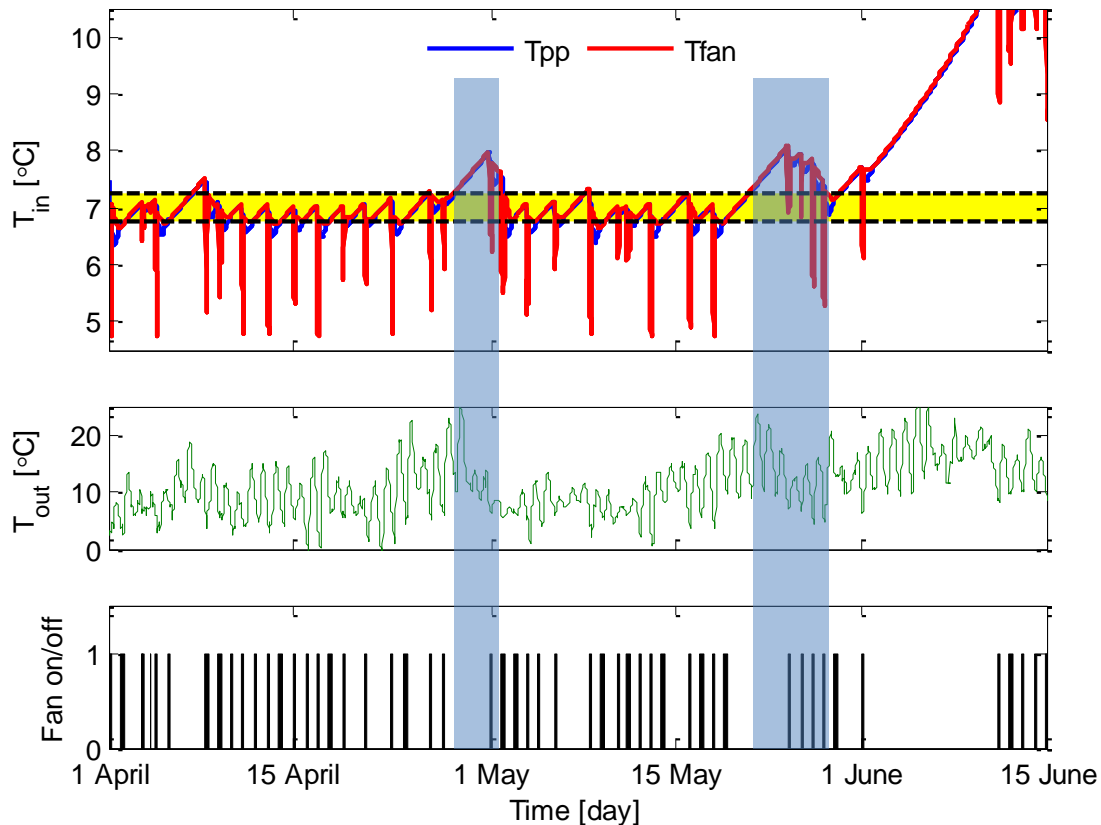
Figure 5-11. Long-time simulation of cooling with outdoor air. Upper plot presents the air and potato temperatures, middle plot presents the outdoor air temperature and lower plot presents the ventilation periods. The two blue areas in the plot indicates the timespan in which the reference potato temperature is above the maximum allowed potato temperature.

Figure 5-11 shows that until the first of June, the reference potato temperature is only in two periods higher than the maximum allowed potato temperature (indicated by the two blue areas in Figure 5-11).

In order to investigate how fast the potato reference temperature increases, the results in the timespan of 22 April until 1 May are presented in Figure 5-12.
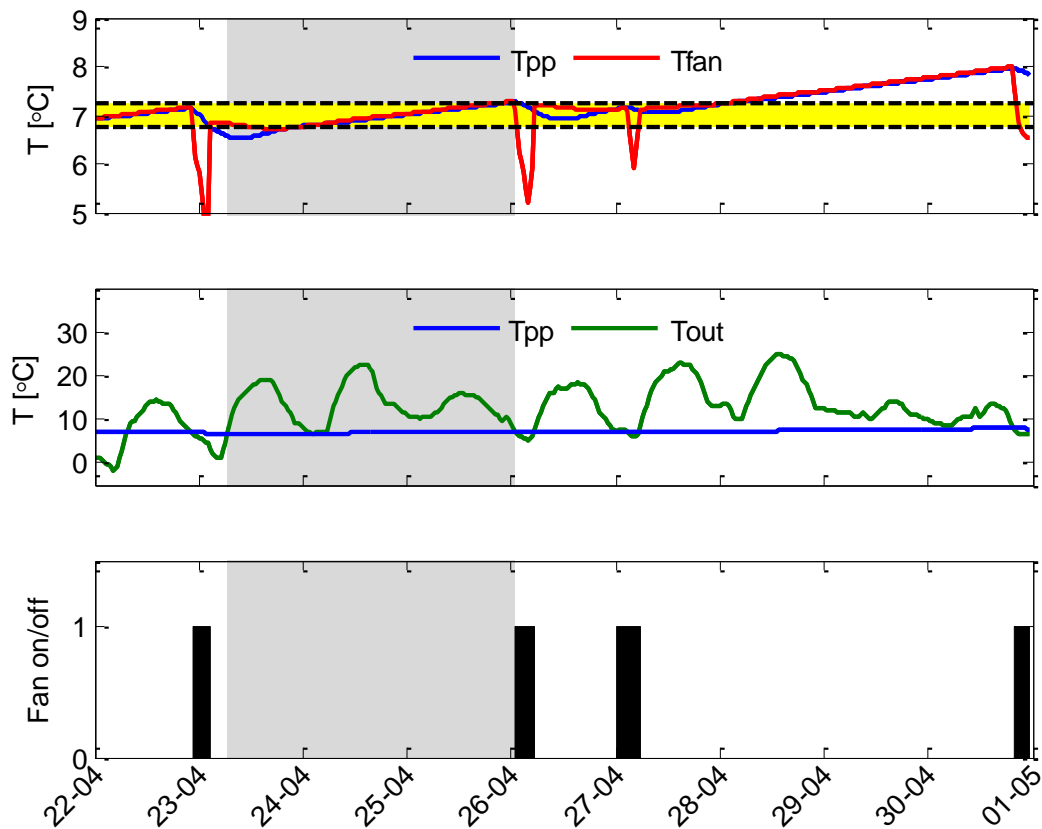
Figure 5-12. Simulation of cooling with outdoor air from 22 April until 1 May. Upper plot presents the air and potato temperatures, middle plot presents the outdoor air temperature and potato temperature and lower plot presents the ventilation periods. The gray area in the plots indicates the time between 23 April and 26 April in which no ventilation occurs due to high outdoor temperature, but the reference potato temperature is below the allowed maximum potato temperature.

The gray area in Figure 5-12 shows that if the outdoor temperature is approximately three day higher compared to the reference temperature (so no ventilation occurs), the reference potato temperature can still be kept below the maximum allowed potato temperature. When the potato reference temperature is already close to the maximum allowed potato temperature or the outside air temperature is for a longer period than three days above the potato reference temperature, the potato temperature is higher than the maximum allowed potato temperature, as indicated by the two blue areas in Figure 5-11.

So, from this simulation, it can be stated that cooling with outdoor air is feasible as long as the outdoor air temperature is no longer than three days above the potato reference temperature and the potato temperature is cooled down to the minimum allowed potato temperature during the ventilation periods.

74

6   Discussion

In this chapter, the results which have been presented in the previous chapters, will be discussed. First, the model limitations are described, followed by model and simulation accuracy issues.

6.1 Model limitations

In the model, the potato quality is based on potato temperature and moisture content, since these two physical quantities are leading in potato quality. However, also other physical and biological processes determine the composition of compounds in the potato and consequently influence the potato quality. In order to focus more on the potato quality, in addition to potato temperature and moisture content, the biological processes related to the contents of sugar, proteins and starch should be included in the model, as well. Moreover, the oxygen, CO_2 and ethylene concentrations in the air also affect the potato quality. Consequently, for modelling of the potato quality, these balances should also be included.

Having a more complete model, also allows the design of more advanced controllers in potato bulk storage facilities. In this research, the ventilation and cooling strategies are only based on the potato temperature. However, including also CO_2 and ethylene balances in the model, ventilation and cooling strategies can be based on these concentrations, resulting in advanced potato quality control.

6.2 Model accuracy

Since no experimental data was available, no databased validation of the model was performed. First, a visual inspection of the simulation results was done in order to investigate if all results are at least in a feasible range. Furthermore, Grubben (2013) presented a model that was calibrated and validated. In this research, similar parameter values related to the physics of the potatoes were used, assuming that the parameter values in Grubben (2013) are correct. Furthermore, validation of the pressure drop over the bulk was performed based on literature values.

A very sensitive parameter related to changes in potato temperature and moisture content is the evaporation coefficient (K_{evap}). Grubben (2013) calibrated the model and found an evaporation value of $K_{evap} = 0.0002 \ [kg/m^2/s]$. However, literature values of this parameter were found in the range of $0.000388 \ [kg/m^2/s]$ (Lukasse, 2007) and $0.0007848 \ [kg/m^2/s]$ (Kondrashov, 2007), so the evaporation coefficient varies by a factor of two. This parameter uncertainty may influence the results of this study.

As described in chapter 4, the 2D model was simplified in order to evaluate the system in combination with a switching controller. The part of the model related to the moving panels was replaced by a ratio which defines the mixing air conditions. Furthermore, it was not feasible to switch very frequently between mechanical cooling and ventilation and therefore, these activities take place simultaneously.

In order to correct for respectively the cooling and ventilation time, the fraction f was determined. This fraction is based on the heating of the air above the bulk during the ventilation period and the cooling of this air during the cooling period (see equation (4-14)). However, due to diffusion, the air above the bulk is heated by the bulk also during cooling period. This diffusion effect is not taken into account by deriving the fraction f. However, compared to forced convection during the ventilation, the diffusion rate is very small and therefore, the influence on the cooling and ventilation periods can be neglected.

By connecting a controller to the model, the original full 2D model was simplified to allow appropriate solutions by COMSOL. Approximations were made with respect to the mixing air conditions (caused by the moving panels) and the functioning of the cooling unit (simultaneously cooling and ventilation). Furthermore, the scenario and sensitivity studies are only performed in 2D simulations, and therefore the average effect of the cooling unit in 3D is projected in the 2D simulations. Due to these simplifications, some dynamics might be lost, and thus reducing the accuracy of the model.

6.3   Simulation accuracy

Due to the numerical solutions of the system, numerical errors are included in the simulation results. Furthermore, stabilization techniques add numerical diffusion to the physical states. It is hard to estimate to what extent the numerical errors influences the final results. In order to check the sensitivity of the final results on errors, the surface plots of the ventilation time and the moisture losses from the potatoes are changed as follows:

- Minima of ventilation period and moisture losses are increased by 5%
- Maxima of ventilation period and moisture losses are decreased by 5%

The original and perturbed surface plots of the ventilation time and moisture loss are presented in Appendix F. Finally, the original surface plot containing the economic costs is compared to the surface plot containing the economic costs after perturbing the ventilation time and moisture losses as described above. A comparison between the economic costs is presented in Figure 6-1.
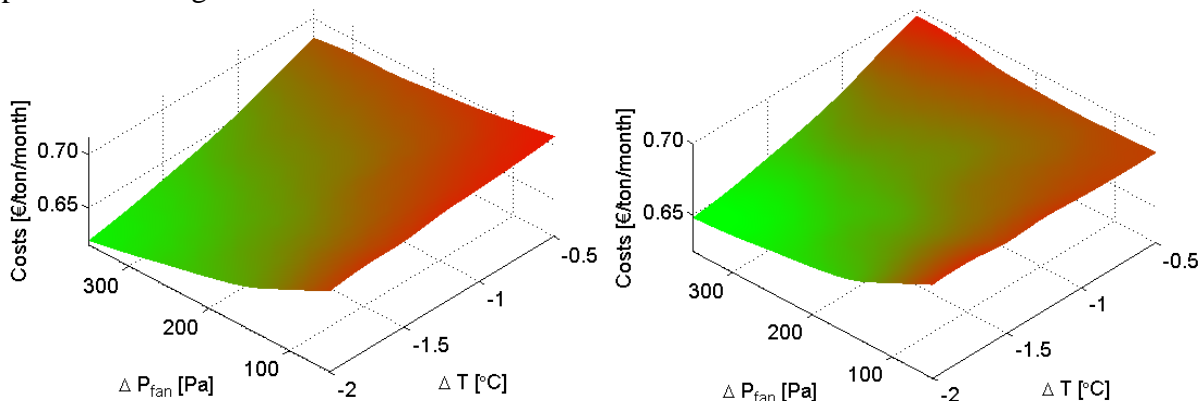

Figure 6-1. Original cost plot (left hand side) and cost plot after manipulating data (right hand side).

Figure 6-1 shows that, although the absolute costs are different, the shape of the surface plots is almost similar to each other. Therefore, comparing the total costs of the scenarios will not lead to different control settings.

7   Conclusion

In a study of Grubben (2013), a spatially distributed 2D model was developed for bulk potato storage. However, not all parts of an advanced storage facility were taken into account in that study. In this research, all parts of an advanced storage facility are modelled, including air conditioning equipment. Based on this model, several scenarios were simulated. With these simulations, the defined research questions can be answered.

The following main research question was defined:

How to set up a dynamic 2/3 D simulation of an advanced climate controlled bulk storage facility?

By coupling all domains of the storage facility using the correct boundary conditions for each state, the total system can be solved in one step. However, 3D simulations entail very long computational times and are therefore not feasible for long term scenario and sensitivity studies. Therefore, the effect of the cooling unit on temperature and humidity was evaluated in 3D (since this effect is not uniform in all directions) and subsequently, the volume averages of temperature and humidity were projected in the 2D simulations.

In these 2D simulations, it is possible to simulate the effects of the air conditioning equipment. However, including a controller that frequently switches the equipment on and off during the simulation resulted in oscillatory behaviour of the system. Therefore, the air domain containing the moving panels was evaluated and a relationship between the mixed air conditions and the opening of the panels was derived. The air domains related to the moving panels were replaced by this relationship. Using this adapted model and a controller based on a specific potato temperature in the bulk, 2D simulations could be performed for several scenarios in which the system is controlled.

What is the influence of the settings of the control input variables on the system behaviour?
Two control input variables of the system are defined, namely the pressure drop over the fan (ΔP_{fan}) and the difference between a specific potato temperature in the bulk and the ventilated air temperature (ΔT). The settings of these control input variables were evaluated on the needed ventilation time and moisture losses from the potatoes by cooling down the potato temperature with $0.5\ °C$. This is done for several scenarios. Based on the simulations, the following rules of thumb were derived:

Scenario with outdoor air cooling
An increase of ΔP_{fan} from $150\ [Pa]$ to $300\ [Pa]$ (at $\Delta T = -1.25\ °C$) results in:

- Decrease in ventilation time of approximately 10%
- Decrease in moisture losses of approximately 7%

Scenario with outdoor air cooling + humidifier
An increase of ΔP_{fan} from 200 $[Pa]$ to 400 $[Pa]$ (at $\Delta T = -1.25\ °C$) results in:

- Decrease in ventilation time of approximately 35%
- Decrease in moisture losses of approximately 30%

Scenario with mechanical cooling
An increase of ΔP_{fan} from 150 $[Pa]$ to 300$[Pa]$ and $\Delta T = -1.25\ °C$ results in:

- Decrease in ventilation time of approximately 25%
- Decrease in moisture losses of approximately 3%

What is the effect of actuators (cooling unit and humidifier) on the system behaviour?
The scenarios in which the different methods of cooling are evaluated, were performed twice, one based on the outdoor conditions in December and one based on the outdoor conditions in April. Compared to the cooling process with outdoor air in December, the following relations are found:

Scenario with outdoor air cooling + humidifier
- Increase in ventilation time in range of $70 - 480$ % (depending on settings control variables)
- Decrease in moisture losses in range of $40 - 55$ % (depending on settings control variables)

Scenario with mechanical cooling
- Increase in ventilation time in range of $58 - 550$ % (depending on settings control variables)
- Change in moisture losses in range of $+21 - -10$ % (depending on settings control variables)

Due to different outdoor conditions, the results of the scenario studies evaluated on data of April are slightly different. Furthermore, due to higher outdoor temperature, not all control settings are feasible, so only large ΔP_{fan} and large ΔT resulted in reaching the goal of cooling down the potato temperature.

What are the optimal settings with respect to the economic costs over a storage period?
The economic evaluation of the performed scenario studies showed that, in December and in April, cooling with a mechanical cooling unit is the most expensive method. This is caused by the extra energy consumption of the cooling unit.

Cooling with outdoor air and a humidifier is most effective in situations with low humidity of the outdoor air (December). Since in April, the outdoor air humidity is relatively high, the effect of the humidifier is limited and therefore, the total costs over the month April are equal in case of cooling with and without humidifier. So, storing according to the following method will result in the lowest costs:

- Cooling with outdoor air and humidifier
- Cooling with outdoor air without humidifier if the outdoor air is already saturated
- Cooling with mechanical cooling unit if outdoor conditions are insufficient to cool down the potato temperature

To minimize the total costs, the control input variables should be set at maximum feasible values, so maximum pressure drop over the fan and maximum allowed difference between cooling air temperature and potato temperature.

8   Recommendations

In this study, the climate in an advanced bulk storage facility is evaluated. From this evaluation, several rules of thumb were defined. These results can be used for further research and applications, which are described in this chapter.

The model used in this research contains only temperature and moisture balances of the air and the product. However, several other processes related to CO_2 and ethylene concentrations in the storage facility influence the product quality, as well. In order to evaluate these phenomena, the model should be extended by including these balances.

This study shows that 2D and 3D simulations of an advanced storage facility are feasible using the software package COMSOL Multiphysics 4.4. However, implementing a low-level controller in this software leads to oscillatory behavior of the system and consequently unstable solutions. To overcome this, a connection between the software packages COMSOL and Matlab should be made. By doing this, advanced controllers can be implemented in Matlab and evaluated by the model in COMSOL. In this way, no assumptions have to be made related to implementing the controller part and consequently the system can be evaluated more accurately.

The results of this study can be used for practical applications. With the use of the "Application Builder", included in the software COMSOL Multiphysics 5.0, an application of the model can be built. This application can be used to provide farmers more insight into the system behaviour and advice farmers by choosing the optimal control settings during the storage period.

9   References

Amos, N. D. 1995. Mathematical modelling of heat transfer and water vapour transport in apple coolstores: a thesis presented in partial fulfilment of the requirements for the degree of Doctor of Philosophy in Biotechnology and Bioprocess Engineering at Massey University.

ASAE Standards.1997.Resistance to airflow of grain, seeds, other agricultural products and perforated metal sheets.

Beukema, K. J., S. Bruin, and J. Schenk. 1982. Heat and mass transfer during cooling and storage of agricultural products. *Chemical Engineering Science* 37(2):291-298.

Chourasia, M., and T. Goswami. 2007. Three dimensional modeling on airflow, heat and mass transfer in partially impermeable enclosure containing agricultural produce during natural convective cooling. *Energy conversion and management* 48(7):2136-2149.

Darcy, H. 1856. *Les fontaines publiques de la ville de Dijon: exposition et application*. Victor Dalmont.

Ergun, S. 1952. Fluid flow through packed columns. *Chem. Eng. Prog.* 48:89-94.

Forchheimer, P. 1901. Wasserbewegung Durch Boden: Zeitschrift des Vereines Deutscher Ingenieure, v. 45.

Grubben, N. L. M. 2013. *Agricultural storage : concepts and modelling*. S.l.: s.n.

Hauke, G. 2002. A simple subgrid scale stabilized method for the advection–diffusion-reaction equation. *Computer Methods in Applied Mechanics and Engineering* 191(27):2925-2947.

Huijsmans, J. F. M. 1985. *Fysische aspecten van de aardappelbewaring : fysische modellering van een geventileerde aardappelstapeling : vergelijking van het horizontale en verticale ventilatiesysteem*. Wageningen: L.H.

Irvine, D., D. Jayas, and G. Mazza. 1993. Resistance to airflow through clean and soiled potatoes. *Transactions of the ASAE (USA)*.

John, V., and P. Knobloch. 2007. On spurious oscillations at layers diminishing (SOLD) methods for convection–diffusion equations: Part I – A review. *Computer Methods in Applied Mechanics and Engineering* 196(17–20):2197-2215.

Ofoli, R. Y., and G. J. Burgess. 1986. A thermodynamic approach to heat and mass transport in stored agricultural products. *Journal of Food Engineering* 5(3):195-216.

Rastovski, A., R. Wustman, and P. Hak. 1985. Horizontale ventilatie bij aardappelbewaring. IBVL.

Rastovski, A., and A. v. Es. 1987. *Storage of potatoes : post-harvest behaviour, store design, storage practice, handling*. [2nd ed. Wageningen: Pudoc.

Sen, Z. 1995. *Applied hydrogeology for scientists and engineers*. CRC Press.

Van't Ooster, A. 1999. Storage of potatoes. *CIGR Handbook of Agricultural Engineering* 4:93-125.

Verdijck, G. J. C. 2003. *Model-based product quality control applied to climate controlled processing of agro-material*. Eindhoven: Technische Universiteit Eindhoven.

Whitaker, S. 1986. Flow in porous media I: A theoretical derivation of Darcy's law. *Transport in porous media* 1(1):3-25.

Zienkiewicz, O. C., R. L. Taylor, J. Z. Zhu, and O. C. Z. L. T. Z. Zhu. 2005. 2 - Convection dominated problems — finite element approximations to the convection—diffusion-reaction equation. In *The Finite Element Method Set (Sixth Edition)*, 28-78. Oxford: Butterworth-Heinemann.

Appendix A

In Figure A-0-1, the cooling process caused by the evaporator is visualized. The process can be described by the following steps:

- Define air conditions at the inlet of evaporator:
  $(T_{in} = 6°C, \ X_{in} = 5.5 \ g/kg)$
- Define capacity evaporator and airflow along cooling plates from specifications:
  $(P_{evap} = 23.5 \ kW, \ \phi_{fan} = 4.25 \ m^3/s)$
- Calculate T_c $(= T_{in} - 7°C)$ and X_c:
  $(T_c = -1°C, \ X_c = 3.48 \ g/kg)$
- Calculate $\Delta H_{cooling}$ and ΔH_{tot}:
  $(\Delta H_{cooling} = 4.4 \ kJ/kg , \ \Delta H_{tot} = 12.2 \ kJ/kg)$
- Calculate R_{enth}, T_{out} and X_{out} using:
  $(R_{ent} = 0.36, \ T_{out} = 3.5°C, \ X_{out} = 4.77 \ g/kg)$

1. Conditions air in			2. Conditions cooling surface			3. Conditions air out		
Temperature	6	°C	Temperature	-1	°C	Temperature	3.473	°C
Relative humidity	95	%	Relative humidity	100	%	Relative humidity	98.3	%
Specific humidity	5.50	g/kg	Specific humidity	3.48	g/kg	Specific humidity	4.77	g/kg
Enthalpy	19.9	kJ/kg	Enthalpy	7.7	kJ/kg	Enthalpy	15.5	kJ/kg
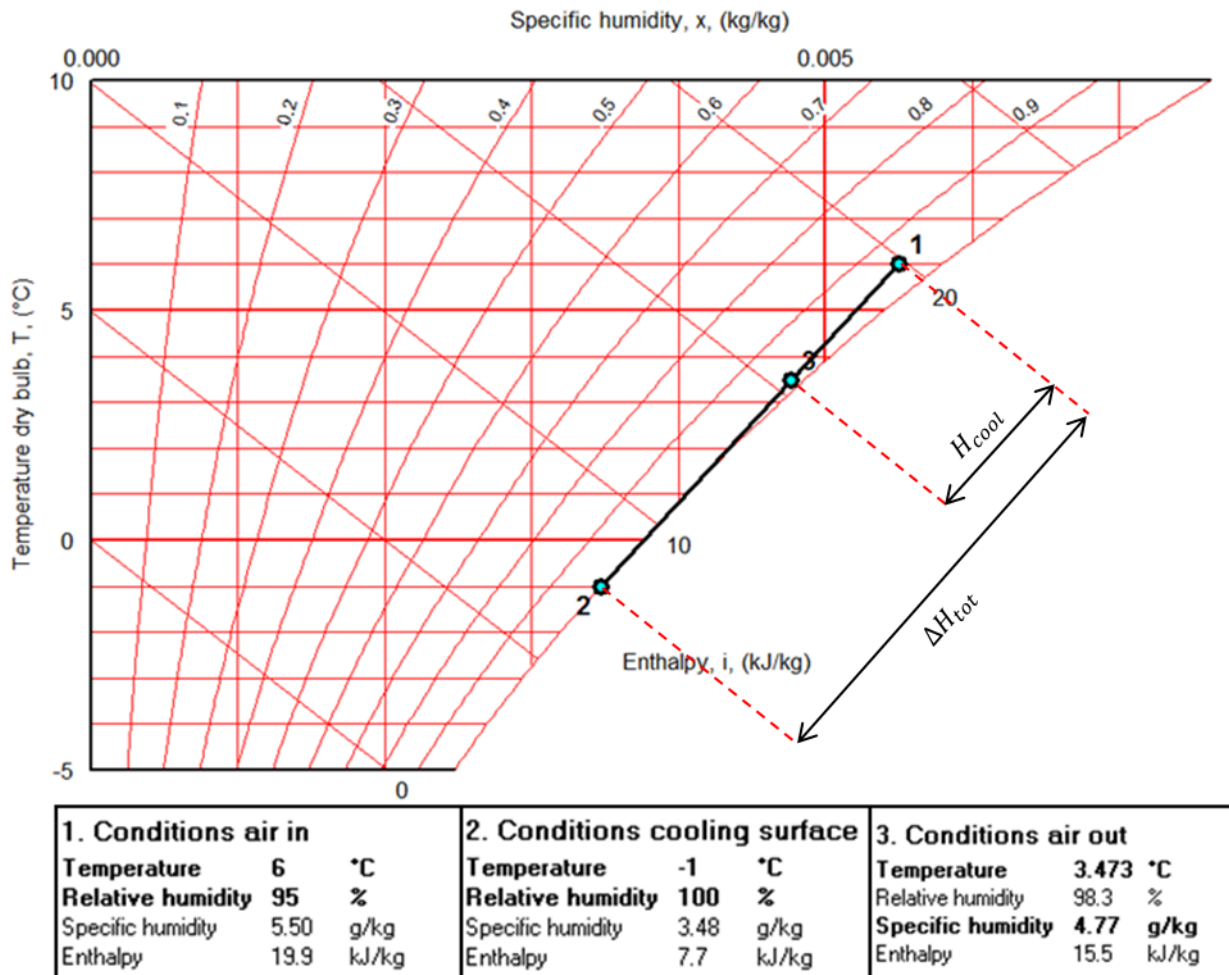
Figure A-0-1. Visualization of cooling process caused by the evaporator in Mollier-diagram. The curved lines in the Mollier-diagram represent the relative humidity fraction. Furthermore, the dry bulb temperature, the enthalpy content and the absolute water content are given in this diagram. Point 1 represent the air conditions at the inlet of the cooling unit, point 2 the conditions on the cooling surfaces of the evaporator and point 3 the air conditions at the outlet of the cooling unit.

Figure A-0-1 shows that both the temperature and the absolute humidity on the outlet of the evaporator (point 3) are lower than on the inlet of the evaporator (point 1).

Appendix B

Specifications of the evaporator used for the calculations on the cooling unit.

Alfa Laval Groningen BV
P.O. Box: 44
NL- 9700 AA Groningen
Phone: ++31 50 5217555
Fax: ++31 50 5264878
Web site: www.helpman.com
Version: 01/2012

Date   Jan 29, 2013
Reference   :
Client Name   :
City   :
Country   :

Air Cooler   Helpman-LEX 26-7 230

Capacity		22.3	kW		Refrigerant	R404A dx		
Required capacity		22.00	kW		Evaporating temperature		-5	°C
Capacity factor		1.01			Liquid temp before exp. valve		30	°C
Air on		2.00	°C	85%	Superheating		4.6	K
Air off		-0.78	°C					
Temp diff	DT1	7.00	°C		Frost	Light		

Fans	230/50/1		Number: 3		Noise pressure level	64.5	dB(A)	5 m
Air volume		15300	m³/h		Sound power	90	dB(A)	
Diameter		457	mm					
Motor		IP55			Throw	20	m	
Speed		1500	rpm					
Power nom/abs.		220 / 370	W					
Adj. therm. relay		2.6	A					

Execution				Connections			
Coil	Copper/Aluminum			Suction	54	mm	
Surface Area	84.2	m²		Liquid	5/8"		
Finspacing	7	mm		**Dimensions**			
Empty Weight (+/-5%)	159	kg		Length	2650	mm	
Internal volume	30.9	dm³		Width	820	mm	
Transport volume	2.3	m³		Height	700	mm	
Remarks							

Dimensions and weights are not valid for all possible options

Appendix C

The ventilation period and moisture losses for the several scenarios evaluated on the first of April:

Outdoor air cooling in April
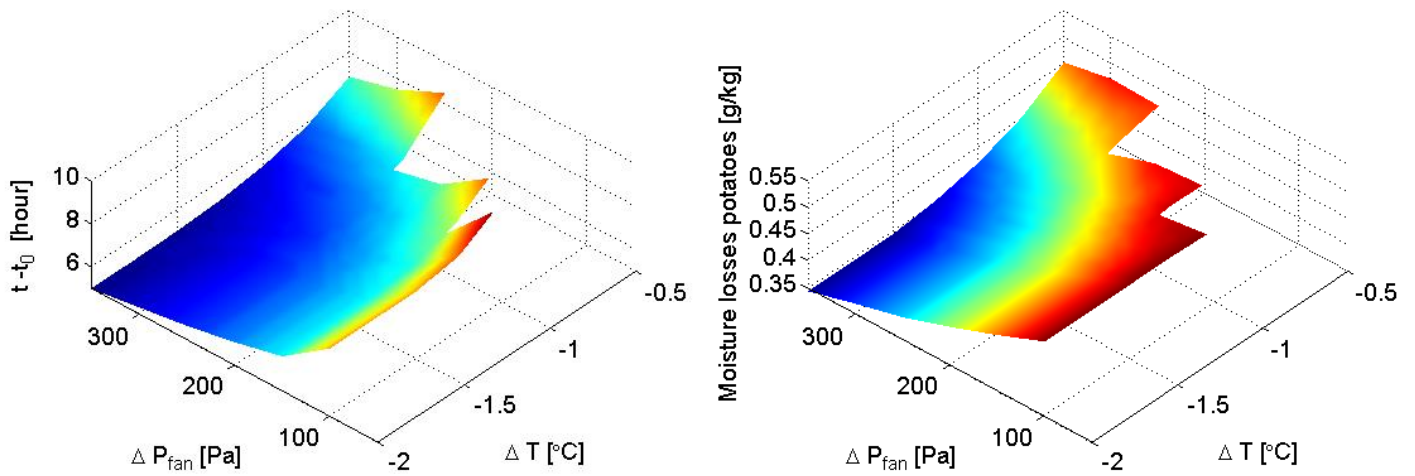

## Outdoor air cooling + humidifier in April
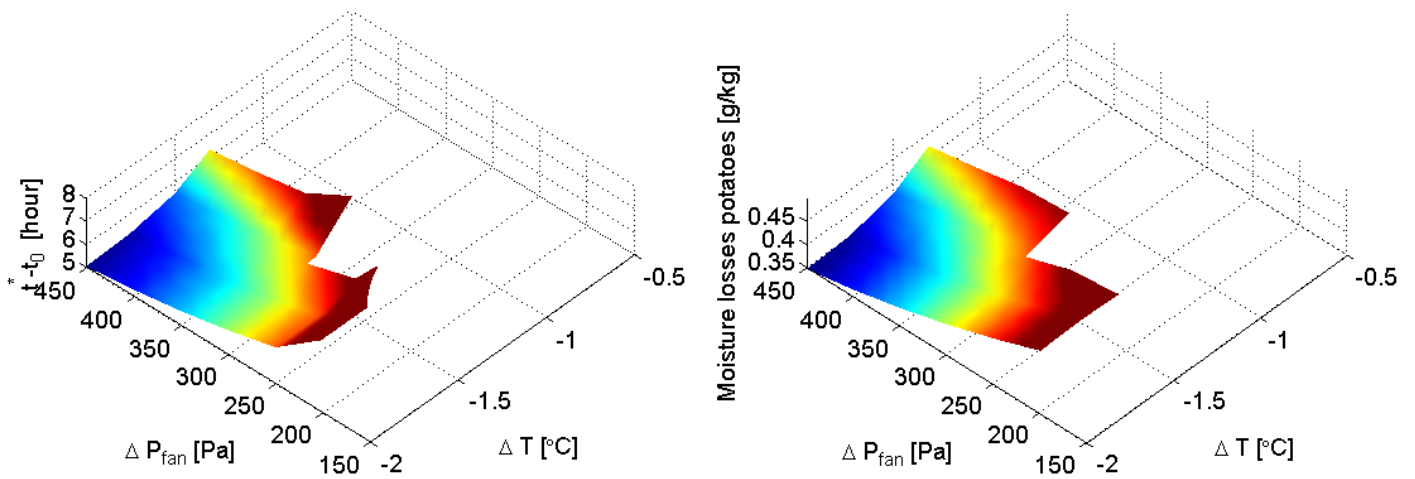
Cooling unit in April
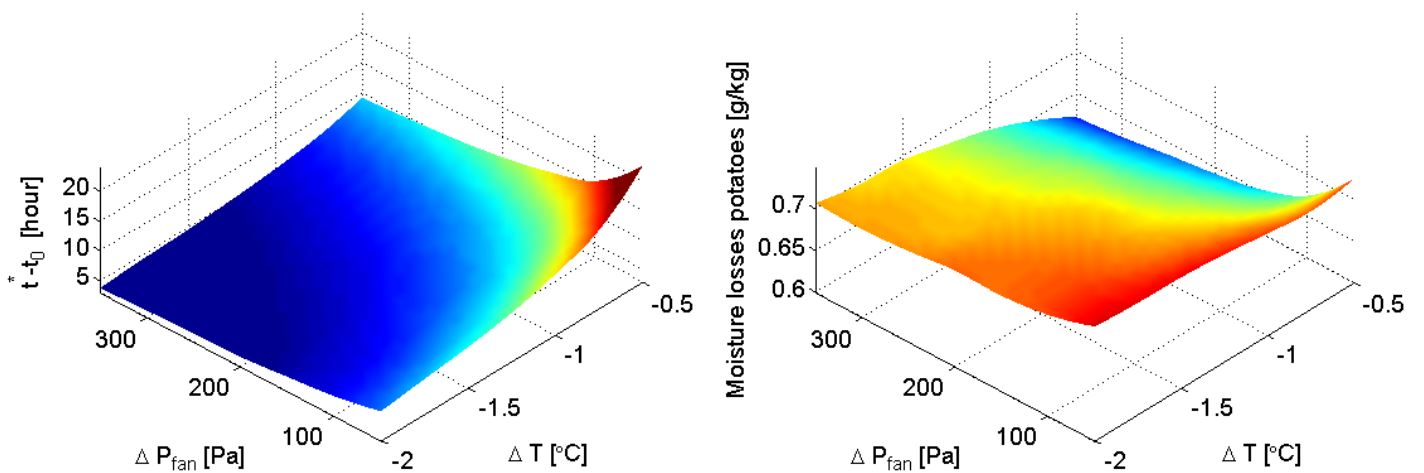
Appendix D

Total costs plots for the several scenarios evaluated on the first of December:

Costs outdoor air cooling in December
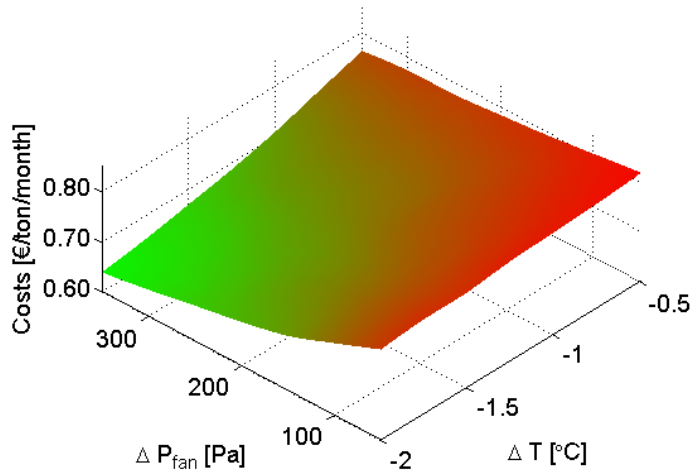
Costs outdoor air cooling + humidifier in December
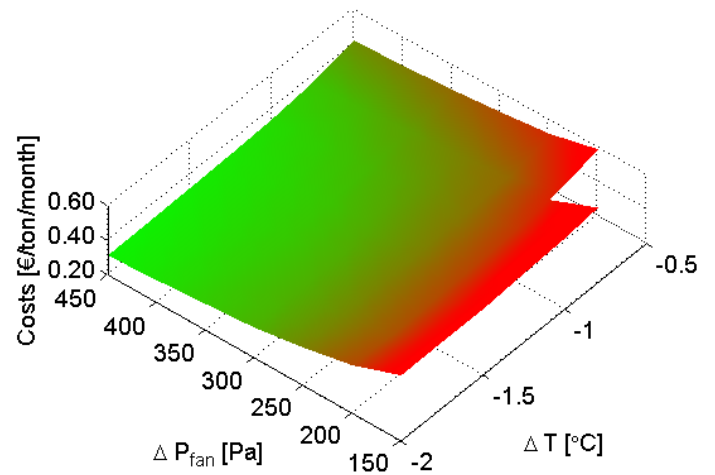
Costs cooling unit in December
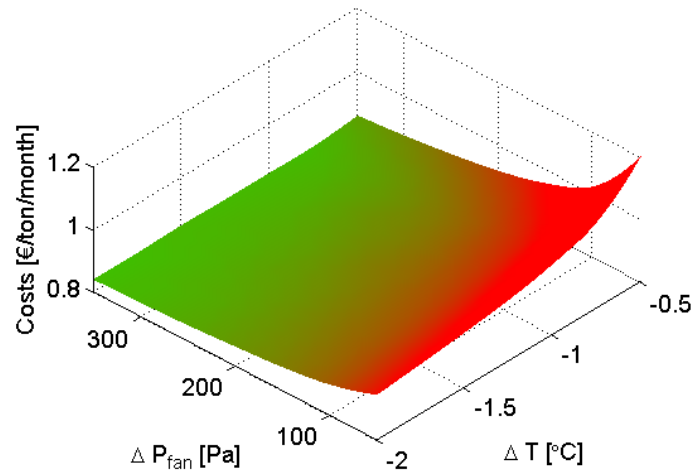
Total costs plots for the several scenarios evaluated on the first of April:
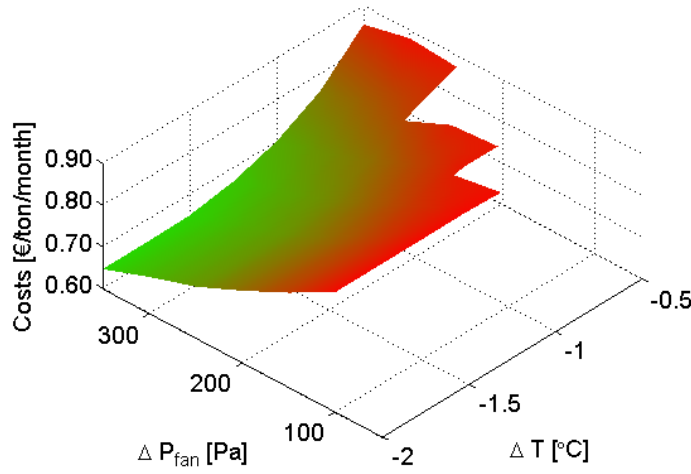
Costs outdoor air cooling in April   **Costs outdoor air cooling + humidifier in April**
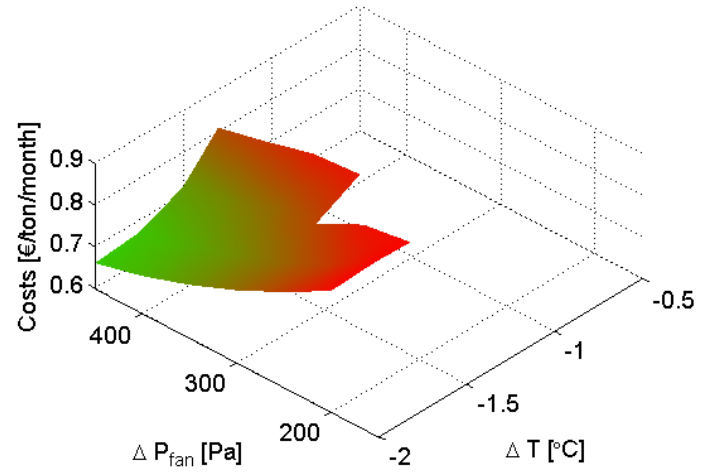
Costs cooling unit in April
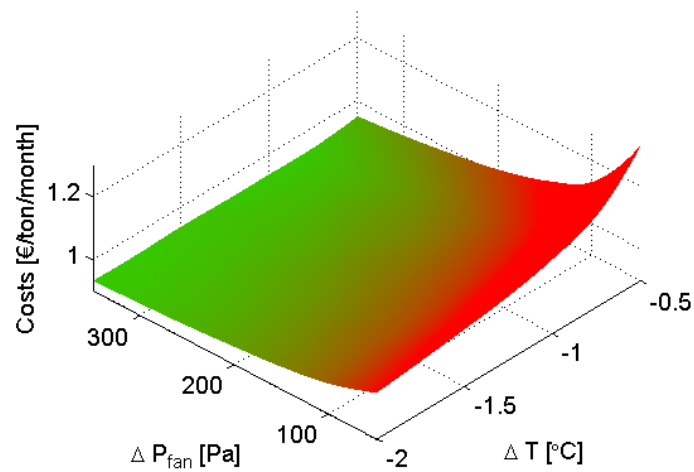
Appendix E

The total costs related to all scenarios in the sensitivity analyses:

**Costs outdoor air cooling in December
(high pot. price, low elec. price)**
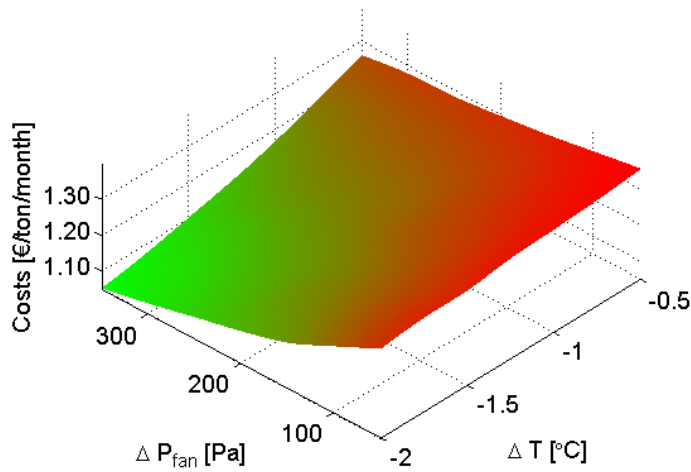
**Costs outdoor air cooling in December
(low pot. price, high elec. price)**
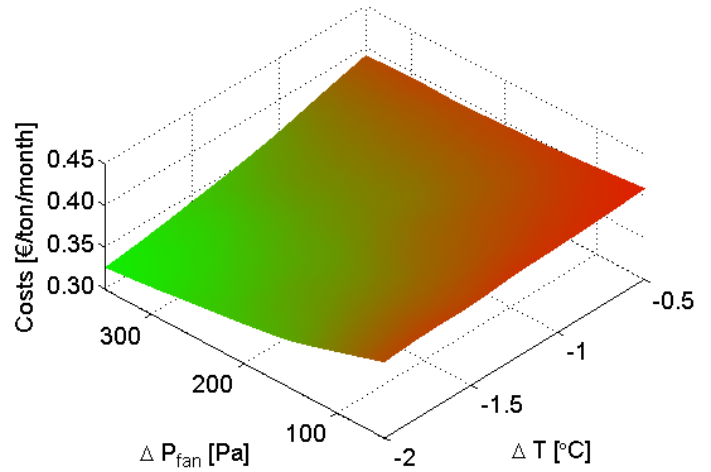
**Costs outdoor air cooling + humidifier in December
(high pot. price, low elec. price)**
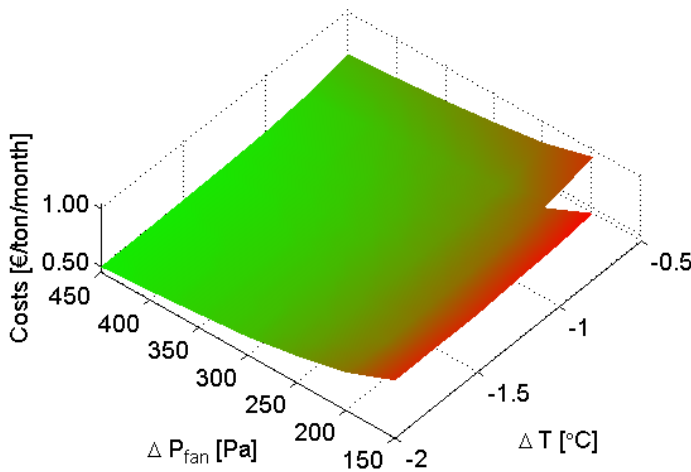
**Costs outdoor air cooling + humidifier in December
(low pot. price, high elec. price)**
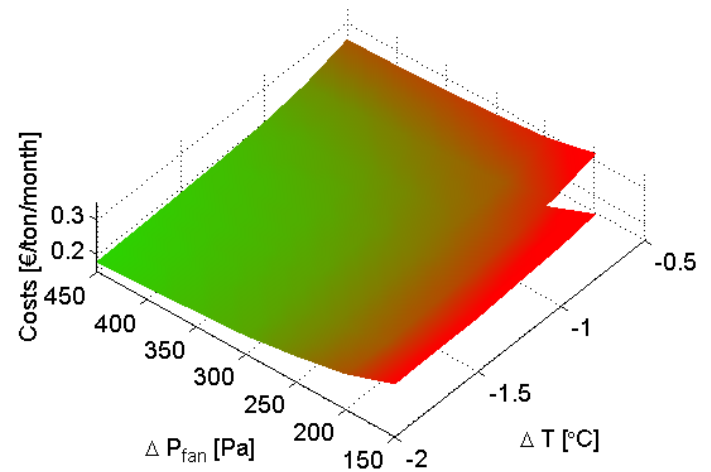
**Costs mechanical cooling in December
(high pot. price, low elec. price)**
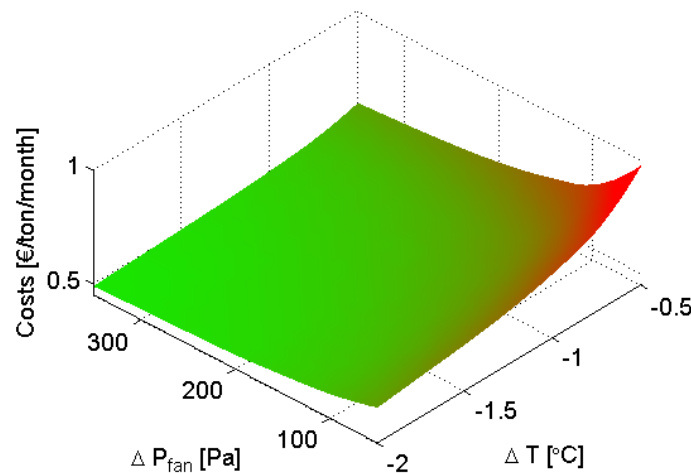
**Costs mechanical cooling in December
(low pot. price, high elec. price)**
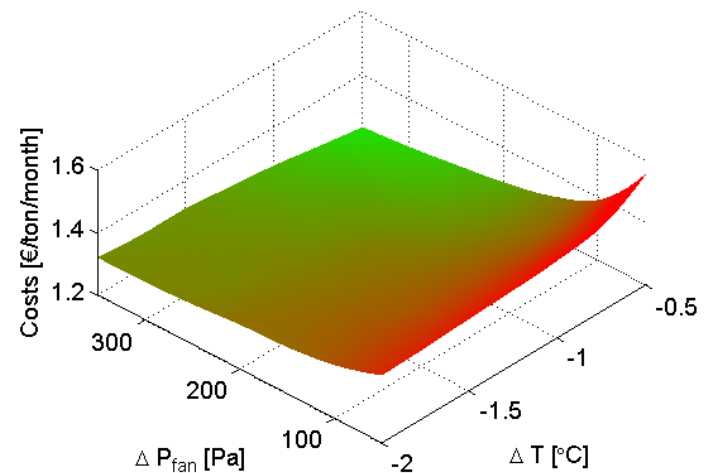
**Costs outdoor air cooling in April
(high pot. price, low elec. price)**
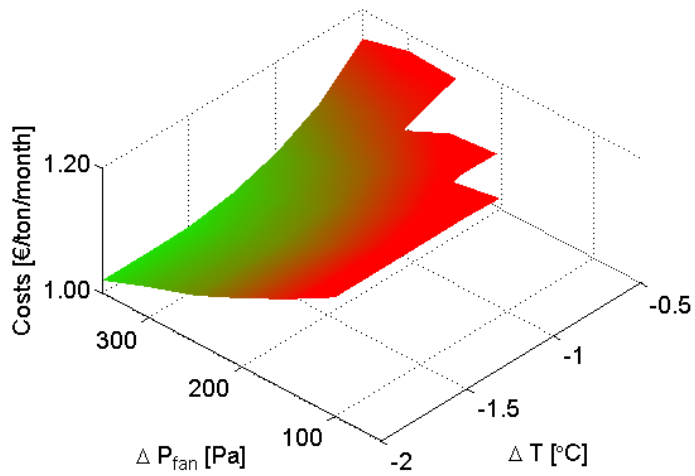
**Costs outdoor air cooling in April
(low pot. price, high elec. price)**
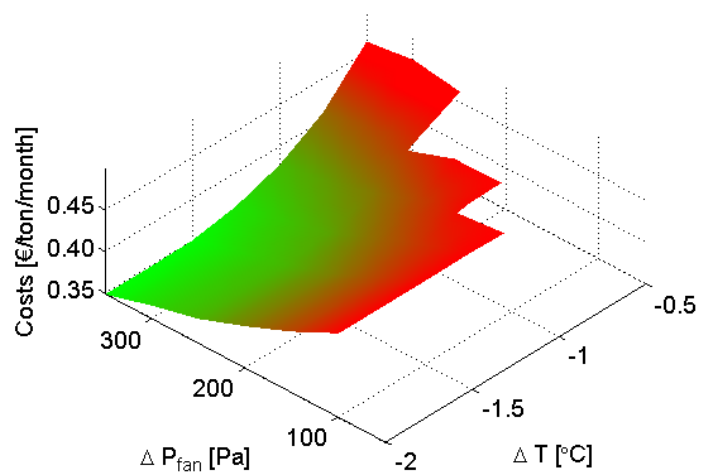
**Costs outdoor air cooling + humidifier in April
(high pot. price, low elec. price)**
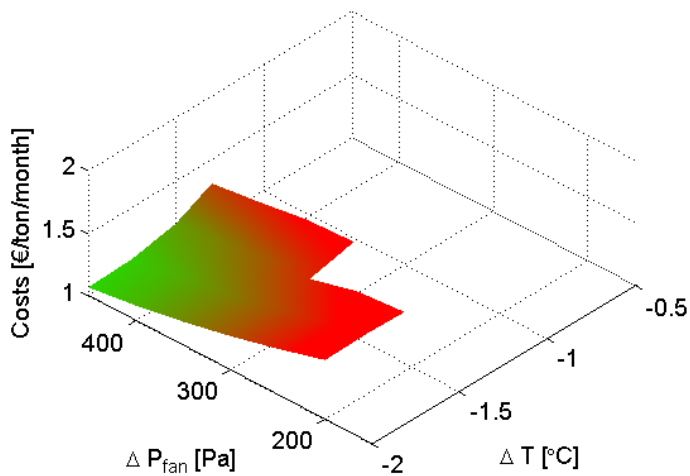
**Costs outdoor air cooling + humidifier in April
(low pot. price, high elec. price)**
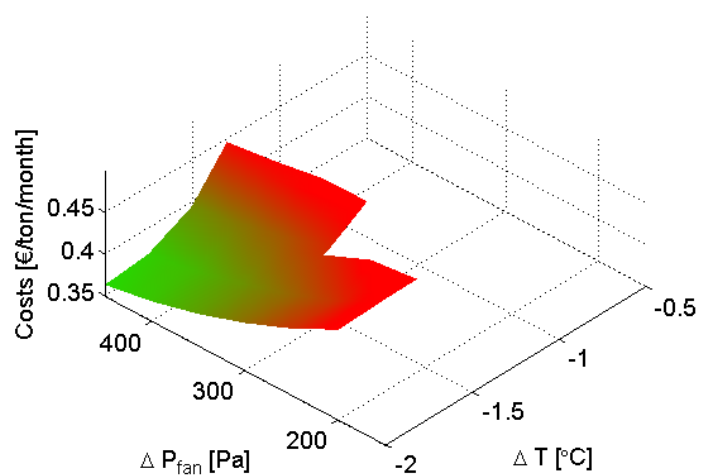
**Costs mechanical cooling in April
(high pot. price, low elec. price)**
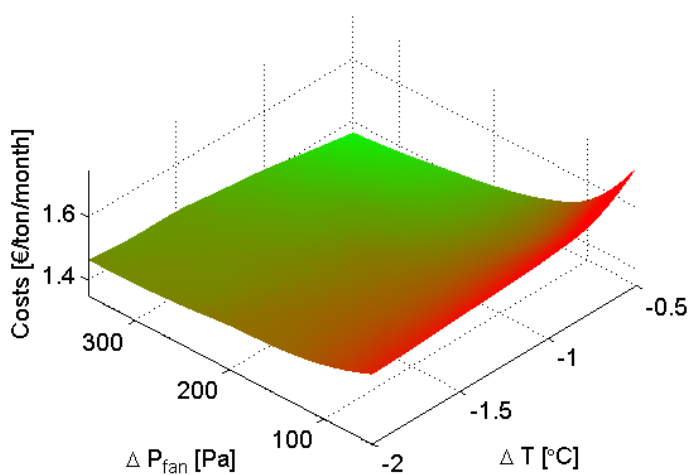
**Costs mechanical cooling in April
(low pot. price, high elec. price)**

94
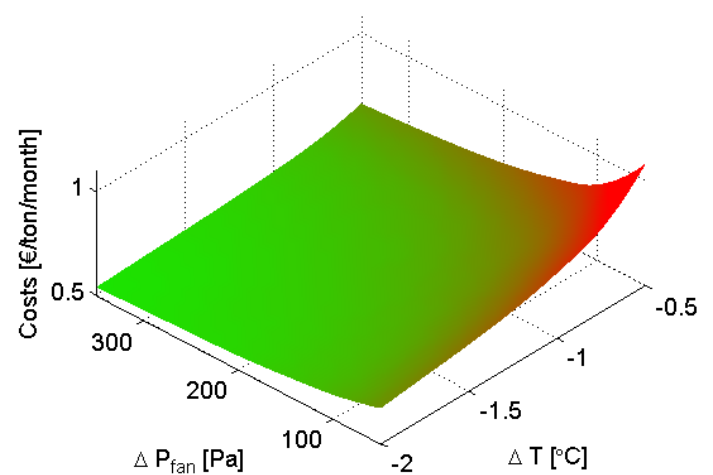
Appendix F

To analyse the sensitivity of numerical errors in the simulations, the original data regarding ventilation time and moisture losses is perturbed (+5 % for lowest values and -5% for highest values):

Original ventilation time   **Perturbed ventilation time**
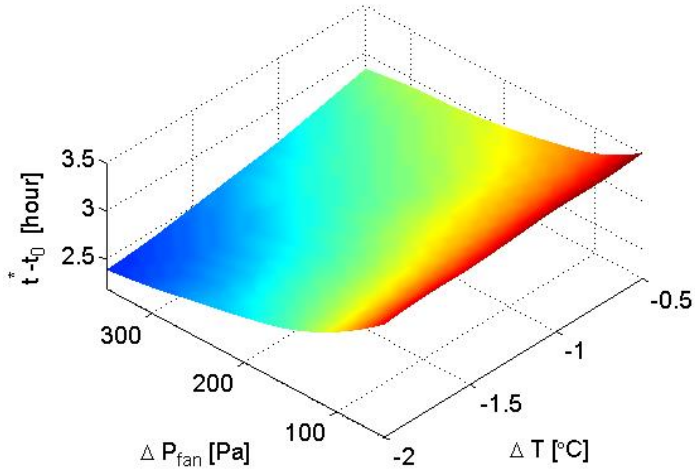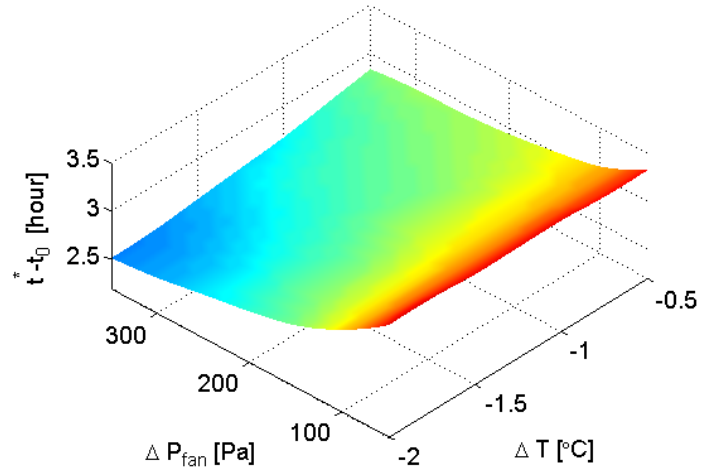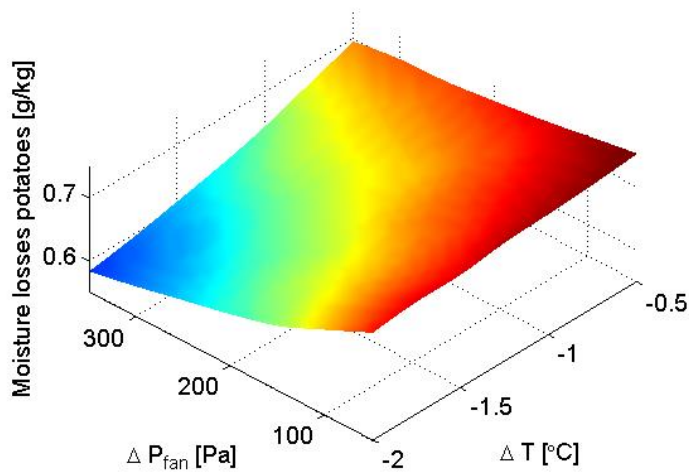
Original moisture losses   **Perturbed moisture losses**